National Library of Canada
Acquisitions and Bibliographic Services Branch
395 Wellington Street
Ottawa, Ontario
K1A 0N4

Bibliothèque nationale du Canada
Direction des acquisitions et des services bibliographiques
395, rue Wellington
Ottawa (Ontario)
K1A 0N4

Your file Votre référence

Our file Notre référence

NOTICE

The quality of this microform is heavily dependent upon the quality of the original thesis submitted for microfilming. Every effort has been made to ensure the highest quality of reproduction possible.

If pages are missing, contact the university which granted the degree.

Some pages may have indistinct print especially if the original pages were typed with a poor typewriter ribbon or if the university sent us an inferior photocopy.

AVIS

La qualité de cette microforme dépend grandement de la qualité de la thèse soumise au microfilmage. Nous avons tout fait pour assurer une qualité supérieure de reproduction.

S'il manque des pages, veuillez communiquer avec l'université qui a conféré le grade.

La qualité d'impression de certaines pages peut laisser à désirer, surtout si les pages originales ont été dactylographiées à l'aide d'un ruban usé ou si l'université nous a fait parvenir une photocopie de qualité inférieure.

Canada

Geometry of Capillary Networks During Normal and Pathological Growth of the Rat Myocardium

A Thesis Submitted to the School of Graduate Studies and Research of the University of Ottawa in Partial Fulfilment of the Requirements for the Degree of

Doctorate of Philosophy in Physiology

Candidate: Sanjay Batra

Supervisor: Dr. K. Rakusan

ISBN 0-315-79991-9

UNIVERSITÉ D'OTTAWA
UNIVERSITY OF OTTAWA

DEDICATION

To my Father, in whose footsteps I have followed with tremendous respect and admiration. To my Mother, for never-ending love, support and friendship.

S+S = ONE!

ACKNOWLEDGMENTS

I would like to sincerely thank Dr. Karel Rakusan whose advice and guidance throughout my course of study has been truly inspirational. You are a consummate scientist, my teacher, colleague and friend. I am indebted to Mrs. Ching-Ju Kuo, and Mr. Jimmy Gao, for their excellent technical assistance. I would also like to thank the members of the Department of Physiology, from who I have learned very much. In particular to Dr. K.J. Kako, for excellent direction over the last four years. To Dr. D.J. Parry, for challenging me to look critically beyond the data. And to the late Dr. Graham Mainwood, who always took the time for graduate students.

TABLE OF CONTENTS

LIST OF TABLES

LIST OF FIGURES

LIST OF COLOR PLATES

ABSTRACT

The aim of this dissertation was to provide a thorough description of the coronary microvasculature at different phases of cardiac contraction, during normal postnatal growth, and pathologically accelerated growth due to pressure and volume overloading. The histochemical technique used to visualize capillaries was novel in that it served to distinguish arteriolar and venular capillary regions by colour. Arteriolar capillary (AC) regions stained blue in colour, positive for the presence of Alkaline Phosphatase in the endothelium. Venular capillary (VC) regions stained red in colour, positive for the presence of Dipeptidyl Peptidase IV. The morphometric methods used to assess capillary geometry from cross and longitudinal tissue sections were classified according to AC and VC regions.

From tissue cross sections, capillaries were represented as a bivariate (CV, blue; VC, red) point pattern in the tissue plane. Our software program for capillary domains served to divide the plane into polygonal regions of tissue, each polygon enclosing one capillary. The area subtended by each polygon, the capillary domain, was closer to the enclosed capillary than any other. From individual domain areas, the equivalent radius of the Krogh cylinder with the same area was calculated. As the distribution of these radii is log-normal, the variability was best characterized by the logarithmic standard deviation (SDlog). In this manner, SDlog, the heterogeneity of capillary spacing was determined.

From longitudinal sections, scale drawings of capillary sets, which consisted of all the capillary pathways that could be clearly followed from the same terminal arteriole to collecting venule served as the basic unit of study. From these capillary sets, we have defined and measured several morphometric parameters, appropriate as indicators of geometrical conditions for oxygen supply. Among these parameters are the minimal capillary length, the shortest contiguous

pathway from arteriole to venule; mean capillary length, the average length of all possible capillary paths from arteriole to venule; and capillary segment length, the distance between two successive capillary branch points.

Chapter 1: To consider the effects of fiber shortening on coronary capillary tortuosity, hearts were arrested at discrete points in the cardiac cycle ($CaCl_2$ or KCl arrest). The degree of fiber shortening was assessed by measurements of both sarcomere length and left ventricular wall to cavity ratio. The principle finding was that increases in capillary tortuosity with fiber shortening were minimal, as compared to data from various skeletal muscles. During cardiac contraction, branching angles are altered rather than corollary increases in capillary segment tortuosity.

Chapter 2: To determine the effects of postnatal growth on the coronary microcirculation, the geometry of capillary nets were studied in male rats at 21, 28, 60 and 240 days of age. Capillary domain areas progressively increased with growth of the heart ($P<0.01$). In all groups, AC domain area was larger than VC domain area ($P<0.01$). The heterogeneity of capillary spacing (SDlog), which is another important determinant of oxygen supply, demonstrated significant increases with age for AC regions ($P<0.01$). With increasing left ventricular mass, there was a lateral expansion of the arterio-venous capillary set, which was displayed by an increase in the number of and distance between adjacent capillary paths ($P<0.01$). Our data indicate that differences in the geometry of arteriolar and venular capillary regions are present by 21 days of age. During postnatal growth, the results from both cross and longitudinal sections, suggest that the geometrical conditions for oxygen supply are notably impaired.

Chapter 3: To consider the effect of pressure overload cardiac hypertrophy on the geometry of capillary nets, we induced chronic pressure overloading by

aortic constriction in neonatal rats. In sham-operated controls, the capillary domain area decreased from the arteriolar to venular capillary regions (499 ± 3 μm^2 and 456 ± 5 μm^2, $p<0.05$; mean ± SEM). In pressure overload hypertrophy, only arteriolar capillary tissue regions increased in size, thus enlarging the difference between arteriolar and venular ends (547 ± 6 μm^2 and 464 ± 5 μm^2, $P<0.01$). Intercapillary distances, measured at various levels along the capillary pathlength, decreased in a stepwise manner in both normal and hypertrophic hearts. In hypertrophic hearts, mean capillary pathlength was significantly longer than in controls, but the total length of the individual capillary nets was reduced. In both groups, arteriolar capillary segment length was longer ($P<0.01$) than venular capillary segment length. Given that PO_2 values are lower on the venular side of capillaries, this spatially distinctive geometry in normal myocardium: smaller domains, shorter intercapillary distances and segment lengths, would provide favorable geometric conditions for oxygen diffusion. In hypertrophy, average intercapillary distance increased, and the distinction in capillary geometry from AC to VC regions was increased.

Chapter 4: These data prompted us to consider what changes occur in capillary geometry following volume overload, where myocyte dimensions and their pattern of organization in the ventricular wall are different from pressure overload. We were interested whether these differences in the tissue remodelling between pressure and volume overload comprised the structural basis for a different pattern of adaptation at the level of the coronary microcirculation. Volume overload cardiac hypertrophy was induced in male Sprague-Dawley rats by experimental aortocaval fistula. In sham-operated controls (CON; n=8), the capillary domain area decreased from AC to VC regions (AC=505 ± 5 μm^2; VC=452 ± 7 μm^2, $P<0.01$; mean ± SE). In volume overloaded hearts (VOL;

n=8), only VC domain areas were reduced from control values ($P<0.01$) and the differences between AC and VC regions were preserved (AC=480 ± 5 μm^2; VC= 395 ± 6 μm^2, $P<0.01$). Minimal capillary length was significantly longer in volume overloaded hearts ($P<0.01$). In the control group, AC segment length was longer than VC segment length ($P<0.01$). In volume overload, AC segment length was also longer than VC segment length, and the divergence between AC and VC regions was increased. These changes in capillary geometry may be secondary to specific changes in the arrangement and dimension of myocytes in the left ventricular wall following volume overload hypertrophy.

Chapter 5: A natural extension of the results of this dissertation would be to consider the influence of these data on models of oxygen transport. Specifically, would alterations at the level of the coronary microvasculature influence myocardial PO_2? To address this question, we have applied these data to a multicylindrical model of oxygen transport that represent myocardial tissue as a set of overlapping Kroghian tissue cylinders. This model allows for the calculation of PO_2 histograms under varying input conditions including domain area, and heterogeneity of capillary spacing (SDlog).

To illustrate the effect of changes in capillary geometry on myocardial oxygenation, we have chosen as an illustration, the results obtained from pressure overloaded hearts. Results of these computations suggest that when realistic morphometric data are used as input parameters in the computation of myocardial PO_2, computed histograms are significantly altered. The effect of realistic morphometric data, as those collected in this dissertation, show that myocardial oxygenation is markedly increased and more uniform than calculations based upon the traditional Krogh cylinder model. These data would call for a modification of the classical Krogh tissue cylinder; the tissue supply volume being better described as a truncated cone rather than a cylinder.

INTRODUCTION

FOREWORD

The purpose of this dissertation is to provide a quantitative description of the coronary microvasculature under conditions of normal and pathological growth. All experiments were conducted in the rat myocardium. The staining technique for the analysis of capillary nets was novel in that it distinguished arteriolar and venular capillary regions by color. Morphometric data were compiled from both cross and longitudinal sections, as a function of capillary region. From cross sections, we determined tissue supply regions surrounding individual capillaries, and the heterogeneity of capillary spacing. From longitudinal sections, we defined and measured several parameters related to capillary length and branching pattern. These data serve as the basis for models of oxygen supply during normal and pathological growth. Following an overall introduction, the dissertation has been divided in five Chapters, as described:

- Chapter 1: study of changes in capillary geometry at discrete phases of the cardiac cycle.

- Chapter 2: morphometric analysis of capillary nets at four stages of normal growth (21, 28, 60, 240 postnatal days of age)

- Chapter 3: study of capillary geometry in hearts exposed to chronic pressure overload following aortic constriction.

- Chapter 4: study of capillary geometry in hearts exposed to chronic volume overload following chronic aortocaval fistula.

- Chapter 5: an integrated discussion and summary of the principal results of the dissertation. Implications of these data to theoretical models of oxygen transport, with calculations of tissue PO_2 profiles under various conditions.

HISTORICAL PERSPECTIVE

The first observation of the circulation was made by William Harvey (1578-1657), who postulated that blood travelled in a circuit from the heart, through the arteries, to the veins and back to the heart in its entirety. This postulate was contrary to the teachings of Galen, whose ideas dominated intellectual thought through the last millenium. Galen's central concept was the unidirectional movement of blood and air within the lungs. Galen described the motion of air (vital spirit) in one direction and waste (sooty residues) in the other though the pulmonary vein. The Galenic system made provision for two types of blood, the nutritional blood of the veins originating from the liver, and the spirituous blood

of the arteries originating from the heart. This system was challenged in Harvey's treatise, De motu cordis, published in 1628. Harvey characterized the quantity and source of the blood that was transmitted from the veins to the arteries by the action of the heart. He described the movement of the blood as a circular motion, analogous to Aristotle's view of the air and rain emulating the circular motion of the bodies above. Harvey reasoned that the quantity of blood ejected by the ventricle with each systole, over a period of time would greatly exceed the quantity of blood in the body. Therefore the blood must follow a circular path from heart to tissues, and back to the heart again. The most salient point in his concept lay in the preservation of the blood rather than it's consumption in the peripheral organs and tissues.

It is not known whether Harvey sought to identify connections between arterial and venous vessels, which he described as porosities of the flesh. Harvey's experiments made it a logical extension that there were pathways for the blood from the smallest arteries to the smallest veins although he was not able to see them with the naked eye. Microscopes were already in use during Harvey's time, and it was just 4 years after his death that the movement of blood through capillaries in the lung would be observed by Malpighi. Marcello Malpighi (1628-1694), used double convex lenses to view direct connections between arteries and veins in several internal organs including the frog lung. Malpighi described tortuous blood containing vessels that formed a network with blood flowing from

arteries to veins, thus completing Harvey's theory of the circulation 33 years after "De motu cordis". Malpighi further suggested that the blood always flowed through tubed vessels, and did not take a random course through the tissues as Harvey presumed. Malpighi was able to describe the blood as a liquid consisting of an infinite number of particles. Subsequently, van Leeuwenhoek, in 1674 was able to make in vivo observations of blood flow in living animals. Using ground lenses with higher magnification, he was able to view individual "globules" streaming through minute vessels that he first termed capillaries. He further described deformations in these globules as they passed through even smaller vessels. And so was born, a complete description of the circulatory system, following from Harvey's original work and ideas. New insights and controversies into the structure, control and function of microscopic vessels continued to evolve over the next two centuries.

It was not until the nineteenth century, that Hall (1831) attempted to distinguish arterioles, capillaries and venules from a structural basis. He described arterial vessels as those that continued to subdivide into progressively smaller branches. Veins continued to enlarge from successive convergences, and capillaries were distinct from either of these. They continued to branch, but did not become smaller or larger. Capillaries maintained nearly constant diameter with successive divergences and convergences. Hall further suggested functional implications, stating that the number and distribution of capillaries was modified

in different tissues in accordance with their specific requirements. Histological methods continued to develop in the nineteenth century which allowed for a more complete description of the capillary wall. In 1865, three scientists, including Auerbach (1865), almost simultaneously described the cellular nature of the capillary wall. This finding was followed by a period of descriptive histology, that was extended to capillary beds in many different tissues.

The next milestone in discovery was to set the basis for the first conceptual models of the microcirculation based upon quantitative histology. In 1922, August Krogh reviewed the state of the art, in giving a series of lectures in the U.S.A. two years after receiving the Nobel prize in medicine and physiology. These materials were previously published in the classic book "The Anatomy and Physiology of Capillaries" (Krogh, 1919).

Krogh suggested that oxygen transport phenomena was dependent upon the number as well as the arrangement of capillaries in tissue. Krogh's first experimental efforts were directed at determining the number, distribution and surface area of capillaries in striated muscle. Based upon his observation that capillaries were uniformly distributed in tissue sections cut perpendicular to the muscle fiber axis, Krogh suggested that each capillary be considered as running in parallel to the muscle fiber, and supplying a concentric cylinder of tissue with the capillary in the center of the cylinder. This "Krogh" cylinder, was completely independent of other capillary-tissue cylinders, and the average cylinder radius

could simply be determined by counting the number of capillaries per cross-sectional area and dividing cross-sectional area by the number of capillaries. The cylinder radius represented the diffusion distance of oxygen from the capillary. With the premise that the rate of O_2 convective transport by the blood greatly exceeded the rate of oxygen diffusion, Krogh concluded that axial diffusion gradients in the tissue were negligible. The Fick equation, solved for a cylindrical geometry was then suitable to quantitative description, and Krogh convinced his mathematician colleague Erlang, to describe this model in mathematical terms. The outcome of this collaboration was the now famous Krogh-Erlang equation, based upon the first law of Fick holding for steady state conditions:

$$\Delta P = P_c - P_x = \frac{M}{K}\left(\frac{R^2}{2}\ln\frac{x}{r} - (x^2 - r^2)/4\right) \qquad (1)$$

where ΔP is the gradient in PO_2 from the capillary to point x (mmHg), P_c is the oxygen pressure in the capillary (mmHg), P_x is the oxygen pressure at point x (mmHg), M is the oxygen consumption (ml O_2/ ml tissue/ time), K is Krogh's diffusion coefficient in ml O_2/cm sec mmHg, R is the radius of the tissue cylinder, r is the capillary radius, and x is the distance from the capillary to any point in the tissue. From this equation it is possible to compute the tissue PO_2 as a function of radial distance from the capillary.

This equation is based upon a number of assumptions and simplifications. As described in the review of Kreuzer (1982), some simplifications include the idea that there is only radial diffusion into the tissue and that the chemical reactions within the blood compartment are ignored, i.e. the oxygen profile at any point in the capillary cross section. The equation also assumed that oxygen consumption was uniform over the tissue, and that this consumption did not depend upon the local PO_2 (zero-order reaction). Krogh further assumed that the capillary wall presented no resistance to diffusion, that there was no facilitation to diffusion by myoglobin, that capillary flow was constant and that there was no interchange of oxygen between adjacent cylinders. Of particular relevance to this dissertation are the following assumptions: that capillaries are straight, unbranched and uniformly distributed; capillary length and radius are constant (which implies no variability in transit time given constant flow). Despite these simplifications, the Krogh model has served as the cornerstone for the analytical study of oxygen supply from 1919 to present day.

It should be further noted that the Krogh cylinder model is not space filling, as the various cylinders leave gaps in the tissue, sometimes referred to as dead corners. Thews (1960) tried to overcome this problem by proposing a space filling hexagonal pattern. In this model, the maximal diffusion distance is defined as the radius of the circumscribed circle of the hexagon. This radius is larger that the Krogh cylinder radius, but serves to cover all regions of the tissue.

Following the original work of Krogh, other investigators have also considered diffusion processes of oxygen and metabolites through tissue. A.V. Hill (1928) extended Krogh's steady state model to the unsteady state. The model of Hill was developed to describe the diffusion of O_2 into isolated nerve preparations from the solution in which those nerves were bathed:

$$Pr = P_R - \frac{\dot{V}}{4D\alpha}(R^2 - r^2) \qquad (2)$$

where Pr is the O_2 tension at a radial position, r; P_R is the O_2 tension at the boundary of the fiber; R is the fiber radius and r is the radial position relative to the fiber; V is the rate of O_2 consumption; D is the O_2 diffusivity and α the O_2 solubility coefficients, respectively. The Hill model characterizes oxygen supply uniformly from the periphery into the muscle fiber, whereas the Krogh model describes oxygen supply outwards into the tissue from a single capillary. These two approaches have been compared (Groom et al. 1984b), and it has been suggested that the Hill model appears to be preferable in situations where the (skeletal) muscle is shortened and capillary to fiber contact length is increased, thus improving gas exchange potential from capillary to tissue. Unfortunately Hill did not apply his mathematical models to various blood vessel-tissue geometries or to conditions representative of living tissues. His results therefore, while advancing mathematical concepts of diffusion processes, did not represent realistic

situations of oxygen supply in living systems. Grote and Thews (1962) developed equations that took into account changes in blood flow, and Hudson and Cater (1965) incorporated other factors such as a non-cylindrical geometry, variations in tissue O2 consumption, variations in oxygen tension along the capillary pathlength and the effect of stirring in the tissue fluid. Groom et al. (1984b) were the first to apply the Hill model to known vascular geometries of mammalian skeletal muscle. Rakusan et al. (1985) considered the effect of myocyte diameter, intercapillary distance and the heterogeneity of capillary spacing on the oxygen supply of normal and hypertrophic rat hearts. They showed that myocardial oxygenation was influenced by the heterogeneity of capillary spacing, a situation that was exacerbated in hypertrophic hearts with longer and more variable intercapillary distances. In addition, they found minimal differences in oxygen profiles calculated with the Krogh model geometry as compared to a model of concentric diffusion.

Roughton (1952) developed equations for a Krogh tissue cylinder under steady and unsteady state conditions. Roughton postulated that oxygen is bound to a substance in the tissue by means of a reversible reaction. This of course represents the case in red muscle where oxygen reversibly binds with the protein myoglobin. Roughton considered several special cases, but solutions to overall equations were not obtained. In addition, Roughton's model treated only the tissue conditions, and not conditions within the capillary. Thews (1960) derived

a number of solutions for cases that were physiologically relevant. He introduced displays of substrate diffusing from capillary with an assumed oxygen profile to the tissue space with various geometries. Kety (1970) was perhaps the first to incorporate intracapillary conditions in mathematical models of oxygen supply. He proposed that the oxygen content of capillary blood would fall linearly from the arteriolar to venular end of the capillary. In combination with the nonlinear oxygen hemoglobin dissociation curve, he provided the first model that included oxygen distributions both within the capillary and the Krogh tissue cylinder.

Rakusan (1971b) described changes in myocardial PO_2 in relation to various oxygen determinants based upon the Krogh-Erlang equation. Using graphical analysis, he considered the individual effects of factors such as oxygen consumption, myocardial blood flow, capillary radius, diffusion distance, and oxygen content within the capillaries on PO_2 at the periphery of the tissue cylinder. The most important factor in affecting PO_2 was the myocardial oxygen consumption. Myocardial blood flow and arterial oxygen content were also important variables in influencing myocardial PO_2. Rakusan found that the cylinder radius was an important factor, only in cases where it was increased, as in cardiac hypertrophy. In his monograph, he stressed the importance of accurate morphometric data in the calculations of myocardial PO_2.

Additional features to the Krogh cylinder model were added by Opitz and Schneider (1950) in a study of oxygen supply to the brain. In this model, the

authors related the anatomy of the microcirculation to the oxygen metabolism of brain nerve cells. Their experiments led to the inclusion of additional terms in the Krogh cylinder equations that included axial diffusion in addition to the previously considered radial diffusion pattern. Detailed solutions to these equations were then obtained by Thews (1960), who further incorporated oxygen gradients in the capillary in addition to the tissue cylinder. Blum (1960) incorporated a semipermeable capillary wall, and considered a constant, linear, and nonlinear (Michaelis-Menten) metabolic rate in the tissue space. Unfortunately, they did not consider a bound substrate in the capillary blood, and thus the results would not apply to gases such as oxygen and carbon dioxide.

Grunewald and Sowa (1977) used digital simulation of three dimensional diffusion patterns to characterize the oxygen profiles within tissue volumes that were supplied by four parallel capillaries. PO_2 histograms were generated under various conditions and compared with histograms derived with tissue electrodes in human skeletal muscles. The highest correlation between theoretical and experimental data was obtained when different microcirculatory units were weight-averaged with a certain proportionality constant. This model however, representing the tissue as a combination of different microcirculatory units, is not consistent with no-flux boundary conditions that were imposed on the lateral boundaries of each unit. To the contrary, it has been shown that different microcirculatory units placed next to each other may exchange significant amounts

of oxygen (Popel, 1982), and the same author developed an analytical solution to quantitate diffusional interactions between different capillary layers of varying flow velocity, inlet PO_2 and O_2 binding capacities (Popel, 1980a). This model is also however based upon a capillary geometry of long, straight capillaries running parallel to one another.

Wieringa et al. (1982) simulated a three dimensional network of straight, parallel capillaries arranged in a hexagonal pattern with randomly placed interconnections between neighboring capillaries. In this model, the locations of arteriolar inflows and venular outflows were randomly generated and the ratio of concurrent to countercurrent flow was 1.15. Eight different network situations were simulated, by varying the number and flow distribution of arterial sources, and the flow through individual capillaries was calculated for each situation. These authors' calculations suggested the presence of a large heterogeneity in the capillary flow rate of adjacent capillaries, suggesting that the anatomy of the capillary network may give rise to areas of profound underperfusion in steady state conditions.

Groebe (1990) developed a model of combined convective and diffusive oxygen transport that allowed for the determination of PO_2 profiles in a cuboid region of tissue with arbitrary microvascular geometries and flows. The model incorporated 3-dimensional calculations, arbitrary input geometry, arbitrary red blood cell velocity and distribution and red blood cell O_2 desaturation along the

capillary. The model was applied to the situation typical of heavily working dog gracilis muscle. The size of the tissue region considered was 500 by 80 by 80 μm, consisting of a central muscle fiber surrounded by 4 (rows of) capillaries. The model elegantly staggered the points of 2 out of 4 capillary origins. Calculations from this model indicated very steep perivascular (near the capillary wall) PO_2 gradients. Further into the muscle fiber, there are low and homogeneous PO_2 values (5 mmHg), with no appreciable PO_2 gradient.

The results of this model appear to be in good agreement to experimental findings obtained by cryospectroscopic measurements of myoglobin saturation in working dog gracilis (Gayeski and Honig, 1986; Gayeski and Honig, 1988) and in the epimyocardium of various mammals (Gayeski and Honig, 1991). In the latter case, results were extremely uniform amongst the different species (dog, cat, rabbit, ferret and rat) despite the tremendous variation in cardiac work/minute, cardiac output, and arterial O_2 content. The median value of PO_2 in equilibrium with myoglobin ranged from 4.3 to 7.0 mmHg. These data, both experimental and theoretical, challenge a wealth of data obtained from direct measurements with both needle and surface PO_2 electrodes (for review see Schuchhardt, 1985) that show a wide range of PO_2 values with values generally an order of magnitude greater than those obtained by Honig's group. Turek et al. (1991) have recently computed histograms of myocardial PO_2 under a variety of conditions, including variations in capillary blood flow, heterogeneity of capillary spacing and

myoglobin-facilitated oxygen diffusion, with and without capillary barrier. With a capillary barrier, tissue PO_2 profiles indicated rather low values that were independent of the above listed conditions. Without a capillary barrier, the effect of the geometrical and functional conditions was considerable. These results are of particular importance in that they clearly indicate that PO_2 profiles may resemble those measured experimentally by PO_2 electrodes or by myoglobin cryospectroscopy, depending upon the choice of input data. These authors accordingly stress the importance of realistic geometrical and functional data for the modeling of myocardial oxygenation.

Certainly the increase in the availability of main-frame computers in the 1960's, and the power of micro-computers in the last decade has allowed investigators to readily obtain data from multi-factorial problems, and change various modelling parameters in an interactive fashion. These modelling parameters include hemoglobin-oxygen kinetics, the role of hemoglobin and myoglobin in facilitation of oxygen diffusion, and morphometric and hemodynamic heterogeneities. Other ideas have called for a reassessment of the Krogh model, most commonly mentioned are intracapillary resistance to oxygen transport and the role of myoglobin facilitated oxygen transport (Honig et al. 1984). Yet despite these theoretical advancements in the theory of diffusion from capillary to tissue, basic entry data regarding the geometry of the microcirculation in various tissues is essential for a better understanding of oxygen transport. In the

heart muscle, these entry data are still not sufficiently available. In addition, most mathematical models of oxygen supply assume a very limited geometry, for example 2-3 straight, unbranched capillaries in computer simulations; which limits the relevance of the output to very specific situations. For the advancement of models of oxygen supply, future models of oxygen supply must incorporate more realistic data regarding the structure and heterogeneity of morphometric data that serve as input parameters in these models.

MORPHOMETRIC METHODS FOR THE ANALYSIS OF CAPILLARY GEOMETRY

To overcome many of the technical difficulties in viewing surface vessels of the beating heart in vivo, the microcirculation may be studied with various post mortem techniques. Perhaps the first method used to identify the vasculature was from thick cleared sections of material in which capillaries have been injected with a dye suspension (Wearn, 1928). Another common method used to visualize capillaries involves the histochemical impregnation of all anatomically present capillaries (Hort and Hort, 1958). Many reactions have been employed such as carbonic anhydrase, Periodic acid-Schiff, and alkaline phosphatase activity. In addition, capillaries may be examined from histological sections based upon counts of endothelial cell nuclei (Linzbach, 1947). The latter method is subject to considerable error, as endothelial cell nuclei may be difficult to distinguish from

the nuclei of connective tissue. Further, the number of nuclei does not provide a direct count of the number of capillaries. Another method is to directly visualize red blood cells within the microcirculation. This method is also subject to considerable error, as red cell density is affected by flow velocity, network geometry and capillary hematocrit. Most recently, a variety of immuno-histochemical techniques that label structural glycoproteins found in epithelial basement membranes, such as fibronectin and laminin have been used to identify capillaries (e.g. Borsi et al. 1987).

As capillaries are generally anisotropic (preferential orientation) structures, the angle of tissue sectioning becomes important in subsequent assessments of capillary geometry. The concept of a planar intercept with zero thickness is an ideal view of the tissue section. In practice tissue sections range from 1μm to perhaps 60-70μm. As the section thickness increases, structures of interest may only be partly captured, or conversely, obscured within the section.

The ideal situation would be to obtain mathematically based three-dimensional (3-D) reconstructions of microvascular networks. Unfortunately, reconstruction methods based upon tissue or optical sectioning are not yet reliably available at the level of the microvessels. In an effort to gain some information regarding the three dimensional geometry of the capillary bed, microvascular corrosion casts have been made and examined with scanning electron microscopy. This technique involved the injection of a compound into the microvascular bed

under study. Upon hardening, the compound becomes rigid, preserving the structural integrity of the microcirculation. The tissue component is digested away, leaving only the microvascular cast which may be examined with a scanning electron microscope. Descriptions of microvessels in the myocardium derived from injected materials have been reported in the literature (Bassingthwaighte et al. 1974; Grayson et al. 1974; Phillips et al. 1979; Potter and Groom, 1983). This method renders a vista into the 3-D organization of microvessels, but does not provide a suitable basis for the quantitative description of the microcirculation. Most studies therefore still rely upon thin 2-D sections cut perpendicular (for cross sections) or parallel (for longitudinal sections) to the axis of anisotropy for studies of capillary geometry. From these sections, information regarding the extent and distribution of capillaries within a given tissue plane may be determined.

CROSS SECTIONS

Many methods for assessing tissue capillarity from cross sections have been advanced in recent years. The central theme to these methods has generally involved the measurement of capillary density, i.e. the number of capillaries per unit of cross sectional area. This measurement is the primary descriptor of the relative contributions of vascular and tissue components in the plane. Notwithstanding this average measurement, tissue supply of oxygen has been

shown to be compromised as the heterogeneity of capillary spacing increases (Turek and Rakusan, 1981); and hence modern approaches have taken into account the spatial relationships amongst neighbouring capillaries.

Capillary Density

$$N_A(c,f)=N(c)/a(t) \tag{3}$$

Perhaps the most commonly reported index of capillary supply in the literature is the average capillary density [$N_A(c,f)$], which is expressed as the number of capillary profiles [N(c)], per unit tissue area [a(t)]. This average measurement unfortunately does not provide any information regarding the variability in capillary supply from different regions within the area from which capillary density is measured. This method, which reduces capillaries to a point pattern in two dimensional space, provides minimal error only when capillaries are straight and parallel (anisotropic) to one another. In cardiac tissue, not all capillaries will necessarily be sampled on cross section, giving rise to oblique capillary profiles. Therefore, careful selection of tissue fields that appear to be cut perpendicular to the capillary axis of anisotropy is imperative. Variations in the extent of shrinkage with fixation or the amount of interstitial space may introduce significant errors to measurements of capillary density.

Capillary to Fiber Ratio (C:F)

$$N_N(c,f) = N(c) \div N(f) \quad (4)$$

Another average value commonly reported as an index of conditions for oxygen supply is the capillary-to-fiber ratio [N_N (c,f)], which is expressed as the number of capillaries [N(c)] to the number of muscle fibers [N(f)]. This index is a useful estimate for comparing different muscles where the absolute size of these two components may differ. However, the C:F ratio is sensitive to changes in fiber area. An example of its use is when reporting adaptive changes in tissue when there is little or no fiber hypertrophy or hyperplasia. In this case, an increase in the C:F ratio would represent a growth of new capillaries. As with capillary density, use of the capillary to fiber ratio tends to obscure tissue heterogeneities, for example the maximal O_2 diffusion distance, which may be critical in oxygen supply and hence tissue viability.

Intercapillary Distance (ICD)

This value is derived from the straight line measurement from the centre of one capillary to another from either cross or longitudinal sections. The shorter the intercapillary distance, the more advantageous are the geometric conditions for

oxygen supply, due to shorter diffusion distances. One half of the intercapillary distance may be taken as the radius of the Krogh cylinder, although this value may not be symmetric when the distance from a reference capillary to several neighbors is not uniform. Regular geometric arrangements that are most often adopted include equilateral triangles, square-array and hexagons, with capillaries located at the apices. Equations are available to determine R, half the mean intercapillary distance depending upon the geometrical array, where ICD is in microns and CD in mm^{-2}:

$$R = 1000 \cdot \frac{\sqrt[4]{3}}{\sqrt{6 \cdot CD}} \quad \text{Triangles} \qquad (5)$$

$$R = \frac{1000}{2\sqrt{CD}} \quad \text{Squares} \qquad (6)$$

$$R = \frac{1000}{3\sqrt{3} \cdot CD} \quad \text{Hexagons} \qquad (7)$$

Method of Concentric Circles

The method of concentric circles is an efficient procedure for obtaining a distribution of capillary-tissue diffusion distances. The sampling method (Loats et al. 1978) uses a template composed of a series of concentric circles with increasing radii, the center of which is overlaid on top of intersection points in a square array. For each point, the circle with the largest radius that doesn't capture any capillaries is recorded. This approach provides an unbiased method of determining the proportion of tissue per given distance from the nearest capillary. Using iterative fitting, Turek and Rakusan (1981) derived the average Krogh cylinder radius from this method and evaluated the heterogeneity of capillary spacing and effect on tissue oxygenation in normal and hypertrophic rat heart. This method has also been shown to be effective in distinguishing between ordered, random, and clustered capillary grouping patterns (Kayar et al. 1982b).

Closest Individual Method

As in the concentric circles method, the closest individual method relies upon nearest neighbor statistics to evaluate the spatial distribution of capillary represented as points in the tissue plane. The closest individual method is derived from ecological survey procedures (Clark and Evans, 1954) where investigators were interested in obtaining distributions of trees and vegetation in field observations. Kayar et al. (1982a) adopted this method to obtain the distribution

of tissue sampling points to the nearest capillary. The tissue sampling points were obtained from a square grid overlay.

Triangulation Method

By drawing straight line segments between neighboring capillaries, intercapillary distance (ICD) is given by the length of these connecting segments. When this procedure is extended over a set of capillaries defined in the plane, the method results in a triangulation pattern, previously referred to as a Delaunay Triangulation (Ripley, 1981). The iterative process is unequivocal, using the convention that no two line segments may cross. When more than one possibility exists, the shorter segment is taken. From the ICD, the area of the Krogh cylinder may be determined as a circle with radius equal to ½ICD. In both skeletal and cardiac muscles, intercapillary distances are compatible with the logarithmic-normal distribution (Renkin et al. 1981; Rakusan et al. 1986). In many areas of biological sciences, this distribution is prevalent. Unlike the normal distribution, where the distribution function is symmetric about the mean, the logarithmic normal distribution is skewed, asymmetric. In a log-normal distribution, it is not differences of equal magnitude about the mean which have an equivalent probability, but rather ratio's of equal magnitude about the mean that have equal probabilities. The index of central tendency in a log normal

distribution is the median; and dispersion is best described by the standard deviation of the log transformed ICD's.

Domain Method

The area and variability of the Krogh cylinder area may be determined in tissue fields by consorting each capillary profile within a Dirichlet cell (Ripley, 1981); a polygon that enclosed a region of tissue nearer to that capillary than any other. This method which was first applied to coronary capillaries on cross-section by Hoofd et al. (1985), partitions the tissue plane into an irregular lattice pattern. The area of individual polygonal tissue regions surrounding capillary profiles, the capillary domain, is taken as the respective tissue supply region. From the domain area, the equivalent radius of the Krogh cylinder with the same area may be calculated. The distribution of these radii is log-normal, the variability being characterized by the logarithmic standard deviation (SDlog). In this manner, SDlog, the index of heterogeneity of capillary spacing may be determined. As the local capillary environment, more than the average tissue value for capillarity, describes better the range of geometrical conditions for oxygen transport, the heterogeneity of domain radii (SDlog) is an important determinant of geometrical conditions for oxygen supply.

LONGITUDINAL SECTIONS

In longitudinal tissue sections, one obvious shortfall is that capillary pathways may not be entirely captured within the thickness of the section. There is generally a trade-off when determining the best section thickness. Sections that are too thin will not have substantial degree of vascular contiguity, which will make following capillary pathways very difficult. On the other hand, sections that are too thick create a problem of focusing at different depths within the tissue and the possibility of missing capillaries at deeper levels within the section.

Capillary Length

> "knowledge of capillary length and it's frequency distribution is essential in modelling O_2 transport and indicator dilution data"
> Honig et al., 1977.

Information regarding capillary lengths in the heart muscle have generally been descriptive and not based upon systematic measurements. This is due to the exigency of developing appropriate facilities for viewing surface vessels of a beating heart in situ; or in the development of morphometric techniques that accurately demarcate capillaries from histological sections. Models of oxygen supply based upon the Krogh cylinder geometry assume that capillaries are indefinitely long, straight and unbranched. In these models, capillary length is

equated with the muscle fiber length, without any information regarding arterio-venous pathlengths, capillary tortuosity or branching pattern. Given the technical difficulties that presently exist in directly measuring capillary length, various 3-D derivatives of capillary-tissue supply may be calculated using stereological methods.

3-D DERIVATIVES

Capillary Length Density (J_v)

Capillary length density (Jv), the capillary length per volume of muscle fibers, is related to numerical density from transverse sections (Na), but also includes a correction factor, c(K,θ) based upon capillary orientation:

$$Jv = c(K,\theta) \cdot Na(\theta) \qquad (8)$$

Under conditions of perfect anisotropy, Jv=Na. For a completely random orientation (isotropy) Jv=2Na. In all known capillary beds, values for K will fall between $+\infty > K > 0$. A simplified method of estimating the coefficient c(K,0) and K using the ratio of capillary counts from cross sections (Na(0)) and longitudinal sections (Na(π/2)) has been suggested (Mathieu et al. 1983).

Knowing c(K,0), an estimate of the capillary length density may be obtained from equation 8, where $\theta = 0$. Given J_v, and knowing capillary circumference (b_c),

and cross-sectional area (a_c), capillary surface (S_v),and volume (V_v) densities may be calculated:

Surface Density (S_v)

$$S_v = b_c \cdot J_v \qquad (9)$$

Capillary surface density is given by the product of average capillary circumference (b_c) and capillary length density (J_v). First suggested for cardiac muscle by Roberts and Wearn (1941), the capillary surface area is expressed per unit volume of tissue, which is an estimate of the total surface area available for gas exchange, and index of blood-tissue exchange potential. The authors calculated the fiber volume from the number and diameter of muscle cells (assuming a cylindrical geometry). The capillary surface area was expressed for a given capillary diameter. The most apparent difficulty in using this method is that input values for cell and capillary diameter, if not representative, will produce exponential error terms when extended to the third dimension.

Volume (V_v) Density

$$V_v = a_c \cdot J_v \qquad (10)$$

Capillary volume density, which is given by the product of average capillary cross-sectional area (a_c) and capillary length density (J_v), provides an index of the relative volumes of blood and tissue, an index of the maximal convective delivery of oxygen and substrates to the tissue.

NETWORK ANALYSIS APPROACH

In 1874 Galton and Watson, [as cited by Harris (1989)] in treating the problem of the extinction of family names, employed probability theory to study the effects of chance upon families or populations. Their mathematical model served as the basis for future studies of branching processes in many different biological disciplines, and recently in studies of the branching phenomenon of microvascular networks. These approaches appear to be well suited to dichotomously branching networks as in the pulmonary airways or larger arterial vessels. However, in highly anastomosing networks, such as the coronary capillary bed, more appropriate, tissue specific methods must be defined. Nonetheless, as more is understood about network models, this approach will become effective in reducing complex network geometry to a distribution of branch points (nodes) of various generation in space that may be mathematically treated for such factors as pressure, flow, and red cell streaming.

FRACTAL MODELS OF MICROVASCULAR NETWORKS

Due to the tremendous heterogeneity in the geometry of biological structures, most quantitative methods describe variances only as a function of a given unit size. As the unit size is reduced, the observed heterogeneity increases. It has been shown that a fractal relationship provides a precise fit to data regarding microvascular networks over a large range of unit sizes. This approach seems to be extremely powerful in describing the underlying heterogeneity of biological data, and has been introduced to microcirculation research (e.g. Bassingthwaighte et al. 1989; King et al. 1990). A possible extension of the results presented in this dissertation may be to incorporate fractal models to describe, for example, the heterogeneity of capillary branching patterns.

CAPILLARIES IN SKELETAL MUSCLE

As compared to the heart muscle, capillaries in skeletal muscle have been studied more extensively. Skeletal muscle is more accessible, not subject to intrinsic contractions, and easier to visualize than cardiac muscle. In addition, the microvasculature of skeletal muscle has a generally more uniform structure than other tissues (Wiedeman, 1984). Capillaries tend to run along the muscle fiber axis, which supports the simple Krogh geometry (Krogh, 1922). Although Krogh alluded to the presence of intercapillary anastomoses, and the heterogeneity of capillary flow pattern (Krogh, 1922), theoretical models of such heterogeneities

were developed only much later. The underlying assumption that there was no diffusional interaction between individual capillaries has certainly been challenged (Popel, 1980b) due to various heterogeneities in capillary geometry (Hammersen, 1968; Plyley et al. 1976), capillary blood flow (Popel, 1980a; Sarelius, 1990) and the oxygen consumption rate within skeletal muscle (Tyml, 1986).

Basic data regarding capillary supply parameters of various skeletal muscles as determined from sections cut perpendicular to the fiber axis are quite extensive. However, data in terms of capillary length parameters as determined from longitudinal sections are less comprehensive. The study of capillaries in tissue is physiologically relevant if one considers the number of capillaries arising from a common arteriole, and therefore forming a unit. Capillary units of repeating geometry have been proposed as functional building blocks of the peripheral circulation (e.g. Chambers and Zweifach, 1944; Eriksson and Myrhage, 1972; Frasher and Wayland, 1972; Gore and Bohlen, 1977; Weibel, 1984; Skalak and Schmid-Schonbein, 1986; Lund et al. 1987).

Honig et al. (1977) measured capillary lengths, segment lengths and the number of anastomoses per capillary length in the rat gracilis at rest and following phasic contraction. These surface vessels were measured by in vivo microscopy, and only capillaries containing moving red blood cells were included in the dataset. Mean capillary segment length (the distance between two successive

anastomoses) was 409 μm at rest and 390 μm after contraction. Mean capillary pathlength was 1154 μm, not including anastomoses.

Lund et al. (1987) employed epiillumination in concert with fluorescein-labelled albumin to determine the three dimensional geometry and flow direction of the capillary bed in hamster tibialis anterior. Capillaries were traced and flow directions noted on acetate overlays to provide three dimensional reconstructions of arterio-venous capillary units. These authors noted that groups of capillaries (12-20) generated from a given arteriole, travelled in parallel, and drained into the same collecting venule. This capillary unit was approximately 800-900 μm long, 200 μm wide and 100 μm in depth. Flow was essentially concurrent within a given capillary unit. Arterio-venous capillary lengths averaged 805 $\pm$ 330 μm ($X \pm SD$). Capillary segment length was 227 $\pm$ 201 μm. These authors proposed that this group of capillaries derived from a common source and terminating in a common venule may served as a functional entity in the regulation of blood flow to skeletal muscle.

Potter and coworkers (1989) measured capillary length parameters using epiilumination in three different muscles of the rat hindlimb (medial gastrocnemius, gracilis and soleus) following perfusion with aquablack (a colloid carbon suspension). Capillary pathlengths were not significantly different amongst these muscles (pooled mean = 588 μm), and showed good agreement with values from rat cremaster (615 μm, (Smaje et al. 1970)), rat extensor hallicus proprius

(535 μm, (Myrhage and Hudlicka, 1976)), and hamster tibialis anterior (805 μm, (Lund et al. 1987)). These values are however much less than the values reported for rat gracilis (1012 μm, (Honig et al. 1977)). Potter and coworkers found capillary segment length to be 204 μm (pooled mean) in these three muscles, which is very similar to values obtained from rat cremaster (210 μm, (Smaje et al. 1970)), cat tenuissimus (200 μm, (Eriksson and Myrhage, 1972)), hamster tibialis anterior (227 μm, (Lund et al. 1987)) and rat soleus (205 μm, (Dawson et al. 1987)). These values, again are smaller by a factor of two than those reported for rat gracilis by Honig et al. (1977).

The diameter of the undeformed erythrocyte is generally equal to or greater than the capillary diameter, which varies between 4-8 μm. Erythrocytes generally travel in single file, leaving only small plasma gaps between the cell and the endothelium. The red blood cells (rbc's) may become quite deformed from their normal biconcave disk shape. The typical Reynolds number in the capillaries is generally less than 0.01 due to the small vessel diameters and low flow velocities. Accordingly, viscous forces dominate flow, and vessel lengths and diameters are the main factors affecting pressure flow distributions in microvascular beds. Capillary diameter, which is also necessary for computations of PO_2 with the Krogh-Erlang equation, may be measured in vivo, or from histological sections. Measurements however, are affected by vasculature and tissue pressures, and the

presence of red cell within the capillaries. The distribution of capillary lengths in a given tissue are generally fixed, unless tissue remodeling occurs.

Ellis and coworkers (1983) developed a computer method to measure capillary diameters in vivo based upon temporal fluctuations in light intensity across the capillary wall due to flow of erythrocytes. This method relied upon the fact that a red cell, or group of red cells travelling side by side, adequately delineated the capillary wall, without the presence of a cell-free plasma layer. An adequate red cell flux would likely be necessary for reliable measurements with this method. The same group (Safranyos et al. 1983) measured capillary diameter in the frog sartorius. This method was then employed along a fixed length of capillary (80μm) to measure red cell density (Ellis et al. 1984). The number of rbc's in this 80 μm length ranged from 0-5. These authors noted significant temporal variability in the lineal density within the same capillary. The presence or absence of red cells at a given time may not indicate whether the capillary is perfused. In light of these data, the authors expressed concern in using changes in the proportion of 'perfused' capillaries as an index of capillary recruitment. At capillary bifurcations the distribution of rbc's between daughter branches is influenced by the ratio of flow rates and the position of individual cells with respect to the streamlines (Schmid-Schonbein et al. 1980). Capillary geometry with respect to bifurcations may then influence rbc lineal density. Given this heterogeneity of rbc distributions in microvasculature, even capillaries originating

from the same terminal arteriole cannot be considered as spatially and temporally equivalent sources of oxygen supply (Groom et al. 1986).

Heterogeneities in microvascular flow may be a function of tissue metabolism, regulated at the arteriolar level (Cousineau et al. 1983); or independent of the degree of metabolism, heterogeneity may be a function of the overall flow rate (Tyml and Mikulash, 1988). In the latter study, the authors considered flow heterogeneity at different inflow rates under constant electrical stimulation of the frog sartorius. These authors showed that the heterogeneity of flow velocity was inversely related to the mean velocity i.e. a flow dependent regulation of flow heterogeneity operating at the capillary level.

Ellsworth et al. (1988) made in vivo measurements of oxygen saturation along the length of individual capillaries of the hamster cheek-pouch retractor muscle using microspectrophotometry. The data were analyzed by a model that considered a block of tissue penetrated by several parallel capillaries. These capillaries had either a uniform or non-uniform distribution in length. Measurement of hemoglobin saturation (SO_2) at the arteriolar end of the capillary were used as boundary conditions, and the predicted SO_2 values at the venular end were compared with experimental data. Under resting conditions, it was observed, that diffusion shunting was so pronounced that the effect of heterogeneities at the arteriolar end were not transduced towards the venular end in the model with uniform capillary length. This was in contrast to the

experimental findings that indicated an increased SO_2 heterogeneity towards the venular end of capillaries. The variability in capillary pathlength was noted as an important factor in measurement of hemoglobin saturation at the level of individual capillaries. These authors stated that more realistic models of oxygen supply should therefore include data regarding the distribution of capillary pathlength.

The role of myoglobin in skeletal muscle of binding with oxygen and releasing it when supply is limiting has been well established. The role of myoglobin in the Krogh cylinder model has been analytically considered under conditions of ischemia (Artigue and Hyman, 1976). The role of myoglobin in facilitating the diffusion of oxygen has been of central interest in mathematical models of recent years (Covell and Jacquez, 1987; Federspiel, 1986; Fletcher, 1980). For reviews see Kreuzer et al. (1991) and Honig et al. (1991)

Recently, Pittman's group (Bennett et al. 1991), considered several statistical tests to estimate the spatial pattern of capillaries in the sartorius, retractor, and soleus muscles of the hamster. These authors generated distributions of: A. distances measured from all capillary pairs, B. distances between first nearest neighbor capillaries and C. distances from sample points in the tissue to the nearest capillary. These data were used to determine if the distribution of capillary profiles in the plane was random, i.e., the null hypothesis of an underlying Poisson process. They demonstrated that capillaries were not

randomly distributed, but rather spaced in a regular pattern in some fields of the sartorius and retractor, and in all fields of the soleus. Results were similar with all three morphometric methods, but method B was found to be most sensitive for detecting regular capillary distributions. The regular capillary distribution in these striated muscles would minimize the tissue fraction located at remote distance from vascular sites, providing advantageous geometrical conditions for oxygen supply.

CAPILLARIES IN THE HEART MUSCLE

This section serves to highlight the variety of approaches and/or interventions that have been used to quantitatively assess capillaries in the heart muscle. It would be ineffectual to describe the profusion of data from tissue sections cut transverse to the principle axis of capillary orientation; therefore, only a brief overview of some prominent works are presented here. What is comprehensive, however, are the studies listed in this section regarding measurements of capillary length in the heart muscle. These data as obtained from longitudinal tissue sections are less abundant as a result of considerable technical restraints, but are of particular relevance to the data presented in this dissertation. Citations of studies regarding capillaries in the heart muscle specific to cardiac contraction, normal postnatal growth, pressure overload hypertrophy, and volume overload hypertrophy are listed in Chapters 1, 2, 3, and 4, respectively.

Along with the brain, the heart is the other critical organ for which a continuous supply of oxygen is essential for normal function, and hence survival of the organism. The oxygen supply of the heart muscle depends upon the degree of capillary supply. An increase in the diffusion distance decreases the myocardial PO_2, which is exacerbated in pathological conditions where the increase in diffusion distance may be accompanied by increases in oxygen consumption and/or a reduction in capillary flow. In such cases, an increase in diffusion distance may lead to hypoxic episodes in the heart muscle (Rakusan, 1971b).

Capillaries may be quantitatively studied directly in vivo or from the examination of thin histological sections. Both of these methods, however, are subject to some technical drawbacks. In vivo studies of coronary capillaries are firstly limited to the most superficial layers of the heart. These measurements must be made in an open chested animal preparation, which is of course not a normal physiological situation. In addition, the difficulty of developing appropriate facilities for viewing surface vessels of the beating heart make recordings often technically inadequate.

Wearn (1928) was the first to employ a suitable method for visualizing the coronary microcirculation. He injected a suspension of India ink in gelatine via the aorta into the coronary vessels of perfused, isolated and beating hearts. Shipley et. al (1937) considered capillary supply in normal and hypertrophied rabbit hearts at various ages. In normal hearts, the average fiber cross sectional

area increased seven-fold from birth to maturity. Over this period, capillary density remained essentially the same, suggesting appreciable growth of new capillaries. This observation was confirmed by a reduction in the fiber-to-capillary ratio from over 5 in the newborn, to less than 1 in the mature heart. In hypertrophied hearts, the average fiber cross sectional areawas greater than in normal hearts. Over this period, there was a reduction in capillary density, and the fiber-to-capillary ratio remained the same, suggesting that growth of new capillaries did not occur. These authors concluded that the growth of new capillaries in normal hearts, which was commensurate with fiber hypertrophy, was absent in hypertrophied hearts resulting in a decreased capillary supply in cardiac hypertrophy. These authors further speculated that the reduction in capillary supply in hypertrophied hearts may hinder gas and substrate exchange, and hence affect cardiac function.

Roberts and Wearn (1941) considered the capillary supply of normal and pathological human hearts of various ages. The average area of tissue supplied by each capillary was 267 μm^2, 299 μm^2, and 403 μm^2 in the hearts of normal children, normal adults, and in hypertrophy, respectively. The capillary supply was similar in normal children and normal adults, but decreased significantly in hypertrophied hearts. These authors calculated the capillary surface area per unit muscle fiber volume (cm^2/cm^3). Values were 1145, 1184, and 625 cm^{-1} in normal children, normal adults, and in hypertrophied hearts, respectively. These data

indicated that during normal growth, capillary proliferation was commensurate with myocyte hypertrophy. In contrast, during hypertrophy, capillaries were pushed further apart, and without corresponding capillary proliferation, capillary supply was diminished.

Since the studies of Wearn and coworkers, countless other groups have measured **capillary density** in the mammalian myocardium under normal and pathological conditions. These data should be considered specific to species, strain, gender, age, and region of sampling. Despite the vast number of publications, results in the literature vary tremendously. Most results for the rat left ventricle tend to vary from 2000 to over 5000 caps/mm^2. This difference has profound implications on models of oxygen transport (Rakusan, 1971a). The most obvious reasons for such variability include method of capillary visualization, failure to correct for shrinkage due to fixation, variations in the angle of orientation of the tissue block, and local heterogeneities in capillary supply.

Brown (1965) used India ink injections through the coronary arteries of isolated and perfused beating hearts to describe the morphological pattern of the terminal vascular bed in 6 different species. Brown described the arteriole as penetrating a muscle bundle at various oblique angles, and furnishing capillaries that often ran in opposite directions and drained into venules quite a distance apart. Collecting venules were formed from capillaries that converged from all directions. Brown also noted that not all of the capillaries from a given terminal

arteriole emptied into the same collecting venule. Ludwig (1971) also characterized the morphology of coronary capillaries in the rabbit myocardium following the injection of India ink. This investigator also noted that terminal arterioles approached the muscle fibers at an oblique angle, and furnished capillaries at various levels and in different directions in the tissue. There was a greater number of anastomoses between neighboring capillaries towards the venular end of the capillary network. In addition, the author stressed the fact that the microvessels arising from a given arteriole often did not empty into the venules nearest them. Similar findings have also been noted in studies based upon in vivo microscopy. Fabel (1968) investigated the microvasculature of the subendocardial and subepicardial regions of the isolated, perfused, beating rabbit heart. In this study, Fabel also described the staggered pattern of arteriolar inputs at various depths within the tissue, and further noted the presence of both concurrent and countercurrent flow direction.

Tillich et al. (1971) studied the capillary bed in the beating cat heart by transilluminating it from within the atrial cavity. These authors were unfortunately not able to look at capillaries in the ventricle, due to its thickness and greater degree of movement. Tillmans et al. (1974) transmitted light through a 20 Ga needle that was inserted underneath the superficial layer of the dog ventricle. The system was designed to keep the heart in focus during cardiac contraction. Martini and Honig (1969), as well as Henquell and Honig (1976),

measured intercapillary distances from freeze-frame photomicrographs of beating rat hearts. In both of these studies, the authors found a significant reduction in intercapillary distance and an increase in the number of perfused capillaries during hypoxic conditions. They reported that approximately 50% and 25% of the capillaries in the right and left ventricles, respectively, were not perfused at rest, which would indicate a considerable capillary reserve in the rat heart. Steinhausen et al.(1978) used epiillumination combined with video-microscopy to study the microcirculation of the epimyocardial layers of the beating rat heart under normal and hypoxic conditions. These authors inserted 5 steel needles into the outer layer of the ventricle to restrict excessive movement and injected a plasma label to improve contrast. They reported intercapillary distances between neighboring capillaries of 18.7 μm, which did not change under conditions of hypoxia. In contrast to Honig's group, these data indicated no functional capillary reserve in the rat heart.

Korecky and coworkers (1982) also measured intercapillary distances of supepicardial capillaries in the rat using freeze frame cinematography. During normoxemia, the average intercapillary distance was 19.2 μm. During hypoxemia, values were reduced to 17.9 μm, which corresponded to a capillary recruitment of approximately 15% over normoxic conditions. Rakusan and Korecky (1982) detected a moderate degree of capillary recruitment (approx. 11%) under hypoxic conditions. The degree of recruitment has been shown to be less in 24 month old

rats (Rakusan and Korecky, 1982) and in cardiac hypertrophy (Henquell et al. 1977).

Rakusan et al. (1967), employing the method of Myers and Honig (1964), measured the capacity of the coronary microvasculature during normal and pathological cardiac growth in the rabbit. These authors found that the capacity of the terminal vascular bed, measured as capillary blood content per gram of tissue, continued to increase until approximately 6 weeks of age. Beyond 6 weeks of age, the capacity decreased in a linear manner, in concordance with increases in heart mass. In hypertrophic hearts, the capacity of the terminal vascular bed, was significantly lower than in normal hearts.

Potter and Groom (1983) used corrosion casting to study the geometry of the microvasculature in cardiac and skeletal muscle. In the heart muscle, the capillaries tended to follow myocyte contours quite closely, with many capillary loops and a high degree of capillary branching. These authors were able to measure capillary diameters in this preparation, without the task of correcting for shrinkage. The casting technique, however, is not suitable to much further quantitative data regarding capillaries geometry.

Previous estimates of **capillary length** in the heart muscle are rare and have not been based upon systematic sampling methodology. Ludwig (1971) estimated distances from the arteriole to venule in rabbit heart using an India ink suspension. Mean distances were reported to be 400 μm for the subepicardial

layers, 300 μm for the intramural layers and 500 μm for the subendocardial layers. These values were reported only as approximations and the number of measurements taken were not given. From injections of dye suspensions of differing color, Toborg (1972) reported that the length of capillary paths from arteriole to venule ranged from 100 to 800 μm, with mean values of 310 μm (in 1 rat heart) and 400 μm (in 1 cat heart). The corresponding length of capillary segments was 65 μm (rat) and 110 μm (cat). Toborg further described the staggered arrangement of microvessels in the heart, with arteriolar inflows and venular outflows being located in an "asymmetric" manner.

Bassingthwaighte et al. (1974) injected a silicone elastomer into a main branch of the left coronary artery of the beating dog heart. Following clearing of the tissue with methyl salicylate, the vasculature could be visualized by reflected or transmitted light microscopy. The author's described the preponderance of different types of branching patterns as well as descriptions of capillary lengths. They described the length of individual capillaries as "indefinite" as they seemed to follow the entire muscle bundle length. In addition, the authors mention the difficulty in determining the typical pathways that a red blood cell may traverse from arteriole to venule. Functional capillary lengths were estimated from two hearts that were perfused with elastomer through the left anterior descending coronary artery while the circumflex coronary artery remained intact and blood perfused. Functional capillary lengths, the distance from the fringe of the

elastomer filled region to the nearest venule, were observed to range from 300-1200 μm; distances to the nearest arteriolar supply were up to 1000 μm or greater. Capillary segment lengths were reported to be 102 μm, following correction for shrinkage.

It has been shown that the extent and geometry of the microvascular bed are important determinants of myocardial PO_2 (Rakusan, 1987). A reduction in capillary density has been associated with a reduction in dP/dt, and ventricular pressure development in the infarcted rat heart (Olivetti et al. 1990). A reduction in capillary supply may also play a role in the reduction of cardiac function in the hypertrophied heart (Rakusan et al. 1980). Given these observations, it would be tenable that an increase in capillary supply may serve to improve myocardial PO_2 and hence cardiac function.

The mechanism of neovascularization in the heart has not been delineated. It has been shown that capillary growth in the neonatal rat heart may be inhibited by protamine sulphate (Rakusan and Turek, 1985). This finding suggests a possible role for heparin, a substance that is released from mast cells, and has been previously considered to be angiogenic (Azizkhan et al. 1980). It is notable that the proliferation of mast cells and capillaries are correlated in spatial and temporal terms in the developing and hypertrophied myocardium (Olivetti et al. 1989b; Rakusan et al. 1990). Protamine has been shown to inhibit the growth of larger resistance vessels as well as capillaries (Taylor and Folkman, 1982).

Flanagan and coworkers (1991) have recently shown that protamine sulphate administration during development of pressure overloaded cardiac hypertrophy in the lamb results in diminished capillary density, diminished maximal coronary perfusion, and increased minimal coronary vascular resistance. Their findings suggest, in agreement with others, that protamine inhibits coronary microvascular growth, which is important for supporting coronary perfusion reserve during developing cardiac hypertrophy. Heparin and heparin-binding growth factors may serve to stimulate vascular proliferation with pressure overload hypertrophy in the young. A variety of factors that modulate angiogenesis have been reported in myocardium including fibroblast growth factor and heparin-like polysacharides (e.g. Sasaki et al. 1989; Kardami and Fandrich, 1989; Casscells et al. 1990).

The effect of exercise on improving capillary supply is still controversial, but most studies report no improvement in myocardial capillarization following chronic exercise training. Certainly results of these studies would depend upon the mode, intensity, duration of the exercise regimen in addition to the species and stage of development of the experimental animal. Tomanek (1970) considered the effects of a 12 week treadmill running regimen on the coronary vasculature of young (40 days of age), adult (130 days) and old (575 days) male rats. There were no differences in myocyte diameter following training, and only the young group showed a significant increase in capillary density as compared to age-matched sedentary rats. This and other studies (e.g. Anversa et al. 1983;

Jacobs et al. 1984) suggest that the exercise induced capillary proliferation is most effectual in younger animals.

The effect of exercise on the capillary net in older animals appears to be equivocal. Anversa et al. (1982) considered the effects of a severe 7-week running regimen on the rat right ventricular microvasculature. Training resulted in significant right ventricular hypertrophy due essentially to increases in myocyte volume. Over the same period, there were significant reductions in numerical capillary density, capillary luminal area, capillary volume density. These changes led to a 14% increase in the calculated maximal diffusion distance, due to the reduced capillary density and lateral expansion of myocytes. These data indicate the lack of capillary proliferation in the face of exercise induced right ventricular hypertrophy. Rakusan et al. (1987) exposed normal and renal hypertensive rats to a chronic 6 week swimming regimen (following 4 weeks of acclimation) to consider the effect of exercise training on capillarization of the left ventricular midmyocardium and subendocardium. The experimental renal hypertension resulted in a reduction in capillary density as well as an increase in the heterogeneity of capillary spacing, when compared to control animals. The swimming protocol did not alleviate these impaired geometric conditions for oxygen supply noted in renal hypertensive rats. In addition, swimming exercise had very little effect in improving capillarization in normal rats. These studies, in addition to similar results of others (e.g. Mattfeldt et al. 1986; Thomas et al.

1990) question the results of other studies that have shown that exercise has a beneficial effect in augmenting the coronary microvasculature (e.g. Crisman et al. 1985).

In addition to the lack of a beneficial effect of exercise on the coronary microvasculature, many studies have shown that during the development of cardiac hypertrophy, coronary microvascular growth is not commensurate with the increases in myocyte volume (see Chapters 3 and 4). Tomanek and coworkers (1990) considered the effects of experimental renal hypertension, induced in middle-aged (15 months) and senescent (24 months) rats, on coronary arterioles and capillaries. Overall, capillary density was shown to be significantly reduced in renal hypertensive hearts from both age groups. This reduction in capillary density was similar in the endomyocardium and midmyocardium in the 24 month rats, but was more marked in the endomyocardium in 15 month old rats. It is notable that while left ventricular mass did not significantly increase in the hypertensive groups, myocyte cross sectional area was significantly increased in both the endomyocardium and midmyocardium. These data suggest that the reduction in capillary density in 15- and 24- month old rats, following late-onset renal hypertension, was not due to left ventricular enlargement per se, but rather represented an absolute decrease (regression) in myocardial capillarization.

In studying compensatory hypertrophy of surviving cardiac myocytes approximately 1 month after myocardial infarction, Anversa and coworkers

(1986b) have observed that in 4-month old rats, the reduction in capillary density is much less than would be expected based upon the observed degree of myocyte hypertrophy. These data suggest that appreciable capillary proliferation may be stimulated in rats of this younger age. The same group has further considered ventricular wall remodelling 1-month following ligation of the left coronary artery in 3-month old rats (Olivetti et al. 1991). In this study, the authors noted that infarct size was quite variable, and animals were accordingly divided into two groups: small infarct (average 38% reduction in total myocyte nuclei) and large infarct (average 60% reduction in total myocyte nuclei). In both infarct groups, the capillary volume fraction (%) was preserved in the surviving myocardium, due to a significant increase in capillary diameter which abrogated the reduction in capillary density. The calculated diffusion distance for oxygen was significantly longer in both infarct groups as compared to controls, being most pronounced in the large infarct group. Despite the observed adaptations to infarction, including recovery of tissue mass, ventricular dilatation, side-to-side slippage of myocytes and capillaries, infarcts of the magnitude observed lead to ventricular failure.

The same group (Anversa and Capasso, 1991) has recently shown that following the onset of ventricular failure due to 8 months of chronic renal hypertension in the rat, capillary proliferation is observed despite the reduction in the densities of coronary vessels 6-40μm in luminal diameter. Capillary density was significantly increased in both the epimyocardium and endomyocardium,

resulting in an overall decrease in the calculated diffusion distance for oxygen of approximately 15%. The authors suggested that the capillary proliferation served to alleviate the rarefaction of intermediate-sized coronary arteries, thus serving to maintain (or improve) the geometrical conditions for the diffusion of oxygen.

It is evident that the stimulus for capillary proliferation is dependent upon many different factors, including the age of the animal, and the nature, severity and time-course of the imposed stress. There is evidence that the angiogenic stimulus may arise from mechanical factors related to changes in local blood flow. For example, the growth of new capillaries has been observed in normal hearts following long term administration of coronary vasodilators such as dipyridamole (Ljungqvist et al. 1984), ethanol (Mall et al. 1980) and adenosine (Ziada et al. 1984), all of which increase coronary blood flow. Turek and colleagues (1987) demonstrated that chronic treatment with nifedipine slowed the reduction in coronary capillary supply in spontaneously hypertensive rats. It appears possible that an increase in coronary perfusion may act as a stimulus for capillary growth.

Observations have been made of exercise-induced bradycardia in association with higher capillary density in active animals (e.g. wild rat) when compared to sedentary animals of similar species (laboratory rat), (Poupa et al. 1970). From these observations, a series experiments have demonstrated that chronic bradycardial pacing increases capillary density and maximal work output in the rabbit heart. Wright and Hudlicka (1981) introduced chronic bradycardial pacing

to normal rabbit hearts at about 50% of normal frequency for a period of 4 weeks. Capillary density was increased by 70% together with an increased coronary flow per beat (Hudlicka et al. 1989). Accordingly, maximal cardiac work achieved following catecholamine challenge was also increased in hearts previously paced. This approach was extended to rabbit hearts made hypertrophic following experimental lesioning of the aortic valve (Wright et al. 1989). In bradycardially paced hypertrophic hearts, capillary density was significantly increased as compared to non-paced hypertrophic hearts. Hypertrophy alone significantly reduced maximal cardiac work. Cardiac pacing of these hypertrophic hearts was shown to return maximal cardiac work levels to normal, thus reversing the depressed cardiac performance due to aortic lesioning. It remains to be seen if the beneficial effects of bradycardial pacing on capillary supply, coronary flow, and cardiac function in rabbits may be of some therapeutic value in humans.

Stereological methods have been applied to characterize the growth pattern of microvessels during cardiac hypertrophy in the rat (Mall et al. 1990; Mall and Mattfeldt, 1990). These authors considered models of cardiac hypertrophy due to 18 weeks of mild physical training (Mattfeldt et al. 1985a), 8 weeks of renovascular hypertension (Mall et al. 1987) and 3 weeks thyroxin application (Mattfeldt et al. 1989), in addition to normal physiologic growth from 5 to 52 weeks of age (Mattfeldt and Mall, 1984). Using measurements of the 2 and 3 dimensional capillary-to-fiber ratios and capillary length density (J_v), these authors

were able to estimate the pattern of capillary growth. The 2 and 3 dimensional capillary-to-fiber ratio's were significantly increased in all of the above mentioned cases except hypertrophy due to renovascular hypertension. These authors concluded that the growth of new capillaries parallel to the axis of anisotropy compensated completely for the increased myocyte cross sectional area (MCSA) after exercise and thyroxin training, and compensated partially for the increased MCSA during normal growth. In contrast, renovascular hypertension induced cardiac hypertrophy was not associated with a proliferation of capillaries parallel to the axis of anisotropy, resulting in a marked reduction in capillary supply.

There is certainly a plethora of information regarding capillaries in the heart muscle that have been collected under a tremendous variety of conditions. Many of these data are not reconcilable, in that they are derived from different animal species, by very different methods of tissue preparation and capillary visualization, and from different regions of the heart muscle. All of these factors make comparisons of data from different laboratories very difficult if not impossible. What is particularly striking is the paucity of data regarding capillary length in the mammalian myocardium. This is generally due to difficulties in developing facilities for viewing surface vessels of a beating heart in situ; or in the development of morphometric techniques that accurately demarcate capillaries from histological sections. The differential staining methodology employed in this dissertation makes it possible, for the first time, to make direct measurements of

coronary capillaries from systematically longitudinal sections of capillary pathways from terminal arteriole to collecting venule.

DIFFERENTIAL STAINING METHODOLOGY

Despite the method used to visualize capillaries (histological or injection with an opaque substance), difficulties still arise in applying reliable standards for the distinction of terminal arterioles, capillaries and collecting venules. Most researchers rely upon tissue cross sections to visualize the smooth muscle layer that is present in arterioles, as the method of differentiation. Others have simply chosen to classify these vessels on the basis of their respective diameter, i.e. all vessels less than 10-20 μm are considered to be capillaries. This limitation may give rise to considerable difficulty in obtaining reliable data specific to capillary geometry.

The original observation by Lojda (1979) that capillaries had a non-uniform distribution of enzymes in the endothelium, which served to distinguish arteriolar and venular capillary regions clearly served as a impetus for the work in this dissertation. The constituents of the incubating media and technical details of these methods are listed in Appendix 1. Briefly, tissue sections were prefixed in a mixture of chloroform and acetone (1:1). The sections were then transferred to a solution sensitive to Dipeptidyl Peptidase IV (DPP IV) in the capillary endothelium for 100 minutes. This treatment stained the venous portion of

capillaries red. Next, the sections were transferred to a solution sensitive to Alkaline Phosphatase (AP) for 25 minutes. This treatment stained the arterial portion of capillaries blue. The transitional zone along the capillary length that demonstrated both AP and DPP IV activity stained a purple color. For the purpose of consistency, this region along the capillary length (approx. 50 μm) was grouped with arteriolar capillaries. Stained tissue sections were available for detailed morphometry. This technique has many advantages, one being that it provides information at specific levels of the capillary bed that were previously not available. We have since employed this method for the study of capillary geometry during normal and pathological growth of the myocardium. Results were derived from both cross and longitudinal sections and classified as a function of Arteriolar (AC) and venular (VC) capillary regions. To the best of our knowledge, we were the first to apply this method to the quantitative analysis of coronary capillary geometry.

It is of interest to note that recent reports have cast doubt on the use of alkaline phosphatase (AP) alone, as a marker of all anatomically present capillaries. For example, Gobel et al. (1990) studied capillary perfusion in 10 different areas of the rat brain. The total number of capillaries was determined by immunohistochemical methods that labelled the capillary wall constituent fibronectin as well as the histochemical AP method. These authors noted that the AP method yielded significantly lower (approx. 30%) capillary counts than the

fibronectin method. This finding, if reproducible, would certainly limit the use of alkaline phosphatase alone as a quantitative marker of cerebral capillaries. Similar findings have also been reported in the canine diaphragm (Reid et al. 1982). Our own data from the rat heart indicate that when AP is used in concert with DPP IV, the former stains approximately 70% of the capillary network (see Table 1). When sections were stained only with AP, approximately 90% of the network is visualized, indicating that there is a considerable overlap in the distribution of these two enzymes along the capillary path from arteriole to venule.

PILOT STUDIES

CAPILLARY CLUSTERING BY HISTOCHEMICAL TYPE

After the introduction of the differential staining methodology to the lab (initial experiments conducted mainly by Mrs. Ching-Ju Kuo), the first endeavour was to develop a strategy to take advantage of this method for the quantification of myocardial capillarization. From the first few hearts, sections cut perpendicular to the axis of anisotropy served to represent capillaries as (AC, blue; VC, red) points arbitrarily distributed in two dimensional space. No pattern was immediately visible. Upon further examination, particularly at higher magnification, it began to emerge, that a given capillary tended to be associated with other capillaries of the same histochemical type. To further examine this

hypothesis, we employed a statistical test, sensitive to departures from a random distribution in the tissue plane. The test criterion was based upon the number of adjacent capillaries of differing histochemical type (AC-VC), which serves as an index of capillary grouping. Most recently this test has been used for the detection of type-grouping in muscle fiber patterns (Venema, 1988).

Ten male rats (Sprague-Dawley; 250-300g) were used in this pilot study. Following anaesthesia with sodium pentobarbital (0.08 mg/100 g BW), hearts were quickly excised, dissected, weighed and frozen in liquid nitrogen. Cryostat sections 16 microns in thickness were exposed to the differential staining technique (Appendix 1), and all data were derived from the midmyocardium of the left ventricle. From tissue cross sections, the position of capillaries in selected fields were digitized with the aid of a graphic tablet linked to a software program (Bioquant IV, R&M Biometrics, Nashville, TN). Line segments connecting adjacent capillaries were then drawn according to the triangulation method. To determine whether the distribution of AC and VC capillary profiles was random, i.e., the null hypothesis of an underlying Poisson process, a statistical test was employed.

A field consisted of N capillaries, with Na arteriolar and Nv venular capillaries (N = Na + Nv). With respect to the histochemical type of neighboring capillary pairs, Nt was the total number of inter-connecting segments. The number of neighbors of the same histochemical type were denoted as either N-aa (both

arteriolar capillaries) or N-vv (both venular capillaries). Neighboring capillaries of different histochemical type were denoted by N-av. In this manner, Nt = N-aa + N-vv + N-av. When capillary type grouping existed, the number of unlike neighbors was less than what would be expected from a randomly distributed pattern. As the number of unlike neighboring pairs follows a Gaussian distribution (Cliff and Ord, 1973), a test of significance (Z statistic), comparing the actual and expected number of unlike neighboring pairs in the field was used. The test criterion that was employed was based upon the number of unlike capillary neighbors (N-av). The mean and variance of the expected number of unlike capillary neighbors (EN-av) in a randomly distributed bivariate point pattern has been previously derived (Cliff and Ord, 1973):

$$EN\text{-}av = 2\frac{NaNv}{N(N-1)} \cdot Nt \qquad (11)$$

$$VarEN\text{-}av = \frac{(EN\text{-}av)^2}{Nt} \qquad (12)$$

For each field, the difference between the actual and expected number of unlike neighbors was estimated by the Z statistic:

$$Z = \frac{N\text{-}av - EN\text{-}av \pm 1/2}{SD(EN\text{-}av)} \qquad (13)$$

For a two-tailed test at $\alpha = 0.01$, the critical Z value was $\pm$ 2.56. Values < -2.56 were indicative of a non-random grouping by histochemical type. Values > +2.56 indicate a repulsion of capillaries of the same histochemical type. The data on the number of AC and VC capillaries per cross-sectional field, and the results of the test for a non-random distribution pattern are presented in Table 1. As all the data originate from the same population of rat hearts, pooled results are also given.

These data suggest that capillary grouping by histochemical type exists in the rat left ventricular midmyocardium. In all hearts, the calculated Z scores indicate that capillaries are distributed in a nonrandom manner, with significant capillary type grouping. There appears to be a level of capillary organization for the myocardium that has not been previously elucidated. The geometrical model being proposed supports the following schema: pre-terminal arterioles run at an oblique angle to the axis of anisotropy. The furnished capillaries may also be staggered in this model (see Figs. 1 and 2). Given this architecture, the arterio-venous (A-V) portions of capillaries would not be in register with one another. Depending upon the angle of the terminal arteriole, neighboring capillaries could be grouped together, and as such, form a bundle of capillaries in register.

TABLE 1 Results of a test for randomness based upon the expected and actual number of neighboring capillaries of different histochemical type.

Heart	N	Na	Nv	Nt	N-av	EN-av	SD EN-av	Z
1	274	47	227	784	159	223.6	7.99	- 8.03
2	248	65	183	706	194	274.2	10.32	- 7.72
3	294	82	212	835	208	337.0	11.66	-11.02
4	271	54	217	743	182	238.0	8.73	- 6.41
5	285	80	205	808	191	327.4	11.52	-11.80
6	307	81	226	864	217	336.7	11.46	-10.40
7	249	48	201	695	140	217.2	8.24	- 9.31
8	297	74	223	830	197	311.6	10.82	-10.55
9	321	96	225	910	224	382.7	12.69	-12.47
10	286	72	214	818	195	309.3	10.81	-10.52
Mean	**283**	**70**	**213**	**799**	**296**	**298.5**	**10.52**	**-10.17**
pooled	**2832**	**699**	**2133**	**7993**	**1907**	**2957.7**	**33.08**	**-31.74**

N=number of capillaries per field; a=AC; v=VC; Nt=total number of neighbors; N-av=number of mixed neighbors; EN-av=expected number mixed neighbors; SD= standard deviation; Z=test statistic.

COMPARISON OF THE RESULTS OBTAINED BY THE DOMAIN AND TRIANGULATION METHODS

As outlined later on in Chapter 3, we noted an inconsistency between the triangulation and domain methods in the analysis of capillaries in hearts exposed to chronic pressure overload. In control hearts, the triangulation method showed that the intercapillary distance was longer on the arteriolar side as compared to the venular side of the capillary net. The domain method conferred similar results, with larger tissue supply regions for arteriolar as compared to venular capillaries. In pressure overloaded hearts, these two methods exhibited different results. The triangulation method showed that intercapillary distance was longer than in controls, but the difference between arteriolar and venular regions was not preserved. The domain method, however, showed smaller tissue supply regions for venular capillaries. Differences between these two methods in the control and pressure overloaded rat myocardium are illustrated in Figure 7. The results of the statistical test for capillary grouping by histochemical type are given in Table 2 and 3 for control and pressure overloaded myocardium, respectively. It is evident that in the pressure overloaded myocardium, capillary type-grouping is diminished, in favor of a more random distribution of capillaries by histochemical type.

To resolve this discrepancy in mathematical terms, we have theoretically compared these two morphometric methods. The triangulation method,

commonly used in the literature, involves the one dimensional measure of inter-capillary distance between two neighbouring capillaries (Fig. 3). The domain method, newer to microcirculation research, takes into account all neighbouring capillaries in the measurement of the tissue supply area, or capillary domain (Fig. 3). To better define the underlying parameters, simulations of capillary fields with various degrees of grouping were generated and analyzed by both methods to compare their sensitivity to grouping phenomenon.

We have reduced the problem to model form, by generating 5 simulations of capillary distribution patterns with pre-defined levels of grouping by histochemical type (Figures 4A-4E). Both morphometric methods were applied to these simulations. The differences in these morphometric methods in terms of tissue supply regions for arteriolar and venular capillaries are illustrated in Figures 5 and 6. The simulations of capillary grouping patterns indicated that the correlation between both approaches: the triangulation method and the capillary domain method, was contingent upon the degree of capillary grouping. In Figures 4A, 4B, and 4C, where the distribution of AC and VC profiles was highly non-random (Z = -18.12, -12.56 and -5.65, respectively), both methods displayed similar results: reduced capillary supply regions for venular capillaries (AC > VC). In figure 4D, where the distribution of capillary profiles was random (Z = -1.9) the first discrepancy in the two morphometric methods was observed: the domain method detected differences in tissue supply region (AC > VC) while the triangulation

method did not show differences in tissue supply region (AC = VC). In Figure 4E, where the pattern was for a repulsion of capillary profiles of the same histochemical type (Z = +5.6), the domain method still displayed the same trend (AC > VC) while the triangulation method showed a reversal (VC > AC). Figure 5 illustrates the tissue supply regions generated by both morphometric methods for all simulations. The triangulation method expressed as percentage of the domain method is shown in Figure 6.

When this interaction is minimal, as in the case of a highly clustered distribution (Simulations A, B and C), there is a large proportion of capillaries surrounded by neighbors of the same histochemical type, i.e., a homogenous environment. This ensures that the triangulation and domain methods will generate the similar results. Take the situation of a reference capillary surrounded by 6 neighbors of the same histochemical type. The triangulation method will yield 6 independent, one-dimensional ICD values (AC-AC). The domain method will yield an averaged, two-dimensional value for domain area from the same 6 neighbors which will be an integration of the 6 individual results of the triangulation method. When the interaction between capillaries of differing histochemical type increases (simulations D and E), the attributes of these two methods begin to digress. The case of a reference arteriolar capillary surrounded by 6 neighbors, 4 AC and 2 VC, will render 4 typical AC-AC values. But the domain method will be influenced by the penetration of the 2 VC profiles

resulting in a modified domain area, the product of a heterogeneous local capillary environment.

In control hearts, a high degree of capillary grouping by histochemical type allowed for a predominantly homogenous population of similar neighbors surrounding a given capillary. As a result, both methods yielded similar results, which agreed with the results of simulations B and C. These data would support a model where transverse arterioles run at an oblique angle to the axis of anisotropy. The arteriole furnishes capillaries that are staggered at various levels in the heart, as a function of the angle of the transverse arteriole and the position that the capillary emanates. Capillaries leaving at any one level would be in register in terms of their arteriolar and venular regions. From tissue cross sections, this arrangement would be manifested by grouping of capillaries of the same histochemical type.

In pressure overloaded hearts, where the degree of capillary type grouping was significantly reduced, the triangulation method did not detect differences between the arteriolar and venular tissue supply regions, while domain areas exhibited significantly smaller values for venular capillaries. These results were similar to those generated in simulation D. In hypertrophied hearts, the observation of less grouping by histochemical type may indicate a sharper angle of the transverse arteriole, which then furnishes capillaries at more dispersed positions in the tissue. Alternatively, this may represent a reduction in arteriolar

unit size, i.e. the number of capillaries furnished by a given arteriole in hypertrophied heart. This trend towards less capillary grouping by histochemical type is likely an attempt of the microcirculation to ensure homogeneous distribution of oxygen to tissue. From cross sections, large zones of venular capillaries, with presumably lower $P0_2$ values, would be encroached by arteriolar capillaries with higher $P0_2$ values to ensure favorable conditions for the diffusion of oxygen in the face of significant cardiac hypertrophy.

To consider which method may provide a more realistic picture of the capillary geometry from arteriole to venule, we have directly measured the distances between capillaries from longitudinal sections (Chapt. 3). The results from these measurements, taken along transect lines at 20% intervals from terminal arteriole to collecting venule, have shown that the tissue supply region decreases in a stepwise manner along the A-V pathlength in both normal and hypertrophied hearts. Accordingly, the method of capillary domains which has demonstrated a similar trend, appears to be preferable to the triangulation method. The method of capillary domains is more sensitive to the local capillary environment and is better able to extract critical information in the face of changes in the extent of capillary grouping.

We conclude that these two morphometric methods do not furnish uniform results over a diverse range of capillary grouping patterns when capillary profiles are reduced to a bivariate point configuration. The underlying variable is the

degree of capillary grouping by histochemical type. As this dissertation represents the first study of coronary capillaries partitioned into two sub-types, it was necessary to reappraise different methods used to analyze capillaries of only one type. This theoretical study analysis provided assurance that the capillary domain method was the most appropriate for the analysis of capillary geometry when capillaries are differentially stained and may vary as to the extent of grouping by histochemical type.

TABLE 2 Results of a test for randomness based upon the expected and actual number of neighboring capillaries of different histochemical type in control hearts.

Heart	N	Na	Nv	Nt	N-av	EN-av	SD EN-av	Z
1	274	47	227	784	159	223.6	7.99	- 8.03
2	248	65	183	706	194	274.2	10.32	- 7.72
3	294	82	212	835	208	337.0	11.66	-11.02
4	271	54	217	743	182	238.0	8.73	- 6.41
5	285	80	205	808	191	327.4	11.52	-11.80
6	307	81	226	864	217	336.7	11.46	-10.40
7	249	48	201	695	140	217.2	8.24	- 9.31
8	297	74	223	830	197	311.6	10.82	-10.55
9	321	96	225	910	224	382.7	12.69	-12.47
10	286	72	214	818	195	309.3	10.81	-10.52
pooled	**2832**	**699**	**2133**	**7993**	**1907**	**2957.7**	**33.08**	**-31.74**

N=number of capillaries per field; a=AC; v=VC; Nt=total number of neighbors; N-av=number of mixed neighbors; EN-av=expected number mixed neighbors; SD= standard deviation; Z=test statistic.

TABLE 3 Results of a test for randomness based upon the expected and actual number of neighboring capillaries of different histochemical type in pressure overloaded hearts.

Heart	N	Na	Nv	Nt	N-av	EN-av	SD EN-av	Z
1	172	50	122	480	166	199.1	9.09	-3.59
2	180	50	130	506	166	204.2	9.08	-4.15
3	210	59	151	597	198	242.4	9.92	-4.42
4	178	68	110	501	194	237.9	10.63	-4.08
5	226	58	168	636	194	243.7	9.66	-5.09
6	224	66	158	640	238	267.2	10.56	-2.72
7	185	41	144	521	136	180.7	7.92	-5.58
8	206	42	164	583	165	190.2	7.88	-3.13
9	173	45	128	494	152	191.3	8.60	-4.51
10	165	51	114	472	165	202.8	9.33	-4.00
pooled	**1919**	**530**	**1389**	**5430**	**1774**	**2172.2**	**29.47**	**-13.49**

N=number of capillaries per field; a=AC; v=VC; Nt=total number of neighbors; N-av=number of mixed neighbors; EN-av=expected number mixed neighbors; SD= standard deviation; Z=test statistic.

TABLE 4 Results of a test for randomness for simulations A-E.

Cond	N	Na	Nv	Nt	N-av	EN-av	SD EN-br	Z
SIM-A	212	62	150	577	58	240	10.0	-18.2
SIM-B	212	62	150	577	114	240	10.0	-12.6
SIM-C	212	62	150	577	184	240	10.0	- 5.7
SIM-D	212	62	150	577	220	240	10.0	- 1.9
SIM-E	212	62	150	577	292	240	10.0	+ 5.2

N=number of capillaries per field; a=AC; v=VC; Nt=total number of neighbors; N-av=number of mixed neighbors; EN-av=expected number mixed neighbors; SD= standard deviation; Z=test statistic.

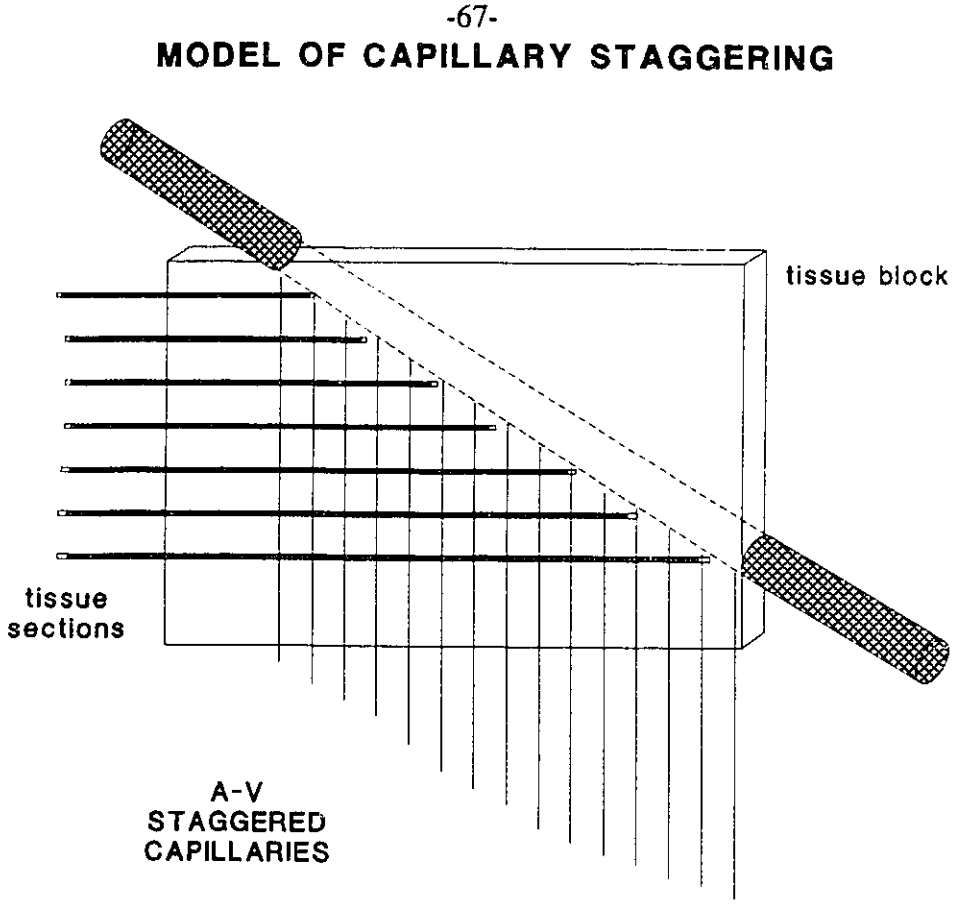

FIG. 1 Model of capillary staggering showing transverse arteriole that furnishes capillaries at different levels in the tissue.

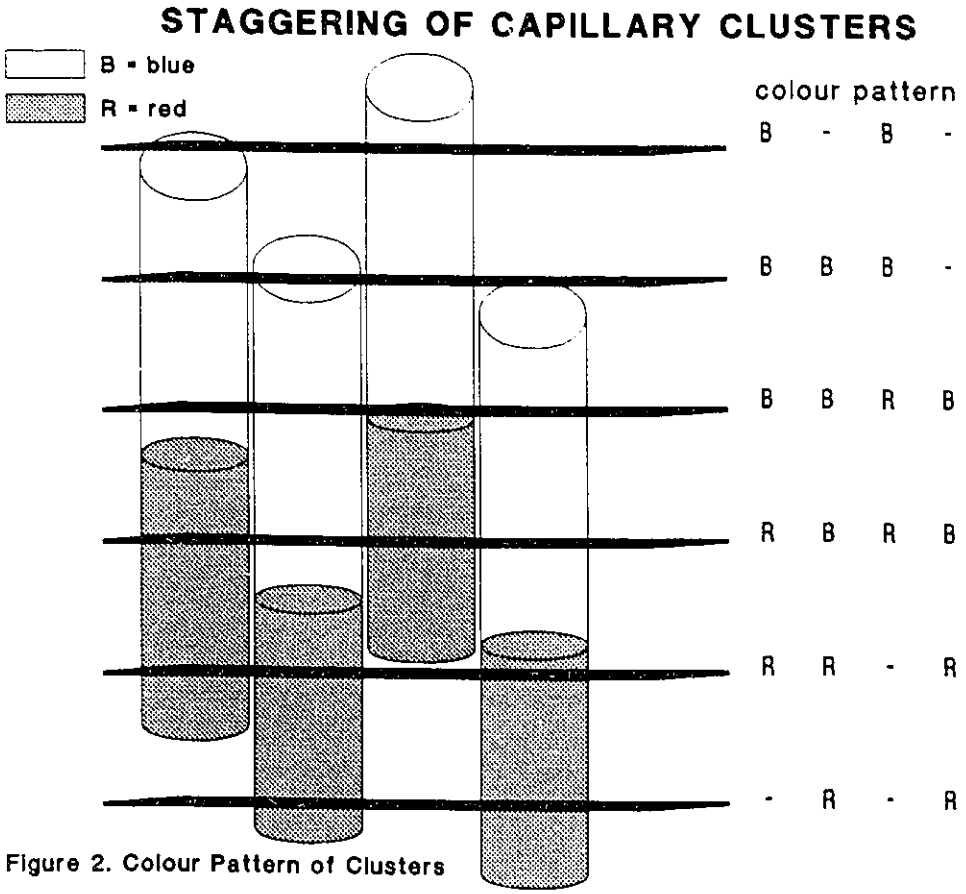

Figure 2. Colour Pattern of Clusters

FIG. 2 Model of capillary staggering showing capillary bundles that are in register with respect to arteriolar and venular ends.

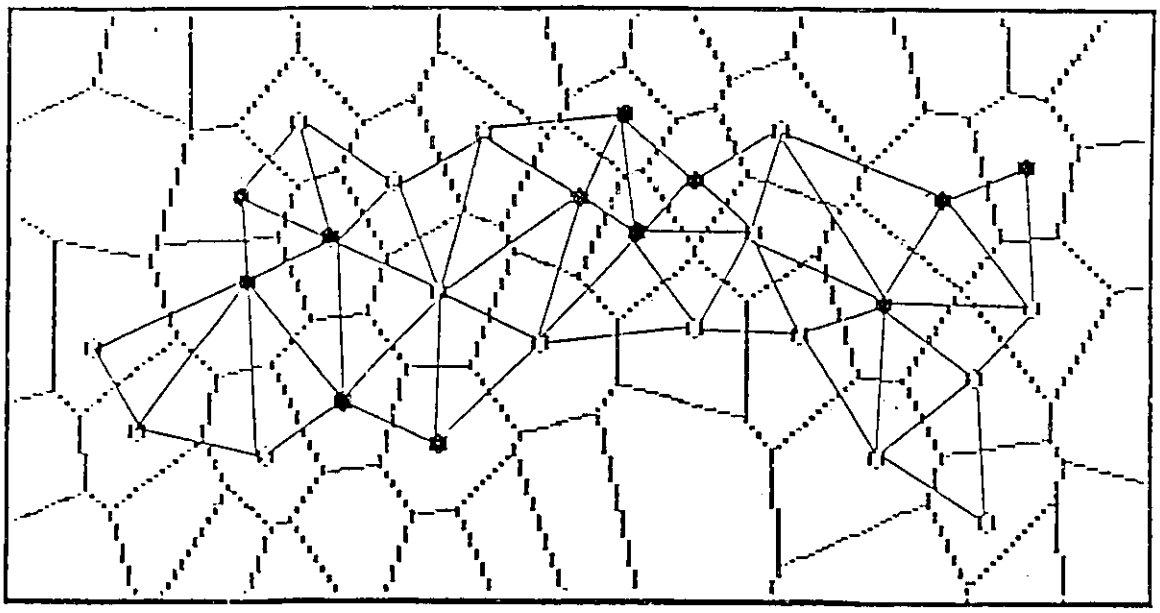

open circles = arteriolar capillaries
closed circles = venular capillaries

FIG. 3 Delineations of Capillary Domains (thick lines) and Triangulations (thin lines) in the tissue plane for 28 capillary profiles. Domains that are not fully enclosed within the field are excluded. Open circles = arteriolar capillaries; filled circles = venular capillaries.

a

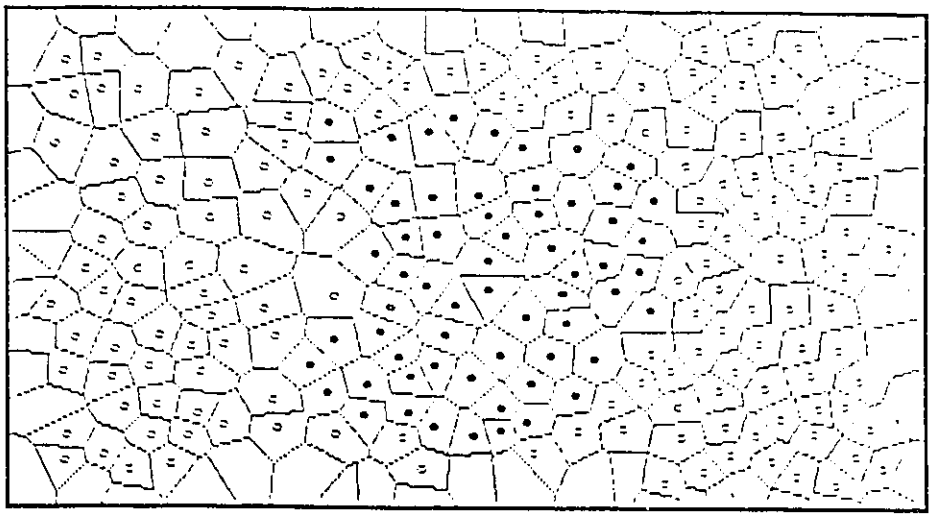

b

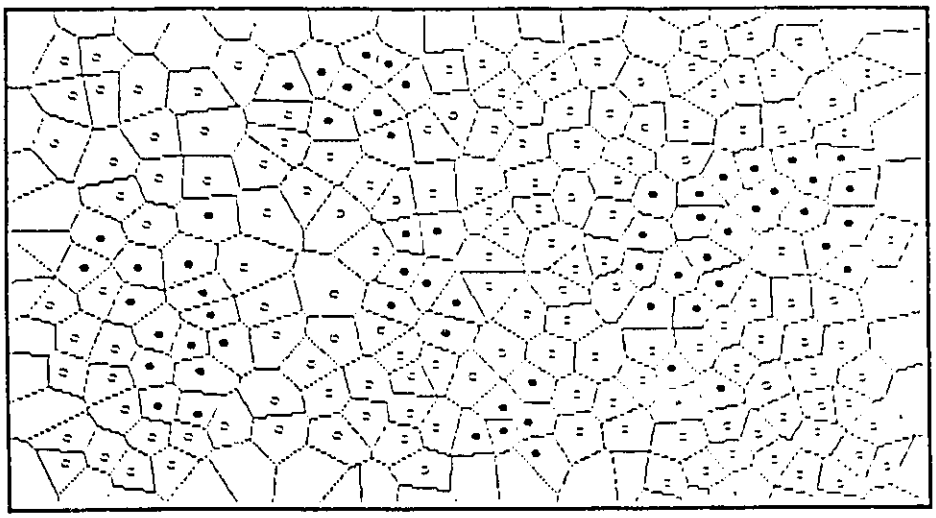

c

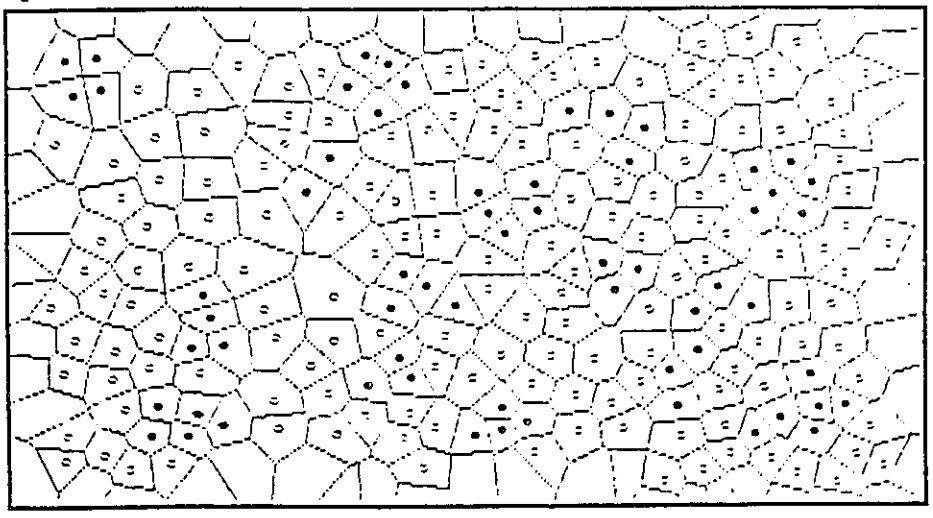

d

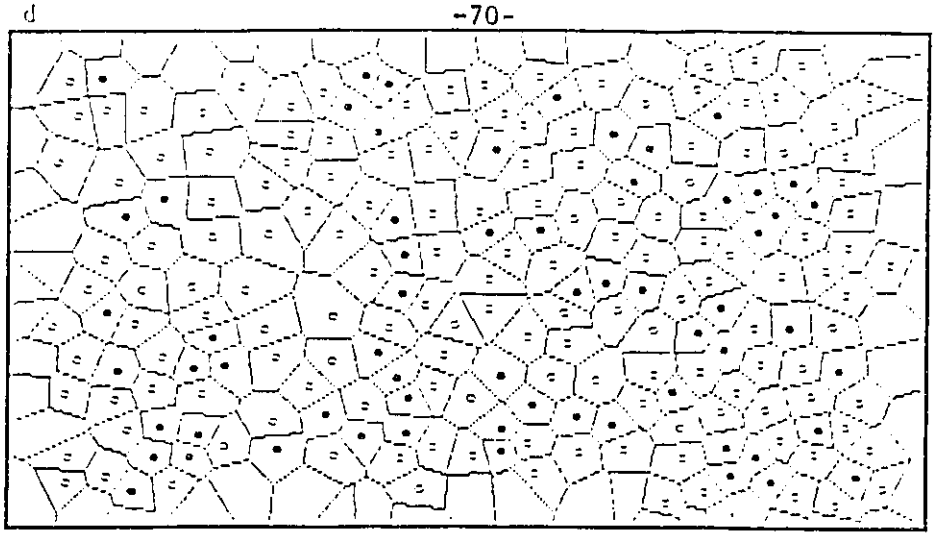

e

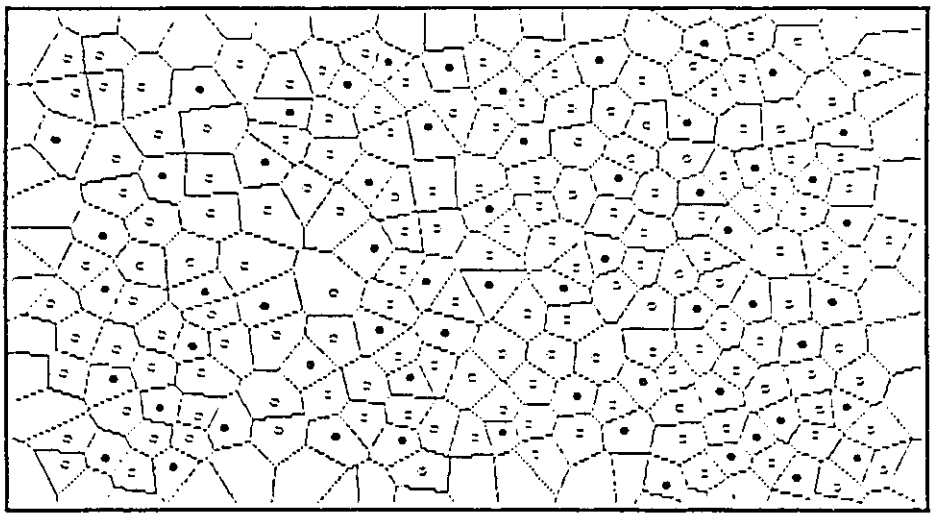

FIGS.4a-e Simulations of capillary profiles in the tissue plane with various degrees of grouping by histochemical type.

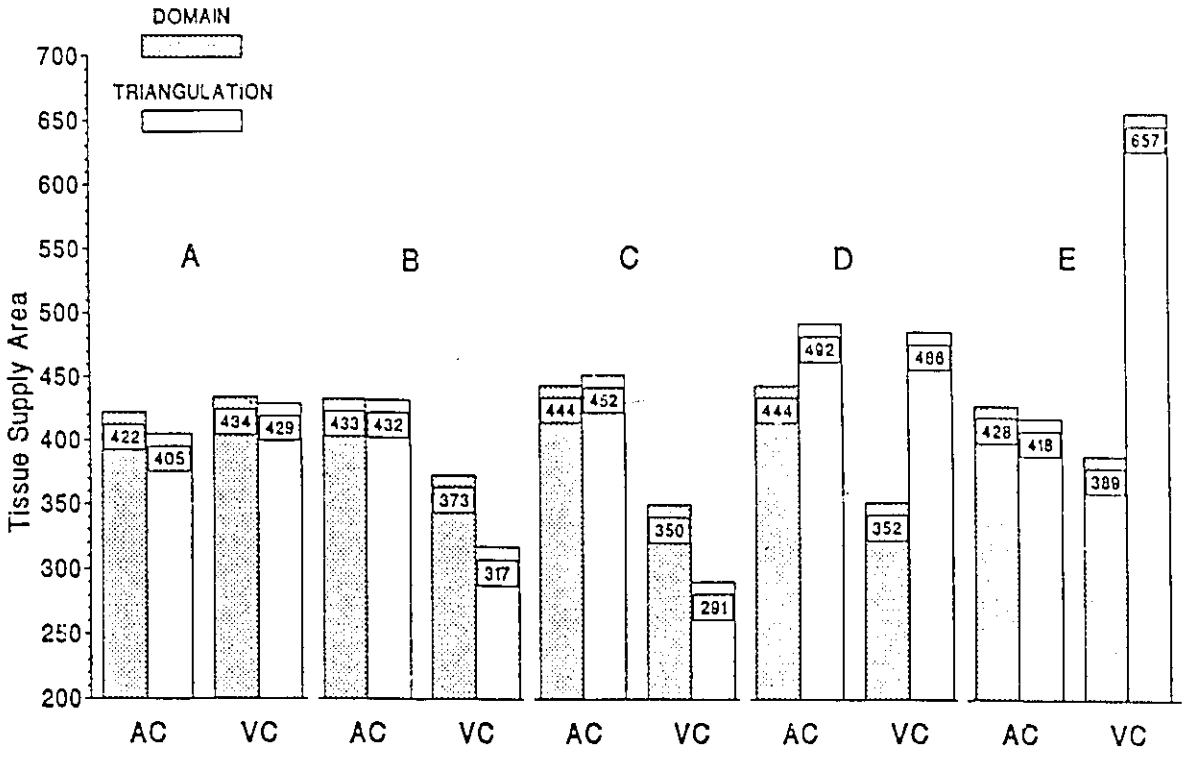

FIG. 5 Comparison of tissue supply regions (μm^2) as determined by the domain and triangulation methods for simulations A-E. Results from the triangulation method (ICD) are represented as area of the Krogh cylinder (πr^2)

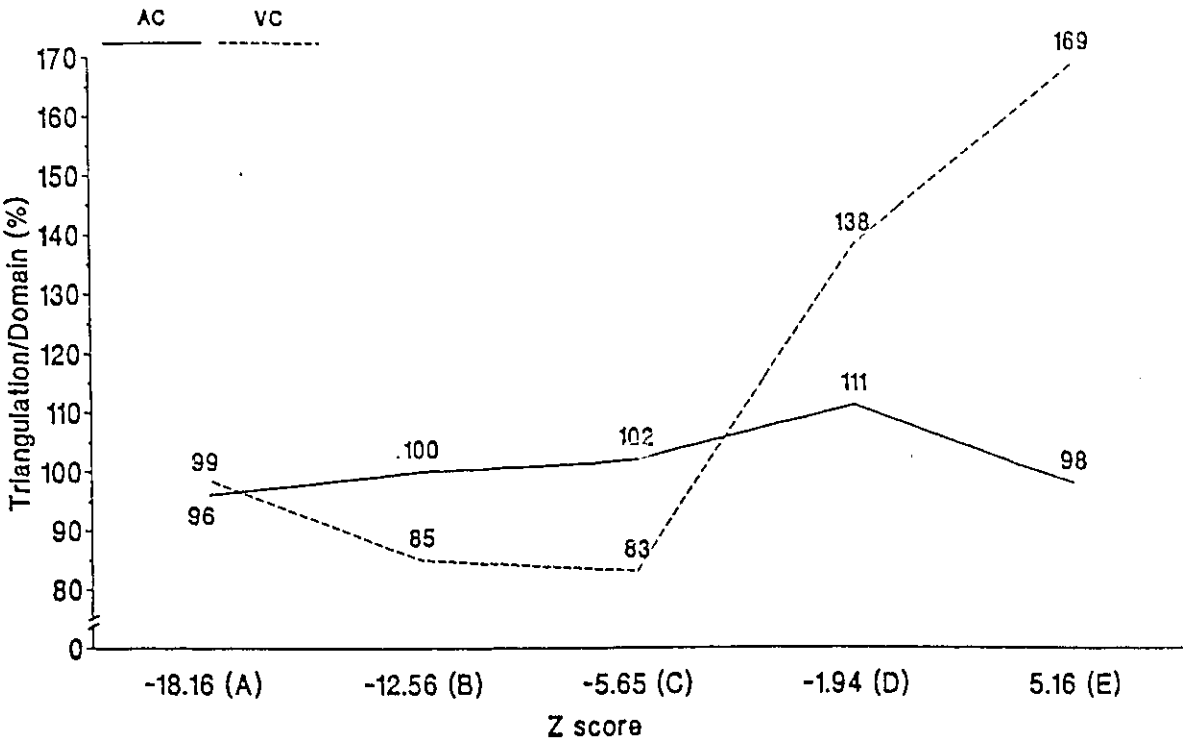

FIG. 6 Results from the triangulation method (ICD) expressed as a percentage of domain area for simulations A-E.

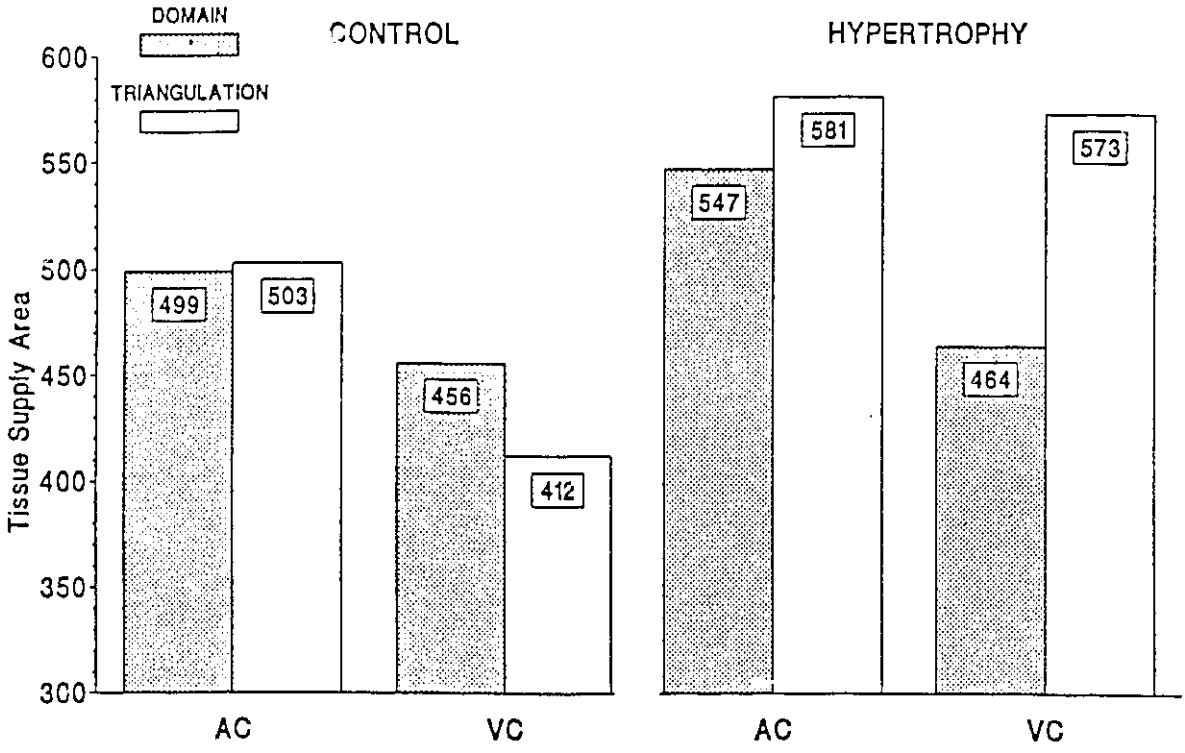

AC = arteriolar capillaries
VC = venular capillaries

FIG. 7 Comparison of tissue supply regions (μm^2) as determined by the domain and triangulation methods in control and hypertrophied heart. Results from the triangulation method (ICD) are represented as area of the Krogh cylinder (μm^2)

PLATE 1 Light micrograph of a transverse section of the left ventricular midmyocardium illustrating differential staining response. Arteriolar capillary regions stain blue. Venular capillary regions stain red.

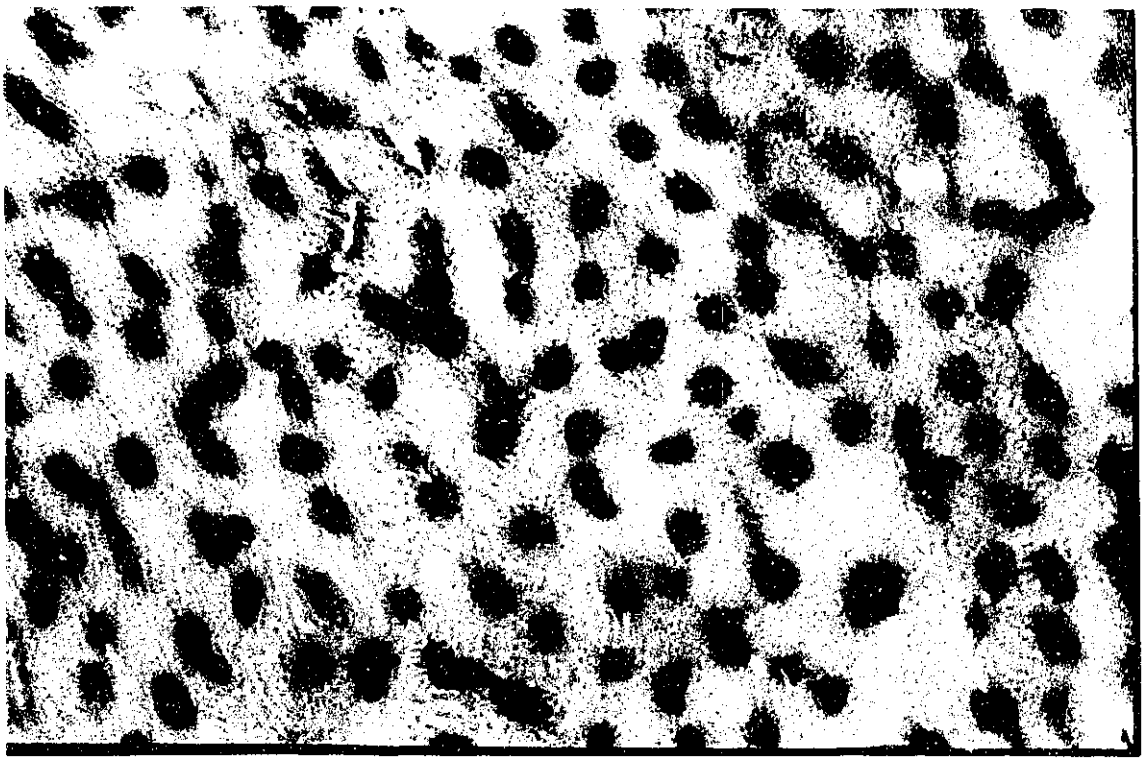

PLATE 2 Higher magnification of a transverse section of the left ventricular midmyocardium. At this magnification, individual myocyte borders may be delineated. Venular capillaries (red) appear to be closer together than arteriolar capillaries (blue).

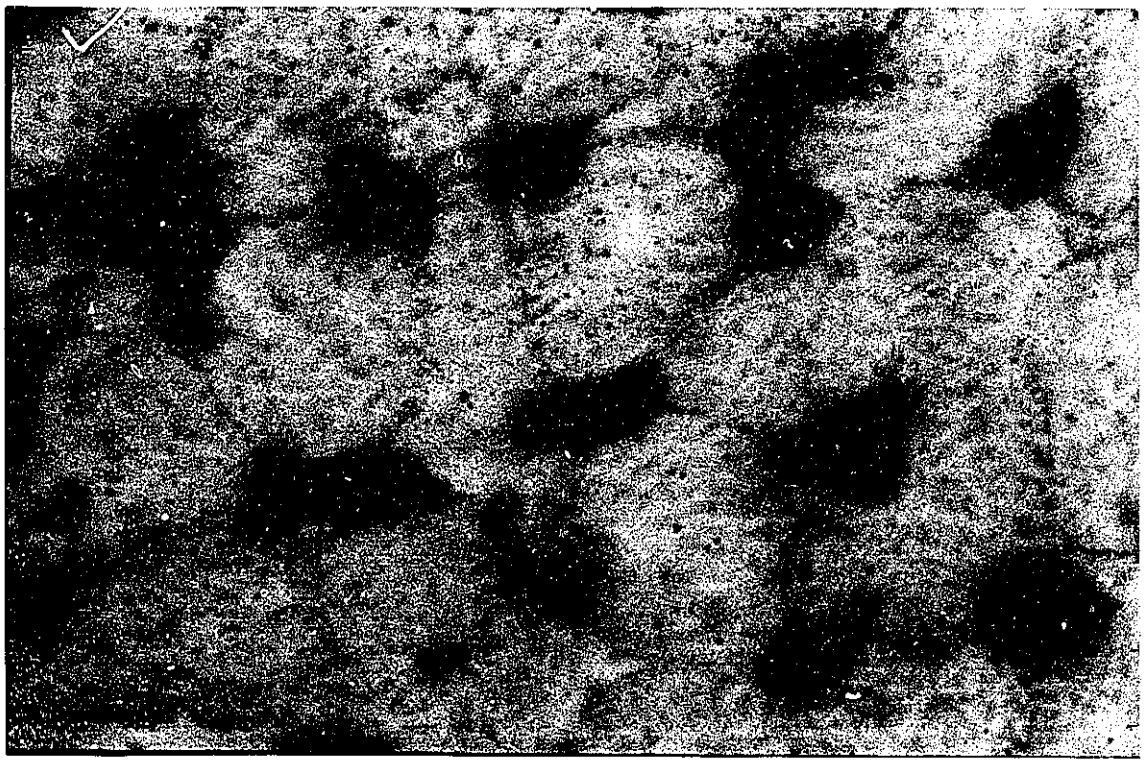

PLATE 3 Longitudinal section at high magnification illustrating anastomoses between neighboring capillaries.

REFLECTION

"We take a handful of sand from the endless landscape of awareness around us and call that handful of sand the world. Once we have that handful of sand, the world of which we are conscious, a process of discrimination goes to work on it...We divide the sand into parts. This and that. Here and there. Black and white. Now and then. The discrimination is the division of the conscious universe into parts. The handful of sand looks uniform at first, but the longer we look at it the more diverse we find it to be. Each grain of sand is different. No two are alike. Some are similar in one way, some are similar in another way, and we can form the sand into separate piles on the basis of this similarity and dissimilarity. Shades of color in different piles - sizes in different piles - grain shapes in different piles - subtypes of grain shapes in different piles - grades of opacity in different piles - and so on, and on, and on. You'd think the process of subdivision and classification would come to an end somewhere, but it doesn't. It just goes on and on".

Robert M. Pirsig

Zen and the Art of Motorcycle Maintenance

BASIS FOR THE DISSERTATION

Realistic models of oxygen transport must be formulated if our knowledge of the underlying biophysical principles of the microcirculation is to be enhanced. Simulations of cardiac oxygen transport phenomena must rely upon accurate morphometric data that serve as input parameters for such models. Despite advancements in the theoretical modeling of oxygen transport, the most fundamental parameters for these models are still not based upon realistic morphometric data and most models still assume a very simple, unrealistic geometry. Furthermore, systematically obtained data regarding distributions of coronary capillary length are not available in the literature.

In preface to the central chapters of this dissertation, we have successfully applied the differential staining technique to the rat coronary microcirculation. This then raised new questions in regards to the appropriateness of various morphometric methods for quantitative analysis of capillary geometry. We have shown in unequivocal terms that from tissue cross sections, the domain method is most germane to the present study.

In the following chapters, capillary geometry from both cross and longitudinal sections has been rigorously analyzed. From cross sections, capillary domain areas and the heterogeneity of these areas were determined. From longitudinal sections, we have established several capillary length parameters, that are described in the appropriate chapters. All results have been classified as a

function of arteriolar and venular capillary regions. The calculation of PO_2 profiles (Chapt. 5), incorporating these data were done in collaboration with Dr. Z. Turek and Dr. L. Hoofd, University of Nijmegen, Nijmegen, The Netherlands. Figures contained in the dissertation that have been previously published, are reproduced with permission.

Various components of this dissertation are in the process of, or already have been published. The following list summarizes the present status of the research presented in this dissertation:

TOPIC	REFERENCE	STATUS
Capillary staggering (Introduction)	Adv. Exp. Med. Biol.	Published
Models of clustering (Introduction)	Adv. Exp. Med. Biol.	In press
Pilot longitudinal data (not incl.)	Adv. Exp. Med. Biol.	Published
Domain/triangulation methods (Introduction)	J. Cardiovasc. Pharmacol.	Published
Systole-Diastole (Chapter 1)	Cardiovasc. Res.	In preparation
Systole-Diastole, San Diego (not incl.)	Circ. Res.	Under revision
Normal postnatal growth (Chapter 2)	Am. J. Physiol.	Under revision
Pressure overload (Chapter 3)	Microvasc. Res.	Published
Volume overload (Chapter 4)	Microvasc. Res.	Published
Modeling of oxygen supply (Chapter 5)	Adv. Exp. Med. Biol.	In press

Complete references may be found in the section: VITA.

STATEMENT OF THE PROBLEM

Since the introduction of the Krogh model geometry over 70 years ago, much work has been done in terms of structure and function relationships in oxygen transport to tissue. It is becoming more recognized that heterogeneities in capillary geometry and capillary flow play a significant role in oxygen supply, which cannot be understood from simply average values of capillary density, capillary length, and red cell flux.

In the heart muscle, even these entry data are still not entirely available. Reports of even the most basic descriptor of capillary supply, the capillary density, in the rat left ventricle range from 2000 to over 5000 capillaries/μm^2. Furthermore, there are no reliable data as of yet regarding capillary length parameters in the mammalian myocardium. Given these shortfalls, the specific direction of this dissertation will be to address the following questions:

1. What is the relationship between capillary geometry and cardiac contraction? i.e. are there differences in capillary geometry at discrete phases of the cardiac cycle?

2. What is the extent of capillary supply as determined from tissue cross and longitudinal sections during normal growth, and accelerated growth due to pressure and volume overloading?

3. Are there differences in capillary geometry from arteriolar to venular capiliary regions?

4. What are the implication of these morphometric adaptations to models of oxygen supply to the myocardium?

CHAPTER 1: CAPILLARY GEOMETRY IN RAT MYOCARDIUM AT DISCRETE PHASES OF THE CARDIAC CYCLE

INTRODUCTION

The pattern of cardiac muscle contraction reflects an integration of many contractile units that, in toto, serve the function of the heart muscle. During cardiac contraction, stresses are developed at the tissue level that may influence the resting properties of the heart muscle. Previous studies of tissue alterations during the cardiac cycle have been limited to non-vascular tissue components, while studies of myocardial capillarization have generally been limited to hearts arrested in diastole. The intrinsic pattern of cardiac contraction, however, raises the question of whether capillary geometry is altered during the cardiac cycle.

Changes in capillary geometry with fiber shortening have already been studied in striated muscle, where capillary geometry changes profoundly with alterations in sarcomere length (e.g. Groom et al. 1984a; Mathieu-Costello, 1987; Mathieu-Costello et al. 1988; Mathieu-Costello et al. 1989b). Specifically, as sarcomere length is reduced below 2.0 μm, capillaries become tortuous and the contribution of capillary tortuosity to capillary length and surface area increases in a curvilinear fashion. This behavior may compensate for the reduced capillary density subsequent to increases in fiber cross sectional area, and capillary length and surface area remain practically unchanged (Ellis et al. 1990). The

dependence of fiber cross sectional area, capillary density and capillary tortuosity on sarcomere length underscores the importance of referencing these measurements to sarcomere length (Mathieu-Costello et al. 1989a).

The purpose of the present investigation was therefore to describe changes in capillary geometry as a function of fiber shortening in the rat myocardium. We have studied the effect of experimentally induced fiber shortening on changes in the tortuosity of individual capillary segments and arterio-venous pathlengths in the midmyocardium.

METHODS

In this part of the study, 14 male Sprague Dawley rats were used (BW = 267±2 g). Following anesthesia with sodium pentobarbital (4mg/100g i.p.), bolus injections of either 100 mM $CaCl_2$ (n=8) or 100 mM KCl (n=6) were made through a catheter in the iliac vein to arrest the heart in "systole" or "diastole", respectively. Following injection, hearts were rapidly excised, weighed, dissected and frozen in liquid nitrogen. From each heart, a tissue block consisting of the middle third of the left ventricle (including septum) was dissected perpendicular to the base-apex axis and was prepared for cryostat sectioning.

Tissue sections were first cut (4-5μm) and stained with Periodic acid-Schiff's reagent to allow for visualization of myofiber Z bands. Tissue blocks were then manually adjusted with respect to the cutting plane (approx. ±5° increments) until

well defined longitudinal sections of the midmyocardium were obtained. Longitudinal sections were identified when a change in orientation of the tissue block gave rise to fiber sections with greater sarcomere length. At the appropriate sectioning angle, cryostat sections were taken (16μm) and prepared for differential staining (see Appendix 1). All data were derived from these longitudinal sections of the left ventricular midmyocardium (LVM). From the sections with PAS, we systematically sampled the free wall of the LVM and measured sarcomere lengths with the aid of a microscope connected to an image analysis system (Bioquant IV, R&M Biometrics, Nashville TN). Morphometric data regarding capillaries were collected and analyzed as a function of arteriolar capillary (AC) and venular capillary (VC) regions. The LVM was systematically sampled for capillary segments (the interval between two successive branch points) that were entirely captured within the 16 μm section. In addition, in fields where it was possible to clearly identify a terminal arteriole, capillary pathways, and the collecting venule, the shortest arterio-venous capillary pathlength was measured.

All results are reported as mean ± SEM. The one-way analysis of variance was used to test for significant differences in appropriate parameters occurring with fiber shortening. For data that were collected as a function of AC and VC regions, a two-way analysis of variance was used to test for differences due to fiber shortening and capillary region, respectively. As conditions of linearity

between dependent and independent variables were generally not met, regression lines of appropriate order were plotted. The coefficient of determination, which is an index of the total variation in the dependent variable that is explained by the regression model, was used to determine the appropriate order of the regression line. The polynomial order, the equation and correlation coefficient (r) of each least-squares regression line is included in the figure legends. Morphometric data that are reported in this study are defined as follows:

Wall/Cavity Ratio (W/C) - The first index of position of the heart with respect to the cardiac cycle was the ratio of the area of the LV wall (including septum) to LV cavity.

Sarcomere length (sl) - The second index of position of the heart with respect to the cardiac cycle. Sarcomere lengths were counted in series of 10 (11 successive Z lines), to provide a values of 10x sarcomere length. A total of 100 measurements were made per heart.

Segment Length (SEG) - The length of the capillary segment as measured by directly tracing the endothelial border of the segment between two successive branch points (nodes). A total of sixty capillary segments were identified and

measured in each heart. These measurements were classified as a function of arteriolar (AC,n=30) and venular (VC,n=30) capillary regions.

Node-Node Segment Length (NODE) - The straight line distance of each capillary segment (SEG) was also measured.

Segment Tortuosity Index (STI) - For each capillary segment, the ratio of the segment length to node-node length (SEG/NODE) served as the index of individual capillary segment tortuosity.

Minimal Capillary Length (MCL) - In fields where capillary pathways could directly be traced from terminal arteriole to collecting venule, the minimal arterio-venous capillary pathlength was measured. A total of 59 pathlengths were measured (3-5 per heart).

Arterio-Venous Capillary Length (AV) - The straight line distance of a capillary path (MCL) measured from terminal arteriole to collecting venule.

AV Tortuosity Index (AVTI) - Similar to STI, the AV tortuosity index was a ratio of the minimal capillary length to the arterio-venous capillary length (MCL/AV), which served as an index of tortuosity along the arterio-venous capillary path.

RESULTS

Results are reported in Table 1.1. Following injections of either KCl_2 or $CaCl_2$ to arrest the heart in diastole (D) or systole (S), respectively, we used two approaches to determine the extent of cardiac contraction: wall/cavity area ratio and sarcomere length. The gross assessment of these hearts indicated that the respective injection gave rise to the desired end-point. However, two hearts that were injected with $CaCl_2$ appeared not be arrested in end-systole, rather at some intermediate position in the cardiac cycle. These "intermediate" hearts had a W/C ratio of 14.6 ± 3, and were classified as third group, (I). Notwithstanding this, the wall/cavity ratio was significantly higher in hearts arrested in systole (S=42.8 ± 4.6; D=7.0 ± 0.5, $P<0.01$). In agreement with gross morphological data, sarcomere lengths were significantly smaller in systolic, as compared to diastolic hearts, and values from intermediate hearts were in between (S=1.81 ± 0.02; I=1.93 ± 0.03; D=2.05 ± 0.02, $P<0.01$). Figure 1.1 displays the relationship between W/C ratio and sarcomere length. Frequency histograms of sarcomere lengths for the systolic, intermediate and diastolic hearts are displayed in Fig. 1.2.

In all phases of the cardiac cycle (S,I,D), AC segments were longer than VC segments ($P<0.01$). The index of capillary tortuosity at the level of individual capillary segments, AC STI, and VC STI, indicated that capillary segments were on average 15% longer than their corresponding node-node lengths ($P<0.05$). There were no differences in the degree of segment tortuosity as a function of

capillary region (AC,VC), or phase in the cardiac cycle (S,I,D). There was a trend for increased segment tortuosity for VC regions as compared to AC regions in 12 of the 14 hearts in this study (Fig. 1.3), but this was not statistically significant. Both of the regression lines in Fig. 1.3 also indicate a trend for increased segment tortuosity at reduced sarcomere lengths, but similarly, the slopes of these lines were not significantly different from zero.

Figure 1.4 illustrates the relationship between minimal capillary length and sarcomere length. Note the high inter-heart variability in this parameter, which appears to be independent of sarcomere length. The number of contiguous capillary segments per capillary length averaged 8±1 (mean ± SEM). The AV tortuosity index displayed a significant relationship with sarcomere length, indicating that with fiber shortening the degree of AV capillary tortuosity was increased (Fig. 1.5). The AVTI is the sum of two components: the tortuosity at the level of individual capillary segments, and the tortuosity due to branching not in line with the arterio-venous axis. This overall tortuosity index was significantly higher in systolic as compared to diastolic hearts ($P<0.01$). Figure 1.6 serves to summarize the data from the present study, showing both the capillary segment and capillary length tortuosity in the systolic, intermediate and diastolic groups. It is evident that the any increased capillary tortuosity with fiber shortening is along the arterio-venous capillary length rather than at the level of individual capillary segments.

DISCUSSION

The preeminent finding in this study was that increases in overall capillary tortuosity with fiber shortening were minimal, as compared with data from various skeletal muscles (Mathieu-Costello, 1987; Mathieu-Costello et al. 1988; Mathieu-Costello et al. 1989b). We noted no increases in capillary segment tortuosity with a reduction in sarcomere length. Interestingly, there was a trend for greater tortuosity in venular capillary regions, but this was not statistically significant. Indeed, an increase in venular capillary tortuosity index would be intuitively appealing; as this would serve to increase the capillary surface area available for diffusion per unit fiber surface area in venular capillary regions where $P0_2$ values are generally lower.

In the special case of an individual capillary length, there was an increase in capillary path tortuosity in systolic hearts despite no increase in capillary segment tortuosity. This would suggest that branching angles at successive branch points along the capillary path may have become less acute, adding to the observed overall tortuosity. It may be that given the high intramuscular pressures generated in systole, and the extensive collagen network, the "weakest" point in the capillary path is at the branch point. During cardiac contraction, branching angles may be altered rather than corollary increases in capillary segment tortuosity.

It should be noted that measurements of individual capillary segments were based upon only those segments that appeared to be entirely captured in the tissue section. We cannot preclude the possibility that some degree of tortuosity was not measured. The planar tortuosity measured, may underestimate the three dimensional tortuosity of capillary segments.

With regard to the reduced capillary tortuosity developed with fiber shortening as compared to skeletal muscle, it is conceivable that the capillary-myocyte struts described above constrain lateral movement of the capillary and reduce or prevent development of tortuosity during fiber shortening. Although the grossly similar appearance of these struts in skeletal muscle argues against such a role (Borg and Caulfield, 1980), it is notable that the collagen content of the heart is about six-fold that of skeletal muscle (Gay and Johnson, 1967). Another possibility is that the high density of capillary branches found in heart affects capillary deformation. It is of interest to note that in the pigeon-pectoralis, a muscle with a high degree of capillary branching, there is also little increase in capillary tortuosity with decreased sarcomere length (Mathieu-Costello, 1991).

What is the Physiological Range of Myocardial Sarcomere Length?

As previously stated, the purpose of this investigation was to determine whether changes in capillary geometry accompany myocyte fiber shortening. Given that the condition of sustained contraction achieved in these experiments,

the observed reduction in sarcomere length may not represent true physiological systole. It is important to relate the sarcomere lengths obtained in this investigation to those that may occur in vivo. Whereas skeletal muscles may produce active tension over a broad range of sarcomere lengths (Gordon et al. 1966; ter Keurs et al. 1988), in vivo, skeletal muscles may only operate over that portion of the length-tension relationship where active tension production is close to optimal. This has been demonstrated in a wide variety of muscles, including carp red muscle (Rome et al. 1988), flight muscles of birds (Cutts, 1986) and human thigh muscles during walking (Cutts, 1989). Cardiac muscle produces less force per unit cross sectional area than skeletal muscle, but the shape of the length-active tension relationship is similar (Spiro and Sonnenblick, 1964). In contrast to skeletal muscle however, the ascending limb of the length-tension curve has been considered the only physiologically functional region in the heart (Spotnitz et al. 1966). Although extreme values of sarcomere length (1.4 - 2.4 μm) have been reported for the cat papillary muscle (Sonnenblick et al. 1963), the normal limits of the ascending limb are generally considered to be 1.5 and 2.2 μm (Spiro and Sonnenblick, 1964; Spotnitz et al. 1966; Sonnenblick et al. 1964). These values correspond well with laser diffraction measurements of sarcomere length over the ascending limb of the length-active tension curve in rat trabeculae at different calcium concentrations (ter Keurs et al. 1988).

At left ventricular end diastolic pressure of 12 mmHg, sarcomere lengths in the subepi and subendocardium averaged 2.18±0.001 μm and 2.13±0.10 μm, respectively (Yoran et al. 1973). Sonnenblick et al.(1964) estimated that sarcomere length will be reduced from 2.1 to 1.7 μm (19%) at physiologic afterload. Assuming a spherical geometry, a circumferential fiber shortening of this magnitude could account for a 40-50% ejection fraction (Sonnenblick et al. 1964). It has been further demonstrated that during postextrasystolic potentiation, sarcomere length shortened from 2.2 to 1.6 μm, resulting in a predicted ejection fraction of approx. 75% (Sonnenblick et al. 1967).

The sarcomere lengths found in the present study most likely incorporate, if not exceed, the range of sarcomere lengths attained in vivo. The method of cardiac arrest used in these studies may not represent physiological limits in the normal cardiac cycle, and the possibility of having attained some non-physiological, contracture of the myocardium was possible. The sarcomere lengths observed in this study would nonetheless be within the limits of all possible sarcomere lengths attainable in rat myocardium.

Regional Heterogeneity in Sarcomere Length

Heterogeneity in sarcomere lengths may occur at different levels, i.e. within a given fiber, between neighboring fibers, or at different regions in the myocardium.

Within fiber: using computer-interfaced optical microscopy, Roos (1987) derived 3-D reconstructions to determine sarcomere length and registration throughout the volume of individual rat myocytes. With the exception of regions where sarcomeres where distorted close to nuclei, sarcomere registration and length periodicity exhibited high uniformity throughout the myocyte. In the present investigations, sarcomeres were often well delineated over the entire myocyte length, and the variability appeared to be greater in hearts arrested in systole. The coefficient of variation for sarcomere length within fibers in systolic hearts averaged 15.4 ± 2.2% (n=22). In diastolic hearts, the coefficient of variation for sarcomere length averaged 7.8 ± 1.4 % (n=15).

Transmural heterogeneity: sarcomere length difference across the left ventricular wall may be dependant upon intraventricular pressure or volume (Spotnitz et al. 1966). However, these differences are typically small and their directional bias is controversial (Spotnitz et al. 1966; Sonnenblick et al. 1963; Sonnenblick et al. 1964; Yoran et al. 1973). Furthermore, at intraventricular pressures of approximately 20 mmHg, these differences appear to be minimized. In the present investigation, no consistent differences were found between sarcomere length across the midmyocardium.

Base-apex heterogeneity: differences in sarcomere length have been reported between the apex and base of the dog left ventricle (Laks et al. 1967). In the

present study, measurements were made at the same level in the left ventricle to minimize such potential bias.

To summarize, a certain degree of sarcomere heterogeneity exists at each level described above. The greater variability observed in systolic hearts likely reflects changes in fiber orientation associated with physiologic systole (or $CaCl_2$ induced sustained fiber shortening). In addition, it may technically be easier to obtain more uniform sarcomere lengths in diastolic arrested hearts, rather than in systolic arrested hearts which likely exhibit various degrees of shortening in both spatial and temporal terms.

It is of interest to note that in our collaboration with Dr. D.C. Poole and Dr. O. Mathieu-Costello, at the University of California, San Diego, we have obtained similar results using an entirely different morphometric approach. The results of this collaborative study are not included in the dissertation. In this study (Poole et al. 1990), we assessed changes in capillary tortuosity with fiber shortening in the subendocardium (endo) and subepicardium (epi) of rats. From 1 μm sections cut transverse and longitudinal to the muscle fiber axis, capillary density, capillary diameter, fiber cross-sectional area, capillary orientation parameter (K), and capillary anisotropy coefficient (c(K,0)), and sarcomere length were determined in each region. Capillary length, surface and volume densities were also calculated (see Introduction for methodology). To briefly summarize these data, hearts arrested in systole had sarcomere lengths in the sub-epi and

subendocardium shorter than those values predicted from measurements of ejection fraction and end systolic volume in humans. There were no differences in morphometric parameters between sub-epi and subendocardium. In both regions, fiber cross-sectional area increased and capillary density decreased with fiber shortening as predicted from the reduction in sarcomere length at constant fiber volume. In contrast to various skeletal muscles, capillary tortuosity did not markedly increase at reduced sarcomere lengths in hearts arrested in systole.

In the present Chapter, we have demonstrated that coronary capillary geometry is much less altered by fiber shortening than in skeletal muscle. To the best of our knowledge, these were the first studies to directly assess changes in capillary tortuosity as a function of sarcomere length in the mammalian myocardium. The development of tortuosity with fiber shortening may be resisted by the presence of a large degree of capillary-to-myocyte collagenous struts. It is worthy of noting that there was a trend towards a greater capillary tortuosity in both systolic hearts, and in venular capillary regions, but these were not statistically significant. In the special case of the tortuosity along the arterio-venous capillary path (approximately 600 μm in length), it appears that the increased tortuosity observed in systolic hearts may be due to a change in capillary segment orientation rather than specific increases in the tortuosity of the capillary endothelium. It is still advisable to collect data regarding capillary geometry from hearts stopped at a well defined stage in the cardiac cycle. The

most uniform and repeatable stage would be end-diastole. All of the studies in the following Chapters investigate the geometry of capillary networks in KCl arrested diastolic hearts.

TABLE 1.1 Morphometric data of midmyocardium in rat heart arrested in diastole, intermediate, and systole

Parameter	Diastole	Intermediate	Systole
W/C Ratio	7.0 ± 0.51	14.6 ± 0.3	42.8 ± 4.6
sl (μm)	2.05 ± 0.02	1.93 ± 0.02	1.81±0.02
AC Seg (μm)	103 ± 5	95 ± 4	99 ± 5
AC Node (μm)	90 ± 3	83 ± 3	85 ± 3
AC STI	**1.14 ± 0.01**	**1.15 ± 0.02**	**1.16 ± 0.02**
VC Seg (μm)	81 ± 4	78 ± 2	84 ± 6
VC Node (μm)	69 ± 3	67 ± 4	72 ± 5
VC STI	**1.17 ± 0.01**	**1.16 ± 0.01**	**1.18 ± 0.02**
MCL (μm)	613 ± 22	583 ± 8	624 ± 17
AV (μm)	516 ± 18	472 ± 16	476 ± 13
AVTI	**1.19 ± 0.02**	**1.24 ± 0.03**	**1.31 ± 0.03**

All values are presented as mean ± SEM. W/C ratio is given by the area of the left ventricular wall (including septum) to the area of the ventricular cavity; sl = sarcomere length; AC = arteriolar capillary; VC = venular capillary; Seg = the length of individual capillary segments; Node = distance between successive capillary branch-points; STI = capillary segment tortuosity index; MCL = minimal capillary length; AV = distance between arteriole and venule; AVTI = arterio-venous tortuosity index.

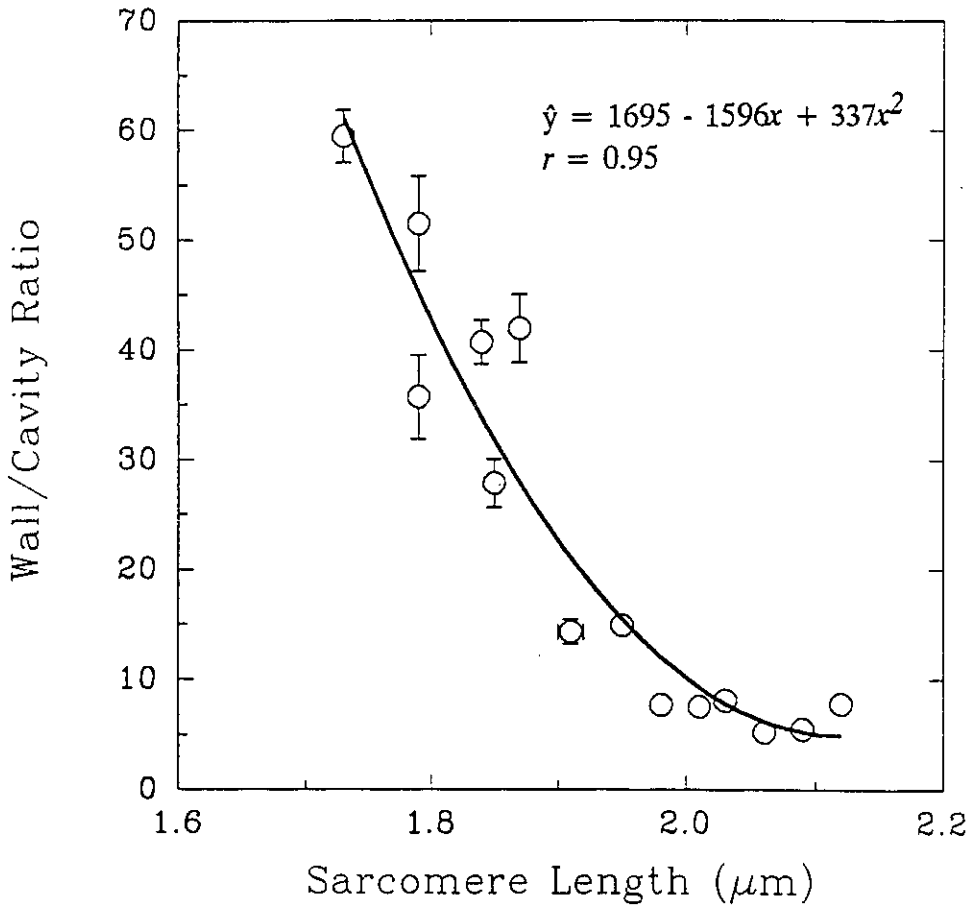

FIG. 1.1 Second order regression line of wall/cavity ratio versus sarcomere length. Symbols represent the mean ± SEM for each heart (n=14).

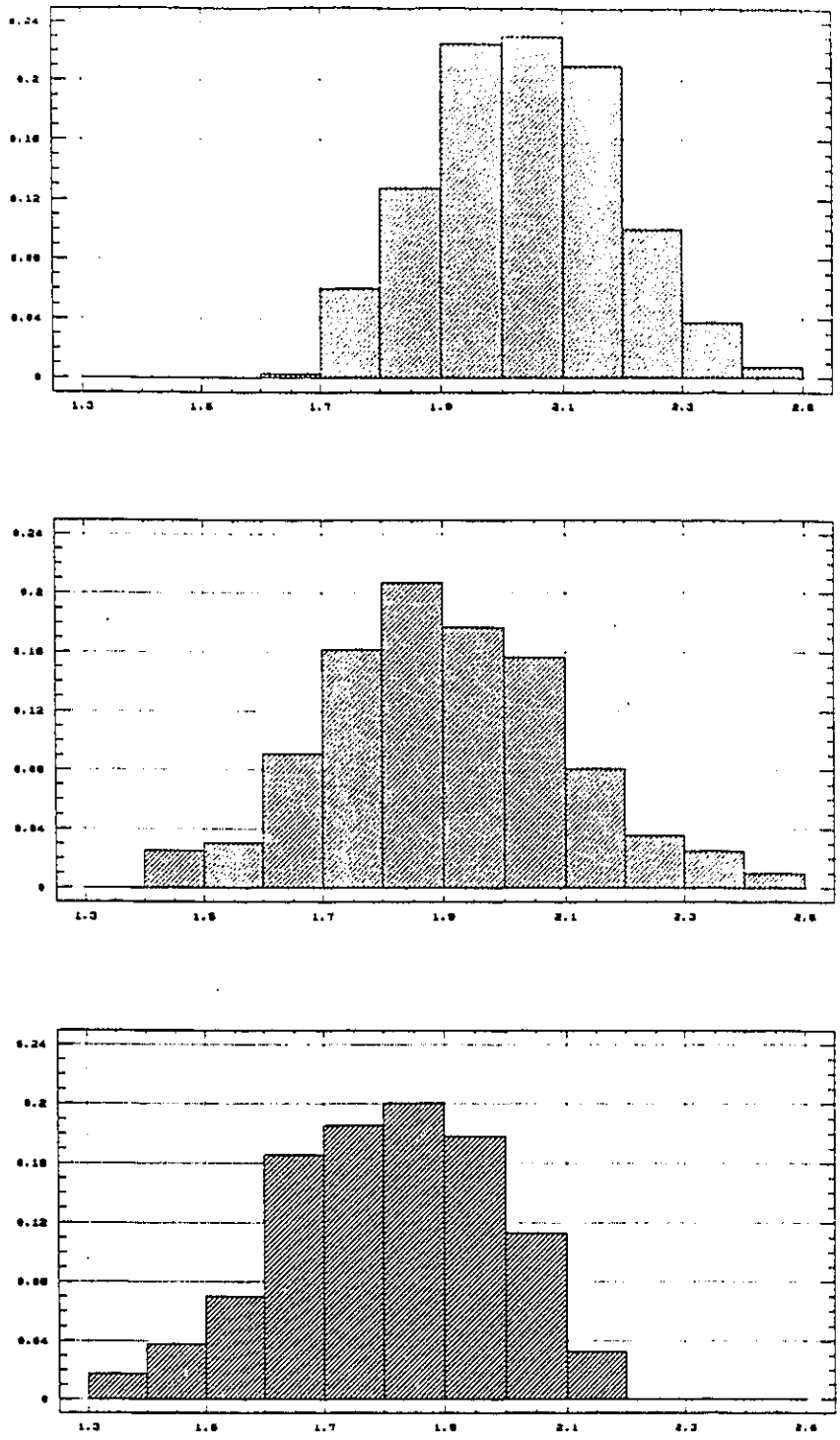

FIG. 1.2 Frequency histograms of sarcomere length in diastolic (upper), intermediate (middle) and systolic (lower) arrested hearts.

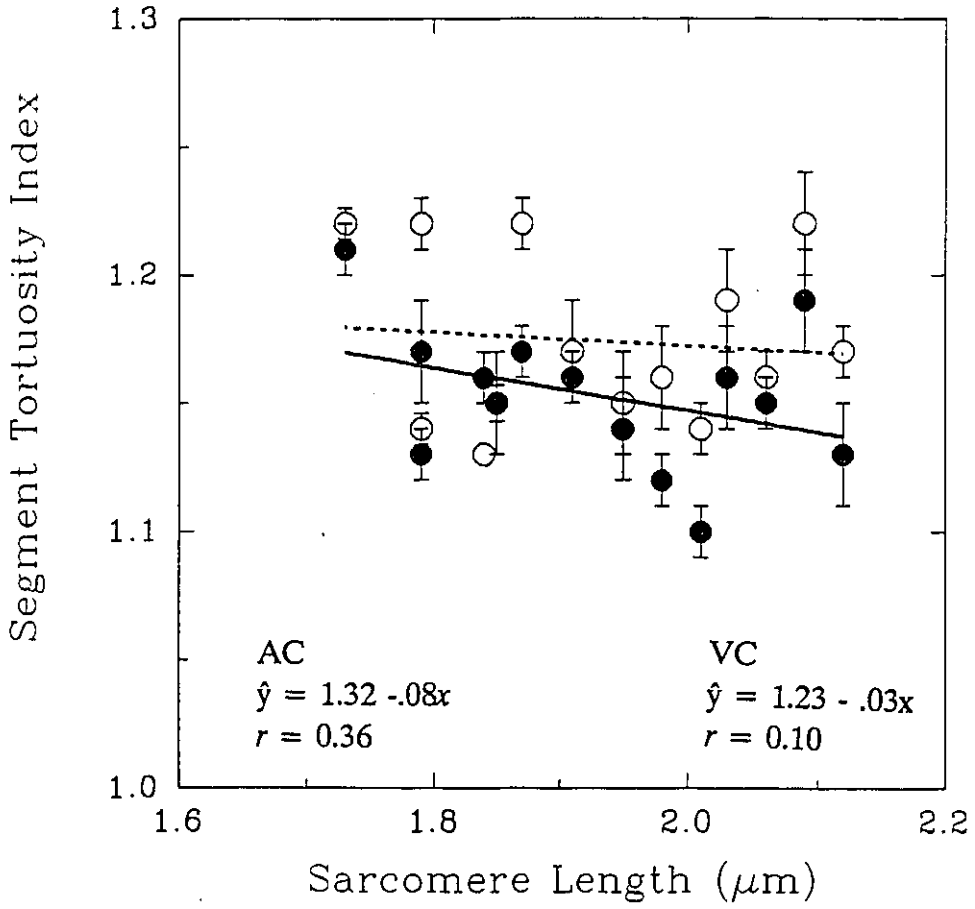

FIG. 1.3 Linear regression lines of arteriolar capillary (AC, solid line and symbols) and venular capillary (VC, broken line and open symbols) segment tortuosity index. Symbols represent the mean ± SEM for each heart (n=14).

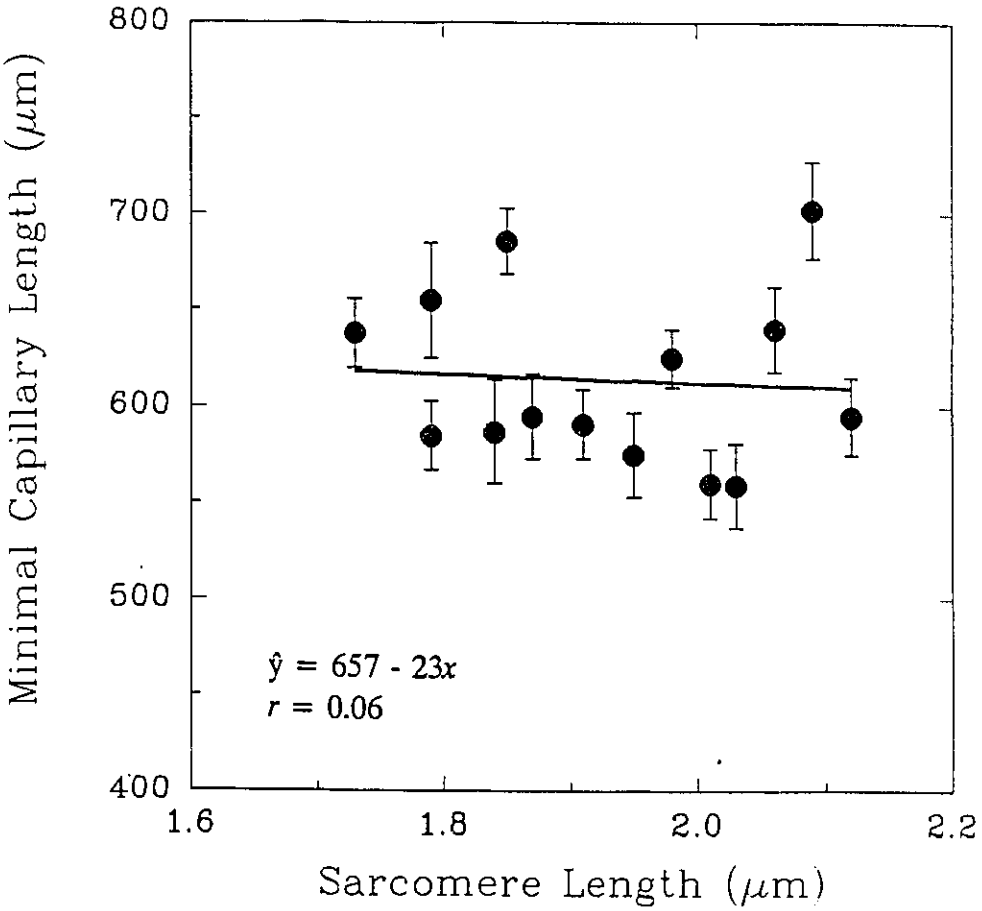

FIG. 1.4 Linear regression line of minimal capillary length versus sarcomere length. Symbols represent the mean ± SEM for each heart (n=14).

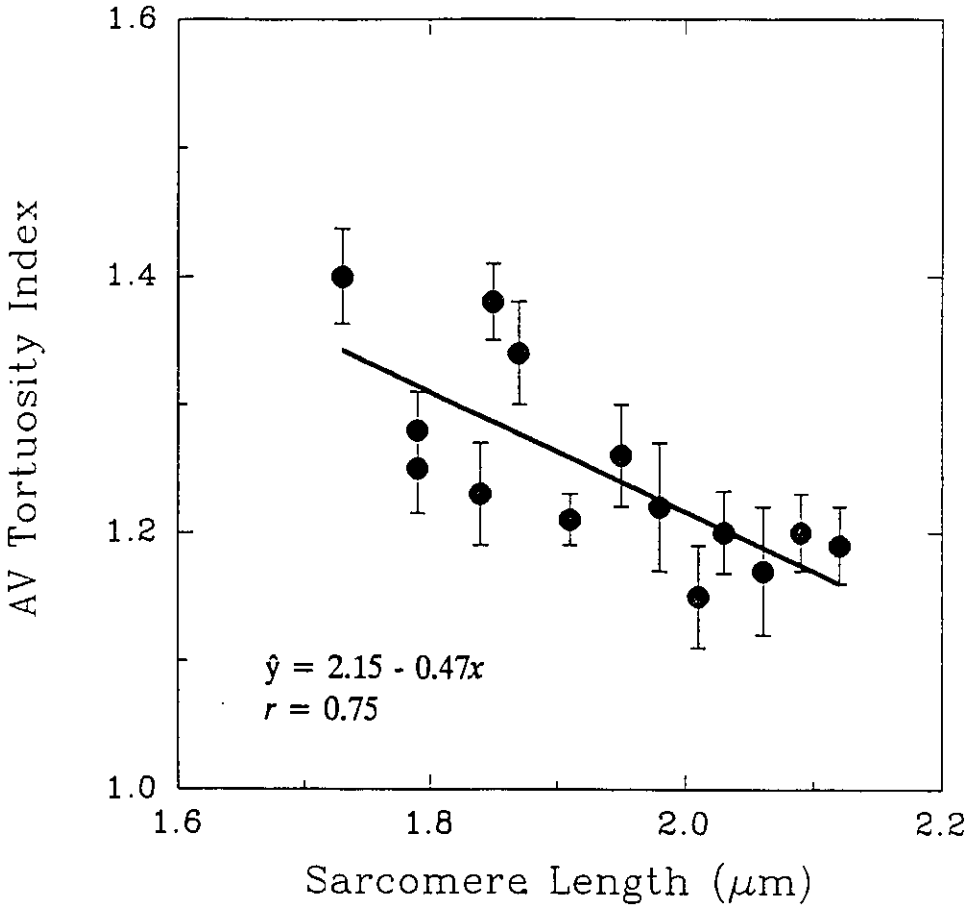

FIG. 1.5 Linear regression line of arterio-venous capillary tortuosity index versus sarcomere length. Symbols represent the mean ± SEM for each heart (n=14).

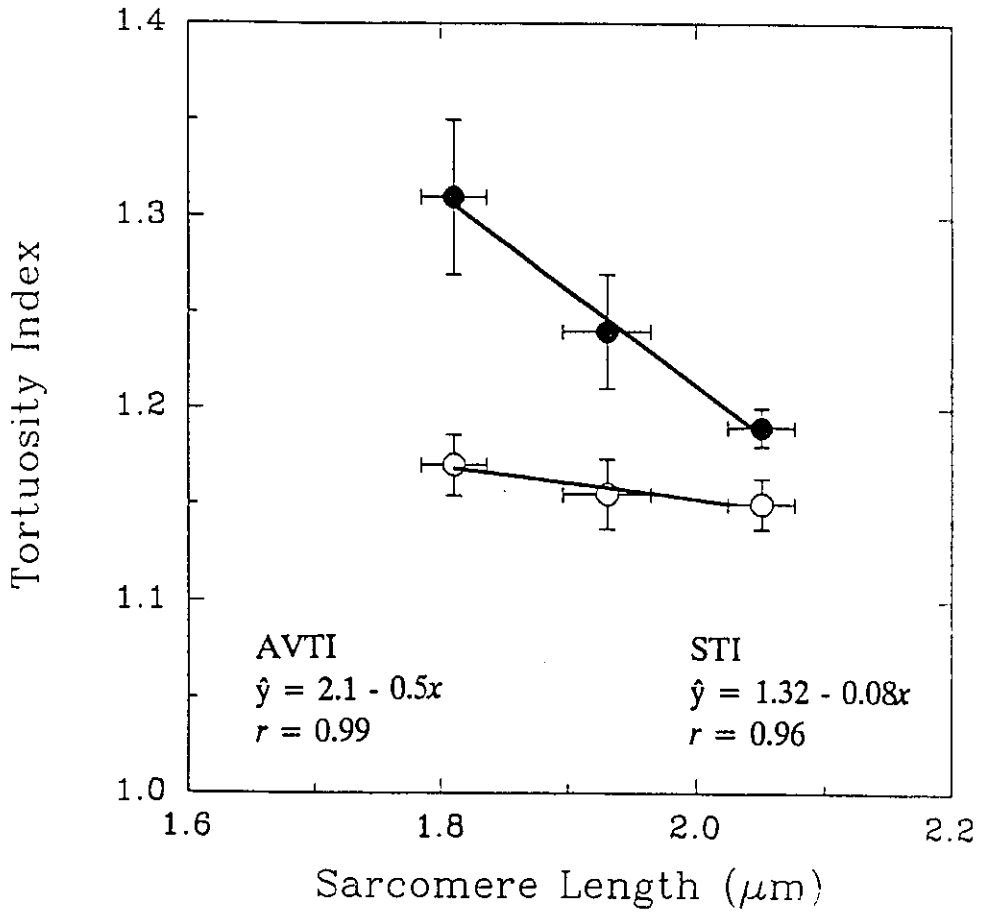

FIG. 1.6 Linear regression lines of arterio-venous tortuosity index (solid symbols) and capillary segment tortuosity index (open symbols) versus sarcomere length. Symbols represent the mean ± SEM for each heart (n=14).

CHAPTER 2: CAPILLARY NETWORK GEOMETRY DURING NORMAL POSTNATAL GROWTH

INTRODUCTION

In Chapter 1, we have described changes in capillary geometry observed as a function of cardiac fiber shortening in the young adult rat myocardium. In this Chapter, we consider capillary geometry in hearts arrested in diastole, at four different stages during the development and growth of the mammalian myocardium. Indeed, this period is characterized by a structural integration of many time-dependent phenomena. Prior to birth, increases in heart mass are associated primarily with myocyte hyperplasia. Then just before birth and extending through the weaning period there is a shift from hyperplastic to hypertrophic growth. Following the weaning period, further increases in heart mass are associated with myocyte hypertrophy (Rakusan et al. 1965). Throughout these stages of development, the increase in cardiac mass is accompanied by an expansion of the capillary network, in an effort to meet the oxygen requirements of the increasing heart size (Anversa et al. 1986c). The quantitative methods previously used to assess capillary supply during growth have primarily relied upon measurements of capillary density and myocardial capillary-fiber (C/F) ratio from tissue cross sections (Rakusan, 1984). Measurements of capillary density only serve as a general index of the geometrical conditions for oxygen supply, as this

assessment does not account for the variability of capillary spacing within the region of tissue from which capillary density is measured. In addition, measurements of capillary density do not provide any information regarding capillary length parameters. Measurements of C/F ratio are not sensitive to changes in myocyte size during growth. These morphometric methods may render divergent results, making the interpretation of capillary supply data during growth ambiguous. For example, following the weaning period, capillary density decreases while the C/F ratio continues to increase. This would suggest that capillary proliferation is occurring during the period of myocyte growth, but this is not sufficient to maintain a constant capillary density. Is growth then characterized by altered conditions for oxygen supply? For the interpretation of these data it is necessary to quantitate capillary geometry in more comprehensive terms.

To this end, we have employed a novel approach to the analysis of capillary nets in the developing rat myocardium from cross and longitudinal sections. As outlined in the Introduction, and detailed in Appendix 1, the histochemical techniques allowed us to distinguish arterioiar and venular capillary regions by color. All data were then collected and classified as a function of capillary region, along the capillary path from arteriole to venule. Given that PO_2 values are lower towards venular capillary regions, the purpose of this study was to determine if there were differences in capillarization toward venules, which would

serve to improve the geometric conditions for oxygen supply. This study presents for the first time, quantitative data regarding the geometry of capillary nets during postnatal growth of the heart, with specific attention to differences between arteriolar and venular capillary regions.

METHODS

Male Sprague-Dawley rats at 21, 28, 60 or 240 days after birth were used in this study. Groups consisted of 8, 8, 18 and 8 animals, respectively. Rats from the 60 day group served as the controls in studies of pressure and volume overload (Chapter 3 and 4, respectively). Rats at 8 and 13 days of age were also considered, but the histochemical methods provided incomplete and therefore unreliable results, suggesting that the enzyme profile of the capillary endothelium was not fully established at these earlier stages of development. Following anaesthesia with pentobarbital sodium, hearts were arrested in diastole (KCl), rapidly excised, weighed, dissected and frozen in liquid nitrogen. From each heart, two tissue blocks were dissected and oriented, one parallel (for cross sections) and one perpendicular (for longitudinal sections) to the base-apex axis. Cryostat sections were taken (16μm) from each block and prepared for differential staining (Appendix 1).

Cross Sections

From tissue cross sections, capillary profiles were represented as a bivariate (AC, blue; VC, red) point pattern in two dimensional space. Three fields per heart, consisting of approximately 200 capillary profiles each were digitized from a graphics tablet and entered into our software program for capillary domains (Hoofd et al. 1985). The capillary domain program serves to divide the tissue plane into polygonal regions of tissue, each polygon enclosing one capillary. The area subtended by these polygons, the capillary domain, is closer to the enclosed capillary than any other. Capillary domain areas were classified according to the histochemical type of the enclosed capillary (AC or VC). From individual domain areas, the equivalent (Krogh) radius of a cylinder with the same area was calculated. As the distribution of these radii is log-normal (Turek and Rakusan, 1981), their variability is characterized by the standard deviation of the logarithmic distribution (SDlog). Accordingly, the index of heterogeneity of capillary spacing, SDlog, was determined for arteriolar and venular capillary regions.

Longitudinal Sections

From tissue longitudinal sections, 4-6 scale drawings were made per heart of capillary pathways from terminal arteriole to collecting venule. A capillary set, which was an extraction of all capillary pathways that could be clearly followed from the same terminal arteriole to collecting venule, served as the basic unit of

study. Capillary set length (CSL) was measured as the total length of all capillaries in the set. The relative contributions of arteriolar (AC) and venular (VC) capillaries to the capillary set were also recorded. Minimal capillary length (MCL) was measured as the shortest capillary pathway from arteriole to venule. The number and length of AC and VC segments (the distance between two successive capillary branch points) in each capillary set were also measured. To assess the profile of the capillary set, the length/width ratio of each capillary set was also determined. In addition, the number of adjacent capillaries, which refers to the number of capillaries within each set running in parallel from arteriole to venule, was also recorded. The capillary set area (CSA), which was the tissue region enclosing the capillary set was also measured from the scale drawings. The overall index of gas exchange potential, as measured from longitudinal sections, was defined as the capillary set length/area ratio. This index served to incorporate the sum of capillary lengths and the enclosed tissue area of each capillary set.

Statistical Methods

All results are reported as mean ± SEM. The one-way analysis of variance was used to test for significant differences in appropriate parameters occurring during growth. For data that were collected as a function of AC and VC regions, a two-way analysis of variance was used to test for differences due to growth and

capillary region, respectively. As conditions of linearity between dependent and independent variables were generally not met, regression lines of appropriate order were plotted. The coefficient of determination, which is an index of the total variation in the dependent variable that is explained by the regression model, was used to determine the appropriate order of the regression line. The polynomial order, the equation and correlation coefficient (r) of each least-squares regression line is included in the figure legends. Differences in the slope and intercept of regression lines between AC and VC parameters were tested for following conversion of LV mass data to a logarithmic scale.

RESULTS

Body mass and left ventricular mass (Table 2.1) showed increases with growth at all levels ($P<0.01$). This study spanned an interval where body mass and LV mass increased by 12.5-fold and 6.5-fold, respectively. The rate of increase in left ventricular mass was less than that of body mass, as suggested by the stepwise decline in LV/BM ratio. As the correlation between age and left ventricular mass was very high ($r=0.95$), all morphometric data have been plotted as a function of left ventricular mass. Note that in Figs. 2.5, 2.7-2.10, two sets of additional data points have been included. These data points were generated from studies of pressure (Chapt. 3) and volume (Chapt. 4) overloaded rat myocardium, and will be addressed in the Discussion of this Chapter, as well as in Chapter 5.

Cross Sections

Data derived from tissue cross sections are given in Table 2.2. Both AC and VC domain areas displayed stepwise increases ($P<0.01$) with LV mass, reaching maximal values by 60 days of age. Figures 2.1 and 2.2 suggest a nonlinear relationship between these domain areas and LV mass. The greatest increases in domain area occur early, and tend to plateau off at LV mass over 600 mg. There was an increased scatter within and between individual heart values with increases in LV mass. On the venular side of the capillary net, the tendency for smaller capillary domains was evident. In all age groups, AC domain area was significantly larger than VC domain area ($P<0.01$). This would indicate greater capillary densities and shorter intercapillary distances towards the venular side of the capillary set, which were established by 21 days of age, and preserved throughout the range of study.

The regression lines of AC and VC domain area versus LV mass on a logarithmic scale (Fig. 2.3) were extrapolated by approximately one order of magnitude above and below the range of observed data. Both AC and VC domain areas demonstrated a significant relationship ($P<0.001$) with LV mass. The slope and intercepts of these lines were not significantly different from one another. Increases in capillary domain areas with LV mass were reflected in a 44% reduction in capillary density from 21 to 240 days of age ($P<0.01$). The heterogeneity of capillary spacing (SDlog) in AC regions was greater in the 240

day group as compared to corresponding values at 21 or 28 days of age ($P<0.01$, Table 2.2).

Longitudinal Sections

Data derived from tissue longitudinal sections are given in Table 2.3. Capillary set length (CSL) values were decreasing with increasing LV mass (Fig. 2.4). The scatter of CSL values within and between hearts was noticeably greater with increasing LV mass. The reduction in CSL (approx. 10%) coincided with an increase in minimal capillary length (MCL, Fig. 2.4) of approximately 20% ($P<0.01$). Accordingly, the contribution of MCL to the CSL increased from 15% (21 day) to 21% (240 day). The capillary set was composed of both AC and VC components. With growth, there was a shift in capillary staining response, which served to increase the AC component at the expense of the VC component (Fig. 2.5).

The length of individual capillary segments within the capillary set displayed progressive increases until 60 days of age (approximately 600 mg LV mass). Beginning at 28 days of age, AC segment length was significantly longer than VC segment length ($P<0.01$). Both AC and VC segment length demonstrated a strong relationship ($P<0.001$) with LV mass (Fig. 2.6). However, the slope and intercepts of these lines were not significantly different from one another. The number of AC and VC segments per set were both significantly reduced with

growth ($P<0.01$). We occasionally observed mixed capillary segments (1-3 per set), that captured the transition zone from arteriolar to venular capillary regions. These mixed segments were significantly longer (197 ± 38 μm; pooled mean ± SEM, $P<0.01$) than either AC or VC segments.

The shape of individual capillary sets was characterized by the length/width ratio (Fig. 2.7). With growth, capillary sets increased more in width than length, resulting in a 50% reduction in the length/width ratio ($P<0.01$). The lateral expansion of capillary set with growth is depicted by an increase in the number of adjacent capillaries traversing the path from arteriole to venule ($P<0.01$, Fig. 2.8). The capillary set area showed an increase of 150% over the course of this study (Fig. 2.9). In combination with the reduction in the capillary set length, the increase in capillary set area gave rise to a significant reduction in capillary length density, as expressed by the capillary set length/area ratio ($P<0.01$. Fig. 2.10)

DISCUSSION

Coronary capillaries and cardiac myocytes comprise the two principal components of cardiac tissue. The importance of the relationship between these two components is underscored by the critical role of capillaries in supplying oxygen to the working myocytes. The geometrical conditions for the diffusion of oxygen are influenced not only by the capillary density, but also by the spatial geometry of capillaries within the tissue. Morphometric data regarding the

geometry of capillaries in the myocardium have generally been limited to average measurements taken from thin sections cut transverse to the myofiber axis. Unfortunately these measurements do not provide any information regarding capillary length parameters, which are necessary for more realistic models of oxygen supply. The purpose of the present study was to obtain these additional data at different stages of normal growth in the rat myocardium.

Hypertrophy as well as hyperplasia of myocytes in the rat heart persists throughout the weaning period (Anversa et al. 1980; Rakusan, 1984). Anversa and coworkers (1980) showed that during the first 11 postnatal days in the rat left ventricle, myocyte hypertrophy and proliferation increased by 2.7-fold and 2-fold, respectively. The number of myocytes layers across the left ventricle reaches adult values at approximately 3 weeks of age (Anversa et al. 1986c). Rakusan and coworkers first proposed that myocyte proliferation ceases at the time of weaning (Rakusan et al. 1965). Others have since suggested that this may occur slightly earlier (Claycomb, 1976) or later (Dowell and McManus, 1978), although the signals that cause myocytes to stop proliferating are still not completely known. During the weaning period, numerical capillary growth surpasses that of the myocytes (Anversa et al. 1986a), and the capillary/fiber ratio increases several fold in the ventricle of the rat (Olivetti et al. 1980; Rakusan and Poupa, 1963; Rakusan et al. 1965). During the first 11 postnatal days in the rat, there are 2- to 3-fold increases in the ratios of capillary volume and surface to myocyte volume

and surface, respectively (Olivetti et al. 1980). The increasing capillary proliferation during this early postnatal period leads to maximal capillary density values at approximately 3 weeks of age in the rat (Rakusan and Poupa, 1963; Rakusan et al. 1965) and 6 weeks in the rabbit (Rakusan et al. 1967).

The present study focused on the post-weaning period of cardiac development, where the increase in cardiac mass is due primarily to myocyte hypertrophy (Rakusan and Poupa, 1963). Korecky and Rakusan (1978) reported similar increases in the diameter and length (68% and 64%, respectively) of isolated myocytes in rats from 75 to 750 gram body mass. A decreasing capillary supply has been commonly observed during this period as the growth of myocytes exceeds that of capillaries (Anversa et al. 1980; Anversa et al. 1986a; Rakusan and Poupa, 1963). Anversa and coworkers (1986a) reported that following the weaning period, capillary density declines with growth until 80 days, and thereafter remains constant until 150 days of age. Despite the reduction in capillary density following weaning, the capillary/fiber (C/F) ratio continues to increase in man until reaching the adult values of approximately 1:1 (Roberts and Wearn, 1941), rat (Rakusan and Poupa, 1963) and rabbit (Shipley et al. 1937).

Mattfeldt and Mall (1987) used an allometric model to describe the growth of capillaries in papillary muscles of rats following weaning (5, 7, 13 and 52 weeks of age). The change in capillary morphometry with growth was characterized by the allometric exponent b, the ratio of growth rates of two logarithmically

transformed variables (e.g. left ventricular mass and capillary length density) according to the linear regression equation $y = ax^b$. The allometric method reduces the description a given morphometric parameter to mathematical terms (b) and may be compared with results from other laboratories. Results of regression analysis indicated that capillary length density was significantly reduced with normal postnatal growth, and similar allometric coefficients were calculated from data of previously published studies (Rakusan and Poupa, 1963; Tomanek et al. 1982; Anversa et al. 1984; Mall et al. 1986). These authors suggested that the reduction in length density may reflect a reduction in relative oxygen consumption during maturation. To summarize, it may be said that cardiac growth is accompanied by capillary proliferation that is not commensurate to the extent of myocyte hypertrophy.

The results of the present study suggested that the developing capillary network was characterized by systematic differences in capillary geometry from arteriolar to venular capillary regions. These differences were already present at 21 days of age, and persisted throughout the age range of the study. Unfortunately, we were not able to obtain reliable results in animals prior to 21 days of age. Following the weaning period, venular capillary domain areas were on average 15% smaller than arteriolar capillary domain areas, suggesting increased capillary branching and/or tortuosity towards the venular side of the capillary net. The increased venular capillary proliferation would provide

advantageous conditions for the diffusion of oxygen in capillary regions with generally low PO_2. Another important determinant for oxygen supply, the heterogeneity of capillary spacing, remained the same on the venular side of the capillary net with increasing age and cardiac mass. In contrast, the heterogeneity of capillary spacing increased for arteriolar capillary regions, indicating impaired geometrical conditions for the supply of oxygen. The overall increases in arteriolar and venular capillary domain areas with increasing left ventricular mass suggest that during growth, capillary supply does not match the increase in myocyte size. This reduction in capillary supply is more pronounced on the arteriolar side of the capillary network, and is coupled with an increased heterogeneity of capillary spacing.

The data derived from longitudinal sections were based upon the scale drawings of capillary sets, which represented unequivocal arterio-venous pathways. These capillary sets should not be viewed as an isolated set of capillaries, however, as there were numerous connections into and out of each capillary set. Given the tortuous nature of coronary capillaries, we were only able to focus on those capillaries forming contiguous pathways from the same arteriole and venule, and therefore remaining in roughly the same tissue plane. From these scale drawings, it was evident that there was a considerable expansion of the capillary set architecture with normal growth. This expansion was most pronounced in a lateral direction, due to an increase in both the number of and distance between

adjacent capillaries. It is of interest to note that the expansion of the capillary sets per unit tissue area was not accompanied by a concomitant increase in the aggregate capillary set length. This would indicate that capillaries in the set were spread less densely over a greater tissue area, as indicated by the reduction in capillary set length/area. These data present for the first time, evidence of a reduction in geometric conditions for the supply of oxygen, as determined from longitudinal capillary sections. Note that previous studies of regarding coronary capillary length measurements are described in the Introduction of the dissertation under the subheading "Capillaries in the Heart Muscle".

Under conditions of accelerated, pathological growth, it has been proposed that the type of cardiac overload influences the resulting pattern of microcirculation (Anversa et al. 1986a; Banchero, 1991; Rakusan, 1987; Mattfeldt et al. 1985b). The typical response to chronic pressure overload is a decrease in capillary density with no change in the capillary/fiber ratio in man (Roberts and Wearn, 1941), rabbit (Shipley et al. 1937) and rat (Rakusan and Poupa, 1966). When the pressure overload was induced in the adult rabbit, Rakusan and coworkers (1967), noted that the relative capacity of the terminal vascular bed, measured as capillary blood content per gram of tissue, was significantly lower than in normal hearts. In contrast, when the pressure overloading was induced in young rabbits, compensatory capillary proliferation occurred, maintaining the capillary supply as in normal animals. The pattern of the microcirculation

following chronic volume overloading is generally noted by a reduction in capillary density, particularly in the subendocardium. For a review, see Rakusan (1987).

In light of these data under conditions of normal growth, we were interested in whether pathological conditions (pressure and volume overload), represented an extension of normal growth at the level of the coronary microcirculation. Therefore, our question may be formulated as follows: how does pathological growth under conditions of pressure and volume overload compare with normal cardiac growth? As Figures 2.5, 2.7-2,10 contain summary data of normal growth (this Chapter), as well as pressure overload (Chapt. 3) and volume overload (Chapt. 4), these Figures will be discussed here. The reader may choose to return to these Figures following the reading of Chapters 3 and 4. An overall summary of capillary geometry during normal and pathological growth will be presented in Chapter 5. To reiterate, pressure overloading was induced by aortic constriction in neonatal rats. Volume overloading was induce by aortocaval fistula in young adult rats.

From Fig. 2.5, it is evident that with increasing left ventricular mass, the extrapolation of the arteriolar capillary set regression line is well fitted by the data point from volume overloaded hearts. The venular capillary set reduction, in both pressure and volume overload is smaller than expected from the prediction line based upon normal growth ($P<0.01$). Given that PO_2 values are lower closer to venular capillary regions, these additional venular capillaries would serve to

maintain optimal conditions for gas exchange. The capillary set length/width ratio (Fig. 2.7) is significantly greater in both pathological conditions as compared to the regression line based upon normal growth ($P<0.01$). Fig. 2.8 demonstrates that the increase in the number of adjacent capillaries with increasing left ventricular mass is well approximated by the data from volume overload. In the case of pressure overload, however, the number of adjacent capillaries is smaller than expected ($P<0.05$) from the normal growth curve, reflecting an increasing cell width which is not accompanied by the additional formation of new capillaries. The increase in capillary set area (Fig. 2.9) with normal growth is underestimated by both pathological conditions ($P<0.01$), but is closer to values expected from the normal growth relationship for the model of volume overload. In Fig. 2.10, the reduction in capillary length density with normal growth does not follow in both pressure and volume overloading ($P<0.01$). This index of capillary supply from longitudinal sections, the capillary set length/area, illustrates that the geometric conditions for oxygen supply deteriorate with normal growth. With both models of hypertrophy, there is a greater level of capillary adaptation than would be predicted from the linear regression line, indicating additional capillary growth, which was however, not commensurate to the increase in cardiac mass. Volume overload appears to maintain the geometric conditions for oxygen supply closer to normal values than the model of pressure overload, and more than that predicted by extrapolation of normal growth. This is in spite of the fact that the

model of pressure overloading was induced in neonatal rats, where the prospect of stimulating additional capillary growth would have appeared to be greatest.

In the present study, we have considered capillary geometry in the rat myocardium from the time of weaning (21 days) to adulthood (240 days). This period is characterized by systematic differences in capillary geometry from arteriolar to venular capillary regions. On the venular side of the capillary net, where PO_2 values are generally lower, the geometrical conditions for oxygen supply are notably enhanced. During normal postnatal growth, data from both cross and longitudinal sections indicate that overall geometrical conditions for oxygen supply are progressively reduced. This reduction in capillary supply parameters appears to be well correlated with the previously observed reduction in myocardial oxygen consumption in the rat during normal postnatal growth (Frolkis and Bogatskaya, 1968).

TABLE 2.1 Body Mass & Left Ventricular Mass Data During Development in Rat Myocardium

	AGE (days)			
	21	**28**	**60**	**240**
BM (g)	41 ± 1	86 ± 2	260 ± 4	513 ± 8*
LVM (mg)	129 ± 3	256 ± 6	605 ± 12	841 ± 25*
LVM/BM ratio	3.1 ± 0.1	3.0 ± 0.1	2.3 ± 0.1†	1.8 ± 0.1†

Note: all values are mean ± SEM; BM = body mass; LVM = left ventricular mass; LV mass includes septum.

* Significant effect ($P<0.01$) of age at all levels.

† Significant difference ($P<0.01$) from all younger age groups.

TABLE 2.2 Capillary Domain Areas and Heterogeneity Index During Development in Rat Myocardium

	Age (days)			
	21	**28**	**60**	**240**
Arteriolar domain (μm^2)	300±7‡	358±10†‡	501±13*‡	531±36*‡
Heterogeneity index SDlog	.063±.003	.057±.002	.066±.004	.073±.003*
Venular domain (μm^2)	258±8	318±5†	456±7*	452±12*
Heterogeneity index SDlog	.066±.003	.069±.003	.067±.001	.071±.003
Capillary density (mm^{-2})	3586±134	2895±124†	2276±112*	1996±148*

* Significant difference ($P<0.01$) from 21 and 28 day groups.

† Significant difference ($P<0.01$) from 21 day group.

‡ Significant difference ($P<0.01$) from matched venular domain.

TABLE 2.3 Capillary Length Data During Development in Rat Myocardium

	AGE (days)			
	21	28	60	240
Capillary set length (μm)	3604±98	3573±181	3148±78†	3209±208
Minimal capillary length (μm)	557±17	581±19	595±10‡	667±46†
AC segment length (μm)	57±2	78±2‡§	93±2†§	87±7†§
VC segment length (μm)	52±1	61±2‡	74±2†	70±1†
Number of AC segments per set	32±3	20±3‡	18±2‡§	24±2†§
Number of VC segments per set	32±3	20±2‡	10±1†	7±1†
Capillary set length/width ratio	7.9±0.8	6.6±0.7	4.4±0.4†	3.8±0.6†
Number of Adjacent Capillaries	3.7±0.2	4.5±0.3	5.7±0.4†	6.2±0.7†
Capillary set area (μm^2)	37503±1517	49222±1511	64609±2223	93713±2262*
Set length/area ratio ($\mu m/\mu m^2$)	0.09±0.005	0.07±0.005	0.05±0.004	0.03±0.005*

* Significant effect ($P<0.01$) of age at all levels.

† Significant difference ($P<0.01$) from 21 and 28 day groups.

‡ Significant difference ($P<0.01$) from 21 day group.

§ Significant difference ($P<0.01$) from matched venular measurement.

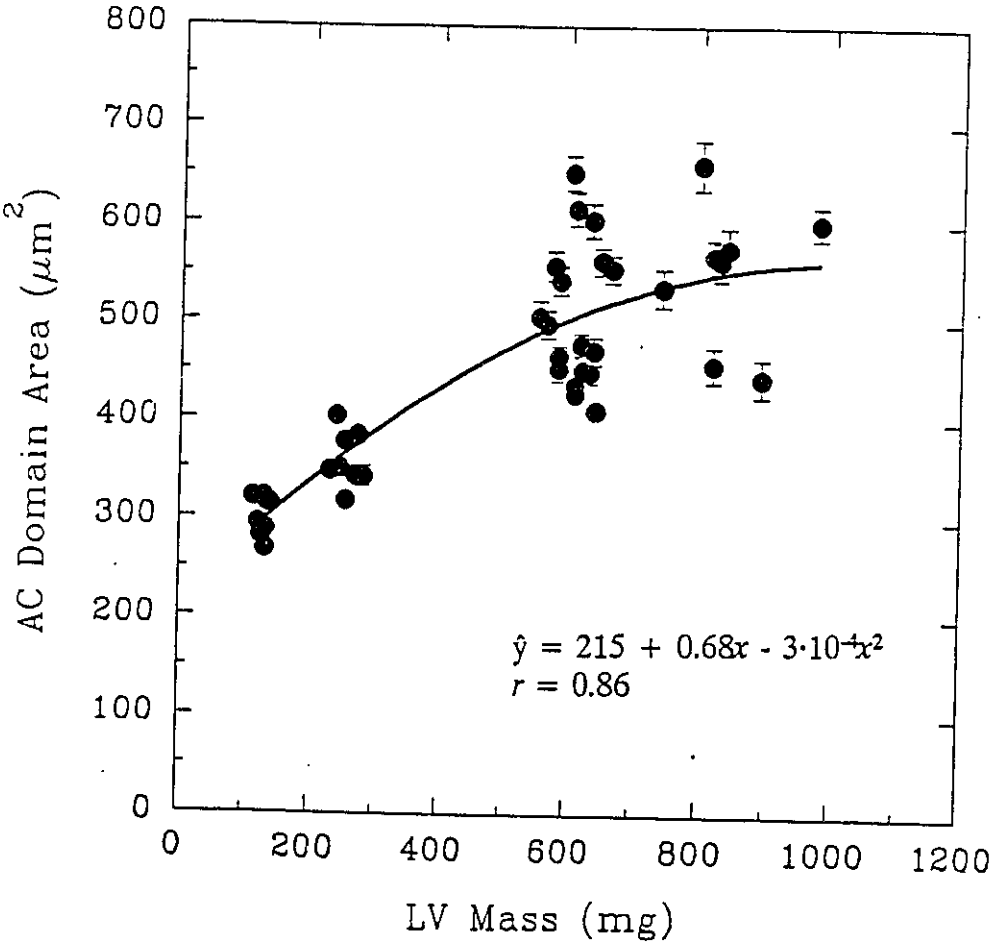

FIG. 2.1 Second order regression line of arteriolar capillary (AC) domain area versus left ventricular mass. Symbols represent the mean ± SEM for each heart (n=42).

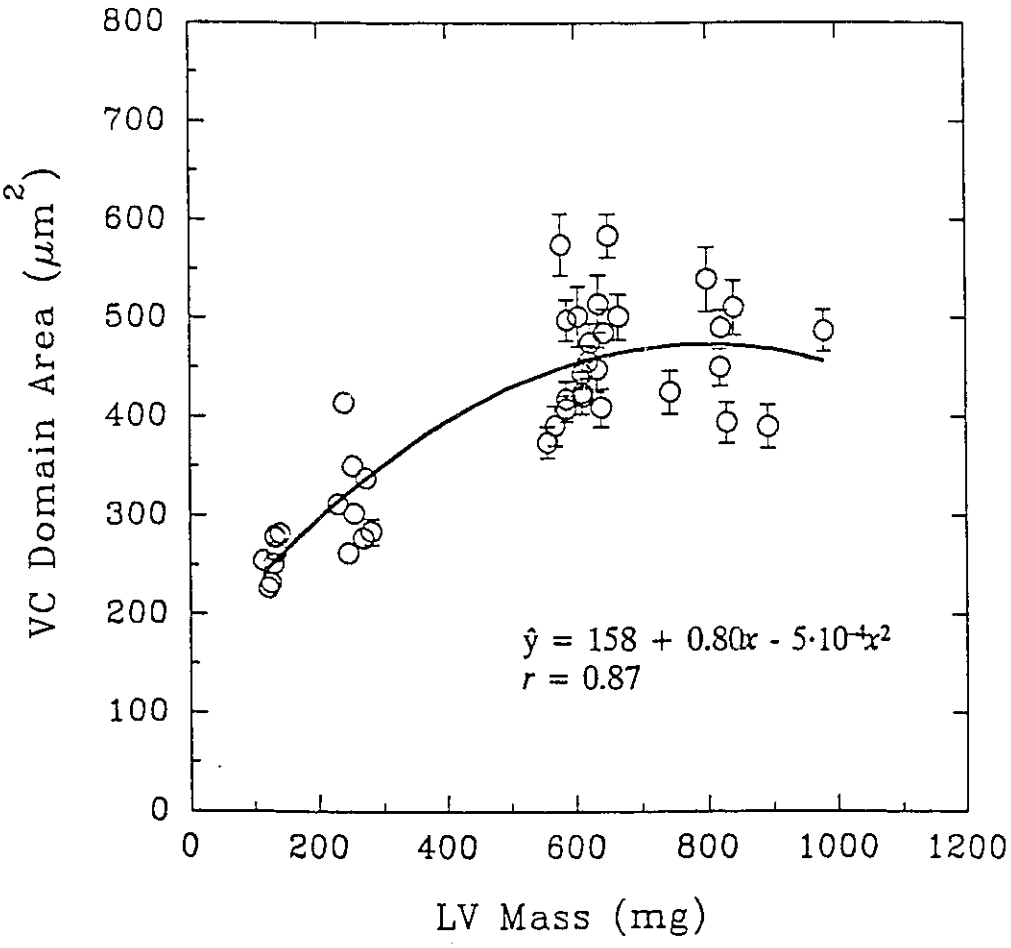

FIG. 2.2 Second order regression line of venular capillary (VC) domain area versus left ventricular mass. Symbols represent the mean ± SEM for each heart (n=42).

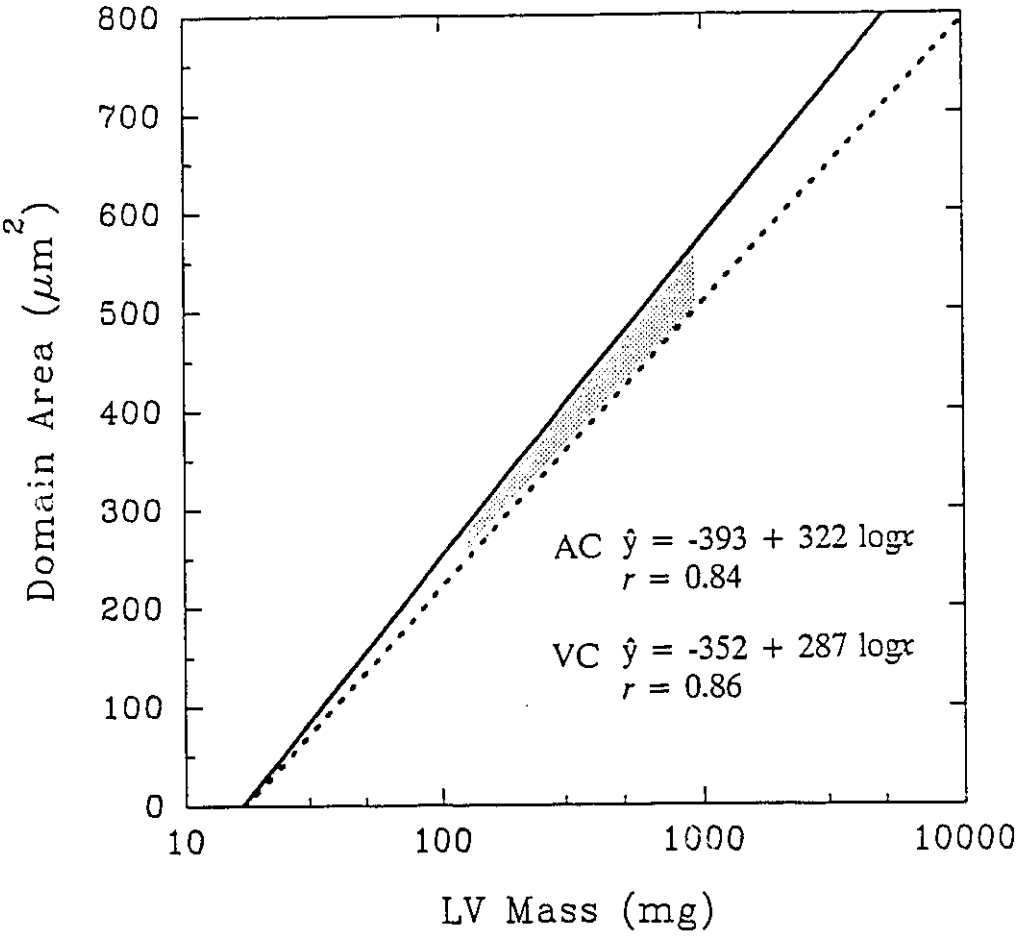

FIG. 2.3 Linear regression lines of arteriolar (AC, solid line) and venular (VC, broken line) domain area versus left ventricular mass. The shaded area represents the interval of observed values.

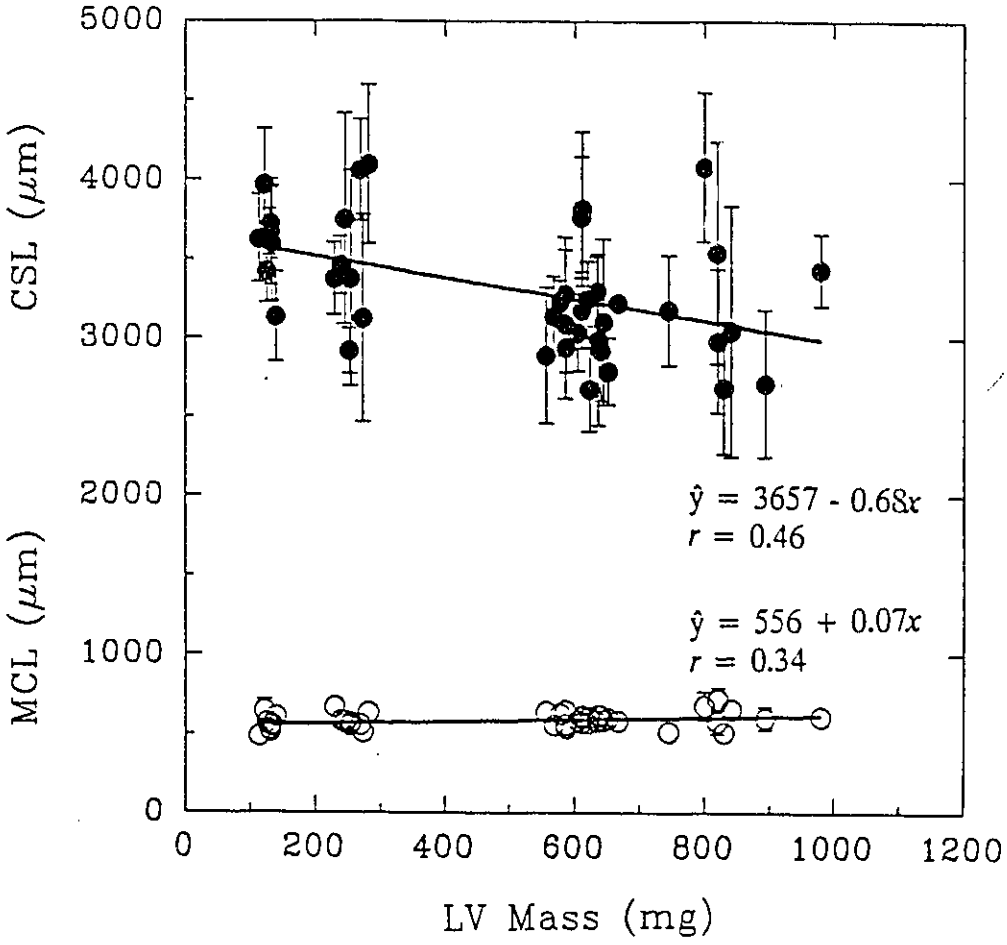

FIG. 2.4 Linear regression lines of capillary set length (CSL, filled symbols) and minimal capillary length (MCL, open symbols) versus left ventricular mass. Symbols represent the mean ± SEM for each heart (n=42).

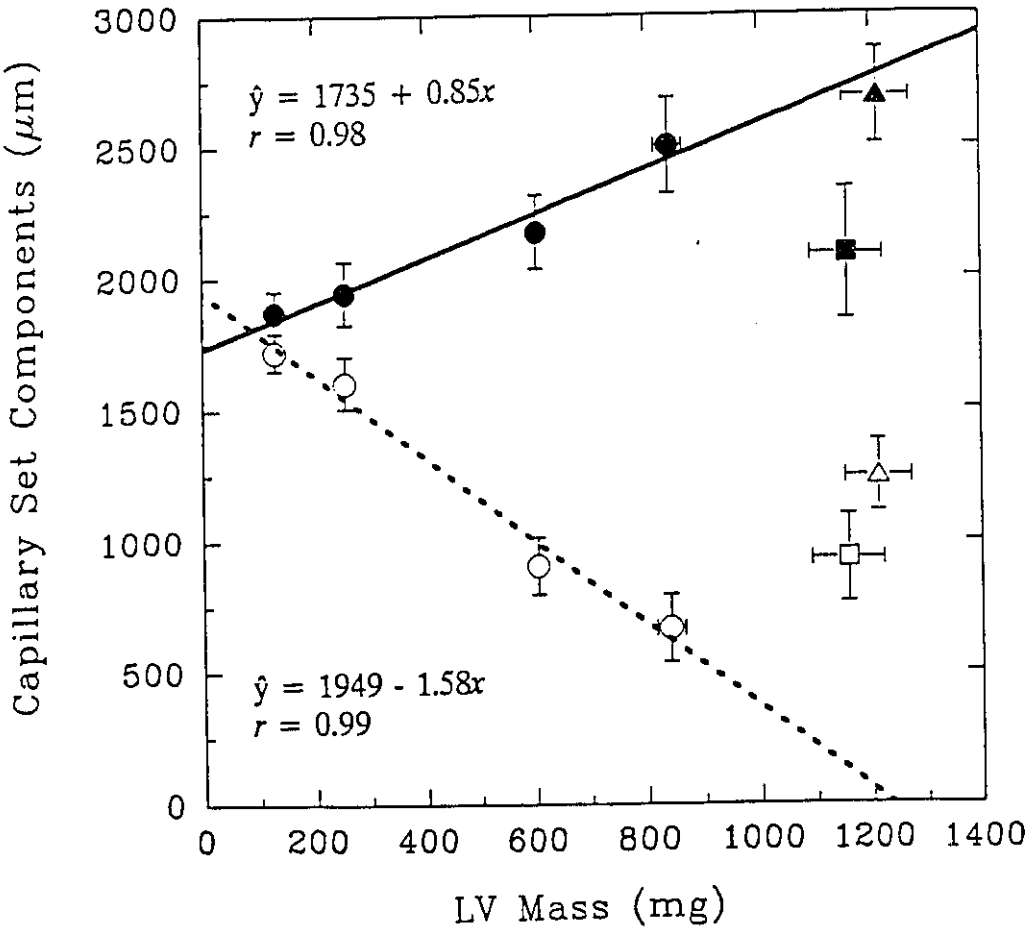

FIG. 2.5 Linear regression lines of arteriolar (AC, solid line and symbols) and venular (VC, open symbols and broken line) capillary set components versus left ventricular mass. The square and triangle symbols represent corresponding values from pressure (Chapt. 3) and volume (Chapt. 4) overloaded rat myocardium, respectively.

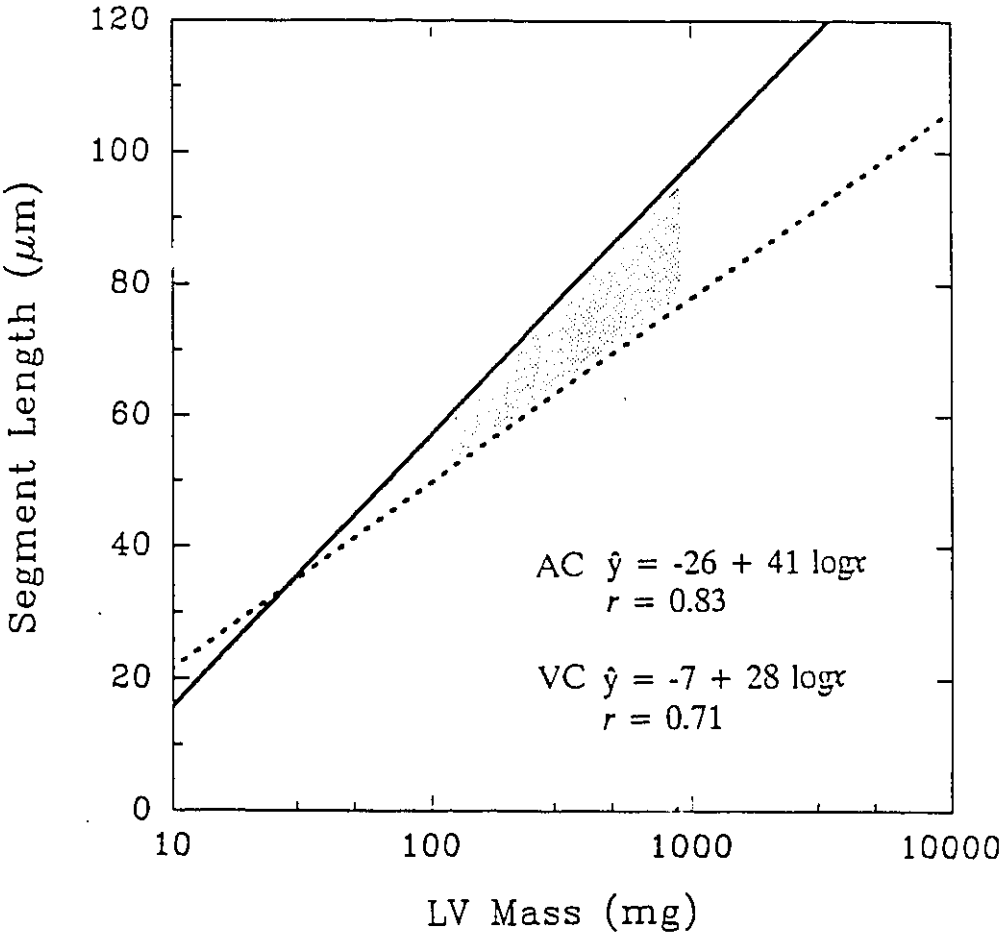

FIG. 2.6 Linear Regression lines of arteriolar (AC, solid line) and venular (VC, broken line) capillary segment length versus left ventricular mass. The shaded area represents the interval of observed values.

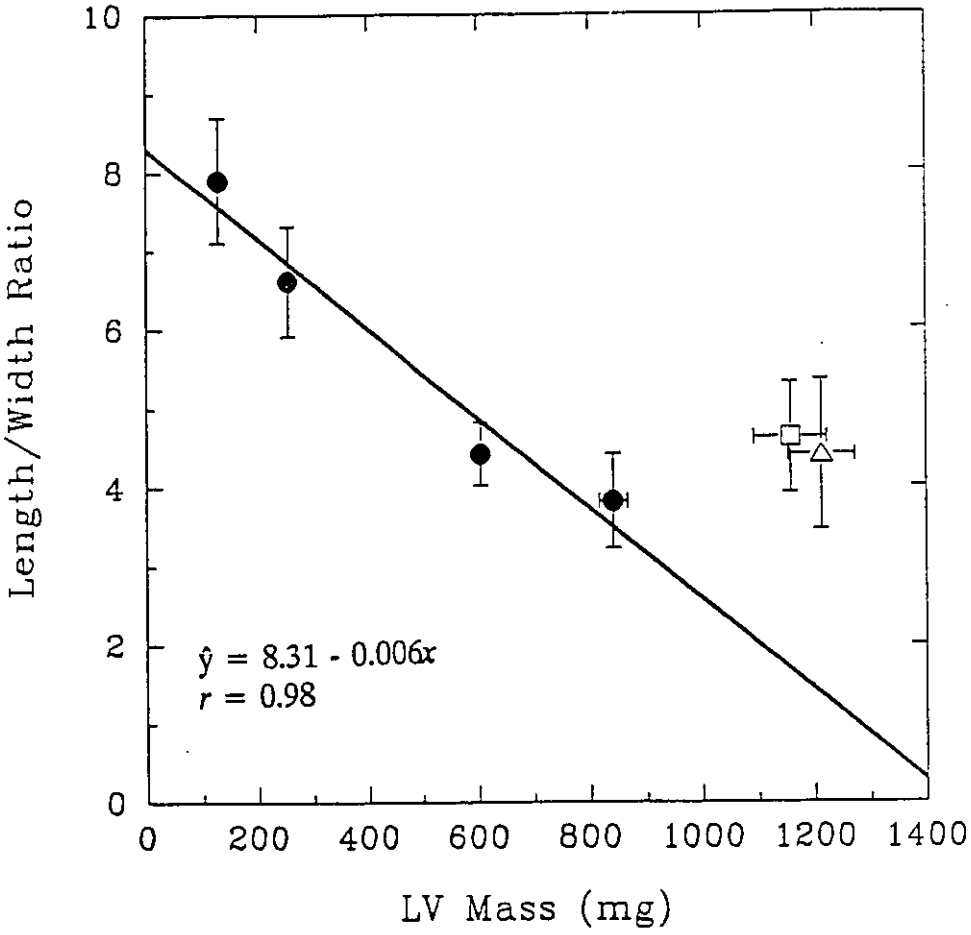

FIG. 2.7 Linear regression line of capillary set length/width ratio versus left ventricular mass. The square and triangle symbols represent corresponding values from pressure (Chapt. 3) and volume (Chapt. 4) overloaded rat myocardium, respectively.

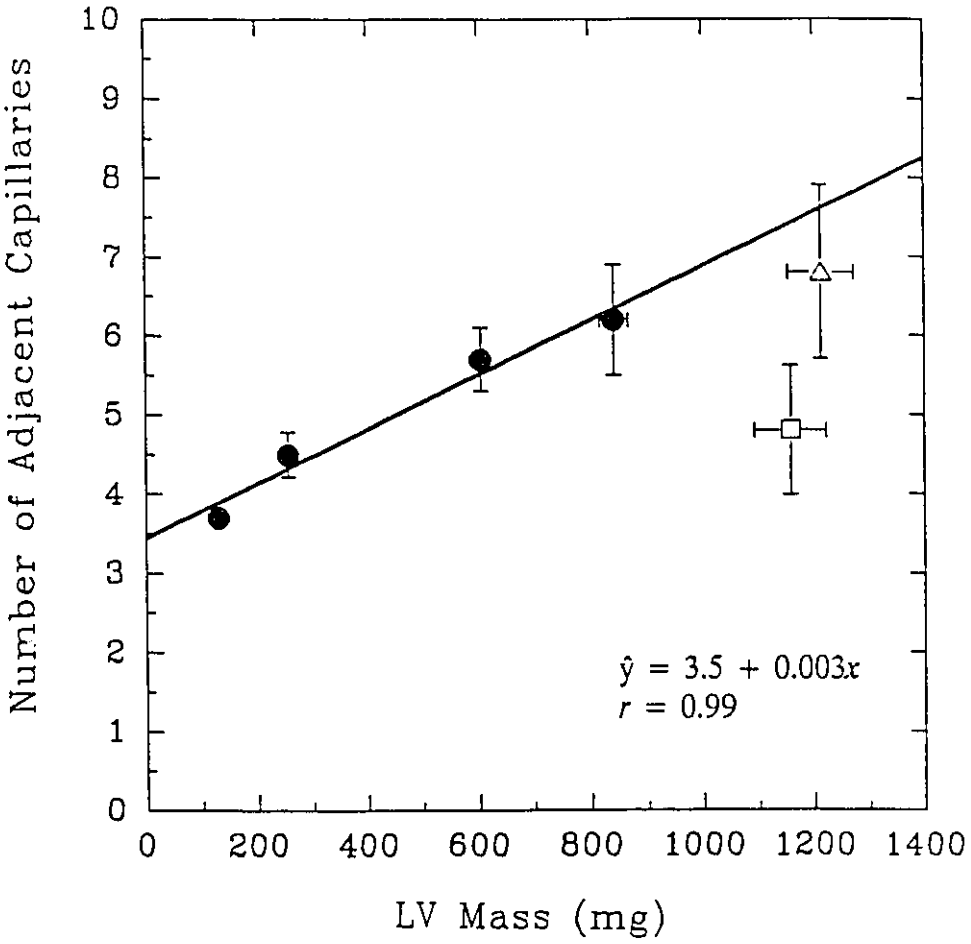

FIG. 2.8 Linear regression of the number of adjacent capillaries versus left ventricular mass. The square and triangle symbols represent corresponding values from pressure (Chapt. 3) and volume (Chapt. 4) overloaded rat myocardium, respectively.

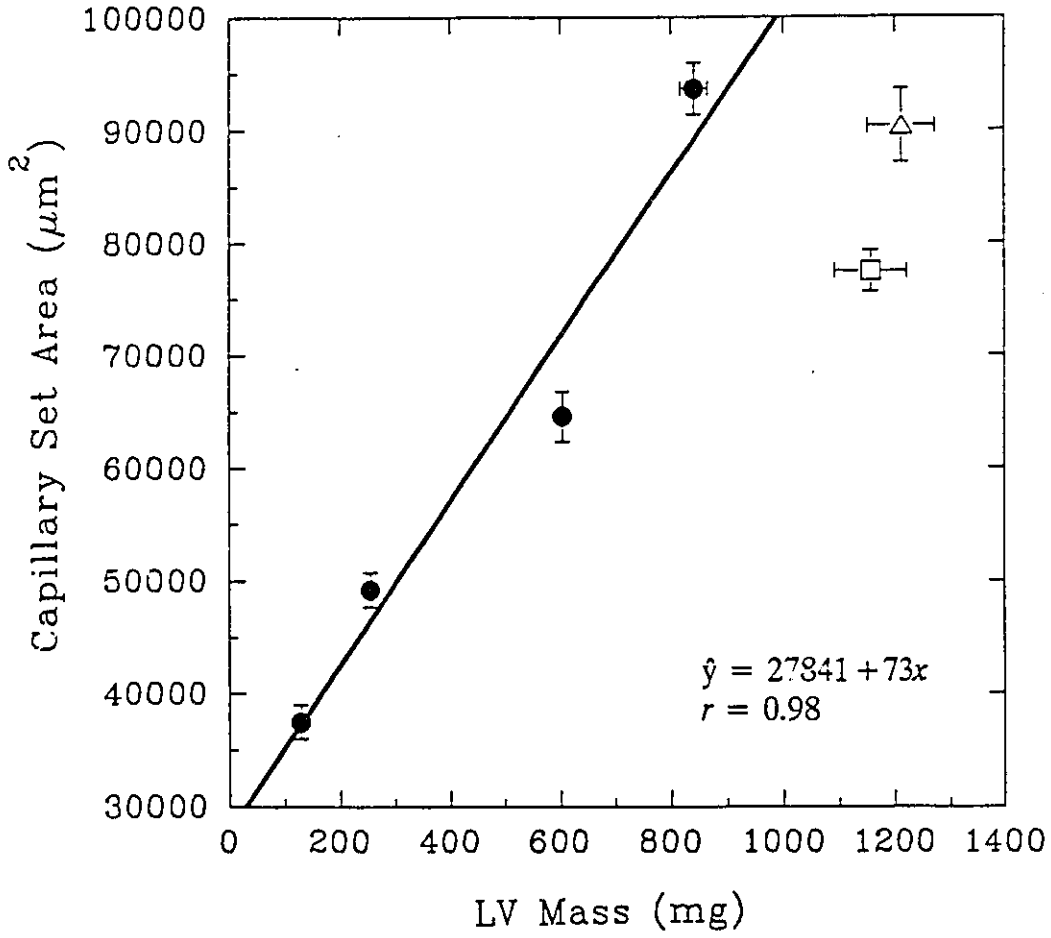

FIG. 2.9 Linear regression of capillary set area versus left ventricular mass. The square and triangle symbols represent corresponding values from pressure (Chapt. 3) and volume (Chapt. 4) overloaded rat myocardium, respectively.

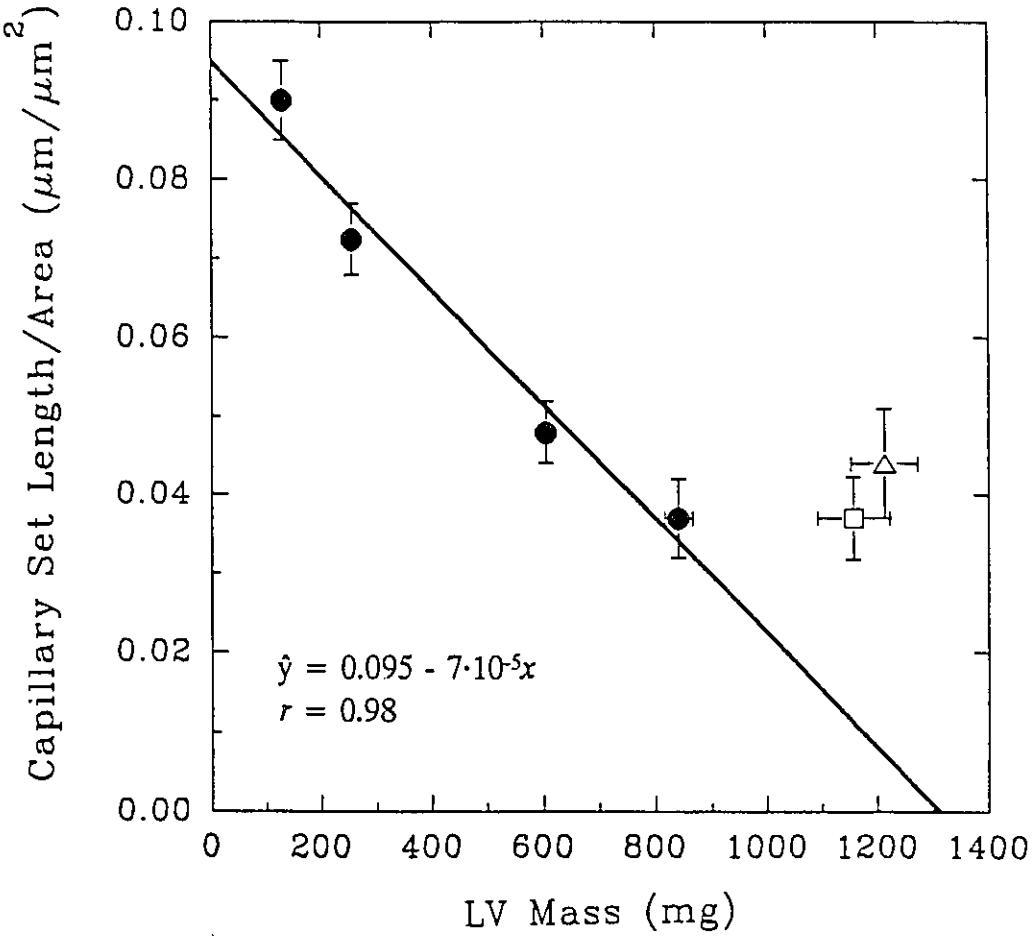

FIG. 2.10 Linear regression of capillary set length/area ratio versus left ventricular mass. The square and triangle symbols represent corresponding values from pressure (Chapt. 3) and volume (Chapt. 4) overloaded rat myocardium, respectively.

PLATE 4 Two-dimensional reconstruction of capillary domains in transverse section. Capillaries are represented as a bivariate point pattern.

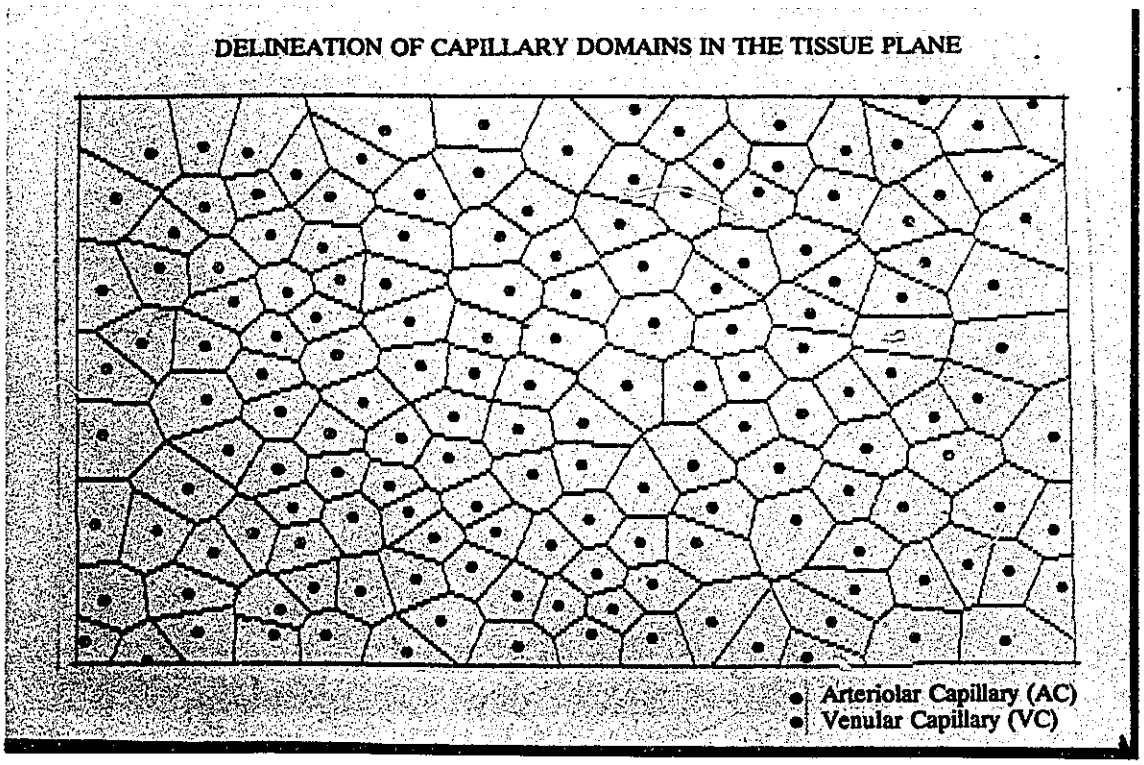

PLATE 5 Two-dimensional reconstruction of a capillary set, delineating capillary pathways from terminal arteriole (A) to collecting venule (V). Solid lines represent contiguous capillary paths that could be followed from the same arteriole to venule. Broken lines represent capillary paths entering or leaving the capillary set, but not contiguous with the same arteriole and venule.

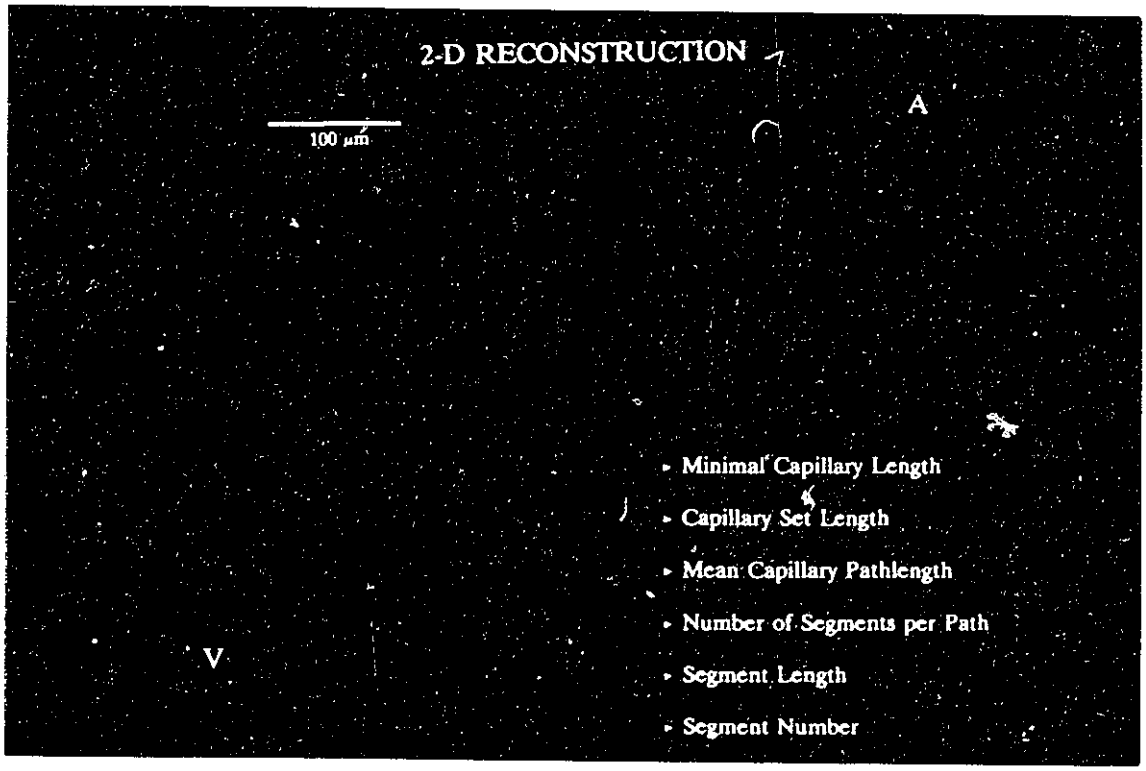

CHAPTER 3: GEOMETRY OF CAPILLARY NETWORKS IN PRESSURE OVERLOADED HEART

INTRODUCTION

The traditional approach to assess tissue capillarization for the modelling of oxygen transport has been the measurement of average capillary density, and the subsequent calculation of the Krogh cylinder radius. An extension of morphometric data on capillarization should certainly include measurements of capillary length and its associated branching phenomena, which would render tangible information in terms of red blood cell pathways from arteriole to venule. As discussed in the introduction to the Dissertation, the ability to obtain these data in cardiac muscle has been impeded, due to the difficulty of developing appropriate facilities for viewing surface vessels of a beating heart in situ; or in the development of morphological techniques that accurately demarcate tortuous capillary pathways from histological sections.

Morphometric techniques have been applied in the present study to evaluate the effect of pressure overload cardiac hypertrophy on the geometry of capillary networks. In this Chapter, we have employed a similar strategy as that used to assess capillary geometry in normal postnatal growth (Chapter 2). From tissue cross-sections, capillary supply regions as determined by the method of capillary domains, and the dispersion of these domains were analyzed. From longitudinal

sections, capillaries were traced from terminal arteriole to collecting venule and pathlengths, segment lengths and number of segments per path were recorded. In addition, distances between capillaries were measured at discrete intervals along the capillary pathlength. The task of following capillaries within longitudinal sections has proven to be rather difficult, which may explain the relative paucity of data in the literature. Part of the restriction lies in the procurement of tissue sections that capture a significant part of the capillary network. Further, it has been difficult to establish valid standards for histologically defining capillaries from arteriole to venule. In an effort to overcome some of these hindrances, we have employed a combination of histochemical methods that distinguished the arteriolar and venular portions of capillaries by color (Lojda, 1979).

It is well recognized that the myocardium, hypertrophied by a pressure overload, is characterized by decreased capillary density and increased variability of capillary spacing. (Rakusan, 1987). However, not much else in known about additional changes in capillary geometry with pressure overload hypertrophy. The present study takes advantage of this differential stain sensitivity, to analyze capillary geometry in normal and hypertrophied rat myocardium, with particular interest in geometry along the capillary pathway from arteriole to venule.

METHODS

Twenty male Sprague-Dawley rats were used in this study (body mass = 257 ± 5 g; mean ± SE). The rats were randomly divided into two groups: pressure overload hypertrophy (n=10; HYP) and sham-operated controls (n=10; CON). Pressure overload cardiac hypertrophy was produced by aortic constriction in 5 day old rats. Anaesthesia was induced with ether and maintained throughout the surgical procedure as required. Following a midline abdominal incision, the intestinal tract was deflected to one side to allow access to the abdominal aorta. A subdiaphragmatic suprarenal ligature was tied around the abdominal aorta, with a 30G hypodermic needle serving as the template. Sham-operated controls were surgically prepared at day five, but a ligature was not tied. At approximately 6 weeks post-surgery, following anaesthesia with pentobarbital sodium (4 mg/100g ip), the heart was arrested in diastole (KCl), quickly excised, weighed, dissected and frozen in liquid nitrogen. Two tissue blocks per heart, one parallel and one perpendicular to principle (base-apex) axis, were prepared for cryotomy. Sixteen μm sections were cut from the middle myocardium of the anterior left ventricular wall. The staining protocol is described in detail in Appendix 1.

Cross-Sections

Tissue cross-sections of the mid-myocardium were prepared by dissecting a block of tissue parallel to the principle axis of the heart and approximately half of the distance from base to apex. Three fields per heart, consisting of

approximately 200 capillaries each, were marked on an X,Y coordinate grid with the aid of a digitizing tablet linked to a software program (Bioquant IV, R&M Biometrics, Inc., Nashville, Tennessee). Average capillary densities were determined for each field, and the average radius of the Krogh tissue cylinder was calculated.

The area and variability of the Krogh cylinder was determined in each field by consorting each capillary profile within a Dirichlet cell (Ripley, 1981); a polygon that enclosed a region of tissue nearer to that capillary than any other, and designated the capillary domain. From the domain area, the equivalent radius of the Krogh cylinder with the same area is calculated. The distribution of these radii is log-normal, the variability being characterized by the logarithmic standard deviation (SDlog). In this manner, SDlog, the index of heterogeneity of capillary spacing was determined.

Longitudinal Sections

Longitudinal tissue sections of the mid-myocardial wall were prepared by cutting sections of tissue perpendicular to the principle axis of the heart. With the aid of a drawing tube attached to the microscope, scale drawings were made in fields where capillary pathways could directly be traced from terminal arteriole to collecting venule. A capillary set, defined as all of the micro-vessels connected to the same feeding arteriole and collecting venule, served as the basic unit of study. Some of these morphometric parameters have been previously defined in

Chapter 2, and are included here with several additional parameters. A total of fifty capillary sets, 4-6 from each heart were delineated for both CON and HYP groups and the following data were collected:

1. Minimal Capillary Length (MCL): the shortest contiguous pathway from terminal arteriole to collecting venule.

2. Capillary Set Length (CSL): all the micro-vessels connected to the same arteriole and venule.

3. Mean Capillary Pathlength: mean measure of all possible pathways that could be traced from arteriole to venule.

4. Number of Segments per Path: the number of segments constituting each pathlength.

5. Segment Lengths: the length of capillary segments (the distance between two ensuing branch points) that were defined as arteriolar, staining positive for Alkaline Phosphatase; venular, staining positive for Dipeptidyl Peptidase IV; and mixed, staining positive for both Alkaline Phosphatase and Dipeptidyl Peptidase IV.

6. Segment Numbers: the number of arteriolar (blue), venular (red), and mixed (blue and red, including transition zone) capillary segments in each set.

To consolidate the results from cross and longitudinal sections, distances between capillaries were measured at discrete intervals along the capillary set in longitudinal sections. Transect lines, drawn at right angles to a line joining the arteriole and venule, at 20% increments were constructed along the capillary set. The distances between capillaries that intersected this line were then recorded and classified according to capillary color. The approach integrated aspects of capillarity from cross-sections, and spatial position along the capillary set from longitudinal sections, into the same 2-dimensional capillary network.

Statistical Methods

Heart weights were compared between the CON and HYP groups with the Student's t-test. To allow direct comparison with other reported data, results are presented as mean ± SEM. Median values, as required for non-parametric analyses are reported only in the figure legends. Frequency analyses were performed for all morphometric data collected in this study. The Kolmogorov-Smirnoff Goodness-of-Fit (one sample) test served as the criterion for testing whether the observed distribution of frequencies for all parameters were

compatible with the normal distribution. The Mann-Whitney test was the non-parametric procedure of choice for two sample analyses of medians. The Kruskal-Wallis One-Way Analysis of Variance by Ranks was the analogous procedure for >2 sample comparisons; it was also applied to the analysis of all capillary length data to consider the variability within and between hearts. The Friedman Two-Way Analysis of Variance by Ranks was used to examine the effect of staining response and position from the terminal arteriole on capillary transect distances for both normal and hypertrophied hearts. The SDlog of the capillary domain radii, were compared by a parametric Two-Way Analysis of Variance. These statistical procedures have been reviewed by Gibbons (1985).

RESULTS

The present model of aortic constriction in neonatal rats allowed for slow-onset pressure overload, resulting in a substantial increase in cardiac mass. Table 3.1 shows data for body mass and heart mass for the control and hypertrophic groups. Left ventricular mass was 92.5% greater in hypertrophied hearts. Left ventricular mass to body mass ratio showed an increase of 109%.

Cross-Sections

Mean values for capillary domain areas are listed in table 3.2. These data were classified into two categories: arteriolar capillary (AC) and venular capillary (VC) domains, for both the control (CON) and hypertrophic (HYP) groups. For

all groups, the Kolmogorov-Smirnoff Goodness-of-Fit test (D statistic) indicated that these distributions were not consistent with the normal distribution. In control hearts, AC domain area was significantly larger than VC domain area (AC = 499 ± 3 μm^2; VC = 456 ± 5 μm^2, $p<0.01$). In hypertrophied hearts, the AC domain area was also larger than the VC domain area (AC = 547 μm^2 ± 6; VC = 464 ± 5 μm^2, $p<0.01$); with only AC domains showing a significant increase from control values, and thus exacerbating the difference between the arteriolar and venular capillary domain areas. The frequency histograms of capillary domain area in Figure 3.1 demonstrate the tendency towards smaller capillary domains on the venular side of capillaries for both control and hypertrophied hearts. In addition to this left shift in VC domain area for both groups, dispersion was lower, as illustrated by the interquartile range (IQR): CON-AC = 197 μm; CON-VC = 189 μm; HYP-AC = 223 μm; HYP-VC = 167 μm. The heterogeneity of capillary spacing (SDlog) was not significantly different between arteriolar and venular capillaries regions ($P = 0.32$). A trend was evident for greater heterogeneity of spacing in hypertrophied as compared to normal hearts ($P=0.06$).

Longitudinal Sections

Mean values for capillary morphometric data from longitudinal sections are given in Table 3.3. In normal hearts, average capillary set length was 3225 ± 103 μm. This measurement was restricted to only those capillaries that formed

contiguous pathways from the same terminal arteriole to collecting venule. Minimal capillary length was 593 ± 15 μm; average pathlength was approximately 10% longer (648 ± 8 μm), which would indicate that most capillary pathways followed the shortest path from terminal arteriole to collecting venule. The length of arteriolar capillary segments was significantly longer than venular capillary segments (AC = 95 ± 3 μm; VC = 75 ± 2 μm, $p<0.01$). Mixed capillary segments, where the transition from blue to red was noted, were relatively few in number (2-3 per set), but their length was more than twice the length of the arteriolar or venular capillary segments. The reason for these very long transitional segments lengths is not clear at the present time. The difference in the number of arteriolar, venular and mixed segments may be attributed to the fact that the majority of enzymatic activity was for Alkaline Phosphatase: approximately 70-75% of the capillary bed stained blue in color. This proportion did not significantly change from heart to heart, or between control and hypertrophied myocardium.

In hypertrophied hearts, the average capillary set length (CSL; Fig. 3.2, right) was significantly shorter ($P<0.01$) than in normal hearts. Minimal capillary length (MCL; Fig. 3.2, left) also showed a trend towards smaller values ($P = 0.23$). In contrast, average capillary pathlength (PATH; Fig. 3.2, middle) was significantly longer in hypertrophied hearts ($P<0.01$). This would indicate that despite no change in the shortest arteriole to venule pathway, other capillary paths were either more tortuous, or exhibited a greater degree of branching, and thus

increased in pathlength from arteriole to venule. There was a greater dispersion of data for minimal capillary length and mean capillary pathlength in hypertrophied hearts, as indicated by the interquartile range (MCL-CON = 104 μm; MCL-HYP = 136 μm; and PATH-CON = 159 μm; PATH-HYP = 247 μm). In contrast, capillary set length showed greater central tendency in hypertrophied hearts (CON = 1138 μm; HYP = 887 μm). The frequency histograms of capillary segment lerigth (Fig. 3.3) show no significant difference in arteriolar capillary segment length between normal and hypertrophic hearts. Venular capillary segment length, on the other hand, significantly increased ($P<0.01$) in hypertrophied hearts. Accordingly, the difference between arteriolar and venular capillary segment length was attenuated, but still statistically significant (AC = 95 $\pm$ 3 μm; VC = 86 $\pm$ 4 μm, $P<0.01$).

From the intercapillary measurements along the transect lines, spacing data was available at discrete intervals along the capillary pathlength from terminal arteriole to collecting venule. From the results presented in Table 3.4, and graphs in Fig. 3.4, it is evident that intercapillary distance showed stepwise decreases along the capillary set from arteriole to venule. The decrease in intercapillary distance was not only as a function of distance from the terminal arteriole, but even along a given transect line there was a trend for shorter intercapillary distances for venular (VC) neighboring capillaries as compared to arteriolar (AC) or mixed (VC-AC) neighbors. In control hearts, intercapillary distances ranged from 23 $\pm$ 1 μm (at 20% of capillary pathlength; AC-AC) to 16 $\pm$ 1 μm (at 80%

of capillary pathlength; VC-VC). In hypertrophy, intercapillary distances were significantly longer than in normal myocardium ($P<0.01$), and the spatial and histochemical differences within and between transect lines were preserved; values ranged from 33 ± 7 μm (at 20% of capillary pathlength; AC-AC) to 19 ± 1 μm (at 80% of capillary pathlength; VC-VC).

DISCUSSION

The objective of compiling this morphometric data has been twofold: first, to provide realistic measurements for models of cardiac oxygen transport; and second, to consider what adaptations occur in pressure overload hypertrophy, at the level of the coronary microcirculation.

All of the data derived from longitudinal sections are based upon the drawings of capillary sets. It should be mentioned that some vessels were leaving the set, and others entering it, as the coronary microcirculation appears to be an infinite branching network. In agreement with Bassingthwaighte et al. (1974) and others, we have observed a greater number of venular outflows to arteriolar inflows in the heart. Accordingly, the capillary sets defined in this study do not represent an isolated set of exchange vessels; indeed, they do form contiguous pathways from terminal arteriole to collecting venule, but this circulation is neither exclusive nor exhaustive.

The preeminent finding in this study was that the capillary domain area decreased from the arteriolar to the venular side of capillaries. In normal hearts,

this decrease would provide for shorter diffusion distances for oxygen on the venular side of capillaries, where PO_2 values are generally considered to be lower. These data would call for a modification of the classical Krogh tissue cylinder; the tissue supply volume being better described as a truncated cone rather than a cylinder. In hypertrophic hearts, the disparity between the arteriolar and venular capillary domain area was even greater. The finding that domain area for venular capillaries did not increase in hypertrophy (and exhibited lesser dispersion) would indicate that the tissue supply region of venular capillaries was commensurate with their PO_2 content. In defense of adequate tissue oxygenation in the face of lower PO_2 values, domain areas were sustained in venular capillaries of the hypertrophied heart, where the risk of failure in oxygen supply is likely to be greatest. Other implication of these morphometric differences between arteriolar and venular capillary regions have already been addressed in the Discussion of Chapter 2.

The data from longitudinal sections established no differences between normal and hypertrophic hearts with respect to minimal capillary length. Capillary pathlength increased in hypertrophic hearts. Capillary set length was significantly reduced ($P<0.01$) in hypertrophic as compared normal hearts which may be related to greater branching between neighboring capillaries; or decreases in capillary density, which would decrease the likelihood of contiguous capillary pathways not being captured in the same tissue section. The increases in average pathlength would indicate that the individual pathways from arteriole to venule

were more tortuous since minimal pathlength did not change with hypertrophy.

The intercapillary distance measurements along transect lines at 20% intervals in the capillary pathlength permitted an integration of the results from cross and longitudinal sections. It was confirmed that intercapillary distance, in accordance with capillary domain areas, decreased from arteriole to venule. These decreases were not abrupt, but rather occurred at gradual intervals along the capillary length. With the differential staining technique, it was only possible to resolve the arteriolar versus venular capillary heterogeneities as a function of the staining response. The transect data showed that intercapillary distance decreased in a stepwise manner along the capillary length irrespective of the differential staining response of the capillary. However, at any given distance from the terminal arteriole, intercapillary distance was related to the stain sensitivity of the capillary. This is indicative of a level of heterogeneity between arteriolar and venular capillaries, at the same distance from an arteriole, in addition to their enzymatic heterogeneity along the capillary length. These data would appear to resolve the discrepancy in the results obtained by the domain and triangulation methods.

The reduction in intercapillary distance at 20% intervals along the capillary path would support the result obtained by the domain rather than the triangulation method. As described in the Introduction to this dissertation, the discrepancy between these two methods appears to be due to changes in the extent of capillary type-grouping between control and pressure overloaded hearts. In control hearts, capillaries are highly grouped (clustered) by histochemical type.

In this case, both methods give rise to similar results. In the pressure overloaded heart, type-grouping is diminished. As a result, the triangulation method, which is a one-dimensional measure of only two capillary neighbors, is not sensitive to changes in capillary geometry. The domain method, on the other hand includes all neighboring capillaries in the measurement of capillary supply area, and therefore provides a more realistic, two dimensional picture of capillary geometry in both control and pressure overloaded heart.

Differences in capillary branching patterns along the capillary pathlength have been alluded to before in studies of India ink injected skeletal muscle. Hammersen (1968) observed greater branching patterns towards the venous ends of capillaries in various rabbit and cat skeletal muscles. Eriksson and Myrhage (1972) described a greater number of capillaries with more anastomoses in the venular part of the capillary bed in cat tenuissimus muscle. Wolff et al. (1975) depicted the developmental pattern of the capillary bed in various organs of the rat, noting an increasing number of capillary branches, mainly on the venular side of the capillary bed, until maturity. These reports however, have only been descriptive in nature.

The present study has quantitatively shown that systematic differences exist with respect to capillary morphometric parameters, from the arteriolar to the venular region of coronary capillaries. In defense of tissue oxygenation, venular capillary domain areas did not increase with hypertrophy. From longitudinal sections, spatial differences in arteriolar versus venular capillary spacing along the

capillary length were maintained with hypertrophy. Further, there was an increase in average capillary pathlength despite no change in minimal capillary pathlength, which is indicative of increased capillary tortuosity or branching specific to venular capillaries. Whether this distinctive geometry on the venular side of capillaries resulting in shorter diffusion distances plays a significant role in oxygen transfer is contingent upon the fact that there are appreciable PO_2 gradients within the tissue. Even if this classical Kroghian thinking should not prevail, this distinctive geometry may play an important role in influencing erythrocyte transit time due to increased venular capillary branching, or by allowing for a greater surface area per volume of tissue for the exchange of oxygen. These results may be interpreted as an adaptation of the capillary architecture to the lower PO_2 values present in the capillaries close to venules.

TABLE 3.1 Body Mass & Left Ventricular Mass Data for Control and Pressure Overloaded Rat Myocardium

	CON (n=10)	**HYP (n=10)**
BM (g)	257 ± 2	253 ± 7
LVM (mg)	602 ± 9	1157 ± 65 *
LVM/BM Ratio	2.3 ± 0.1	4.6 ± 0.3*

all values are mean ± SEM; BM = body mass; LVM = left ventricular mass; LVM includes septum.

* Significantly different from CON at $P<0.01$; Student's t-test.

TABLE 3.2 Capillary Domains Areas and Heterogeneity Index for Control and Pressure Overloaded Rat Myocardium

	CON	HYP
Arteriolar Domain (μm^2)	499 ± 3 #	547 ± 6 *#
Heterogeneity index SDlog	0.067 ± 0.02	0.072 ± 0.02
Venular Domain (μm^2)	456 ± 5	464 ± 5
Heterogeneity index SDlog	0.066 ± 0.01	0.067 ± 0.02
Capillary Density (#/mm^2)	2247 ± 112	2118 ± 142

* Significantly different from CON at $P<0.01$; Mann-Whitney Test.

Significantly different from matched venular domain area at $P<0.01$; Mann-Whitney Test.

TABLE 3.3 Capillary Length Data for Control and Pressure Overloaded Rat Myocardium

	CON	HYP
Minimal Capillary Length (μm)	593 ± 15[a]	574 ± 17[b]
Capillary Set Length (μm)	3225 ± 103[c]	2887 ± 109[c]
Capillary Pathlength (μm)	648 ± 8[ad]	705 ± 11[bd]
Number of Segments per Path	8 ± 1	7 ± 1
Arteriolar Segment Length (μm)	95 ± 3[e]	95 ± 3[f]
Venular Segment Length (μm)	75 ± 2[e]	86 ± 4[f]
Mixed Segment Length (μm)	228 ± 10[e]	210 ± 13[f]
Arteriolar Segment Number	20 ± 1	17 ± 1
Venular Segment Number	9 ± 1	9 ± 1
Mixed Segment Number	3 ± 1	3 ± 1

Variables denoted by the same letter are significant from one another at $P<0.01$.

[abcd] Mann-Whitney Test.

[ef] Kruskal-Wallis ANOVA.

TABLE 3.4 Transect Distances (μm) at Discrete Intervals Along the Capillary Set for Control and Pressure Overloaded Myocardium.

	CON				HYP			
	AC-AC	**AC-VC**	**VC-VC**	**X_a**	**AC-AC**	**VC-VC**	**VC-VC**	**X_a**
20%	23 ± 1	20 ± 1	16 ± 2	22 ± 2	33 ± 7	24 ± 2	-	31 ± 4
40%	21 ± 1	20 ± 1	17 ± 1	20 ± 1	25 ± 1	25 ± 2	21 ± 4	25 ± 1*
60%	20 ± 1	19 ± 1	17 ± 1	19 ± 1	23 ± 2	23 ± 1	23 ± 2	23 ± 1*
80%	19 ± 1	18 ± 1	16 ± 1	17 ± 1*	23 ± 3	25 ± 2	19 ± 1	22 ± 2*
X_b	**21 ± 1**	**19 ± 1**	**16 ± 1#**		**27 ± 2**	**24 ± 1**	**20 ± 1#**	

AC = arteriolar capillary; VC = venular capillary; X_a = weighted mean by transect line; X_b = weighted mean by histochemical type;

* Significantly different from X_a value at 20% interval;

Significantly different from X_b value for AC-AC.

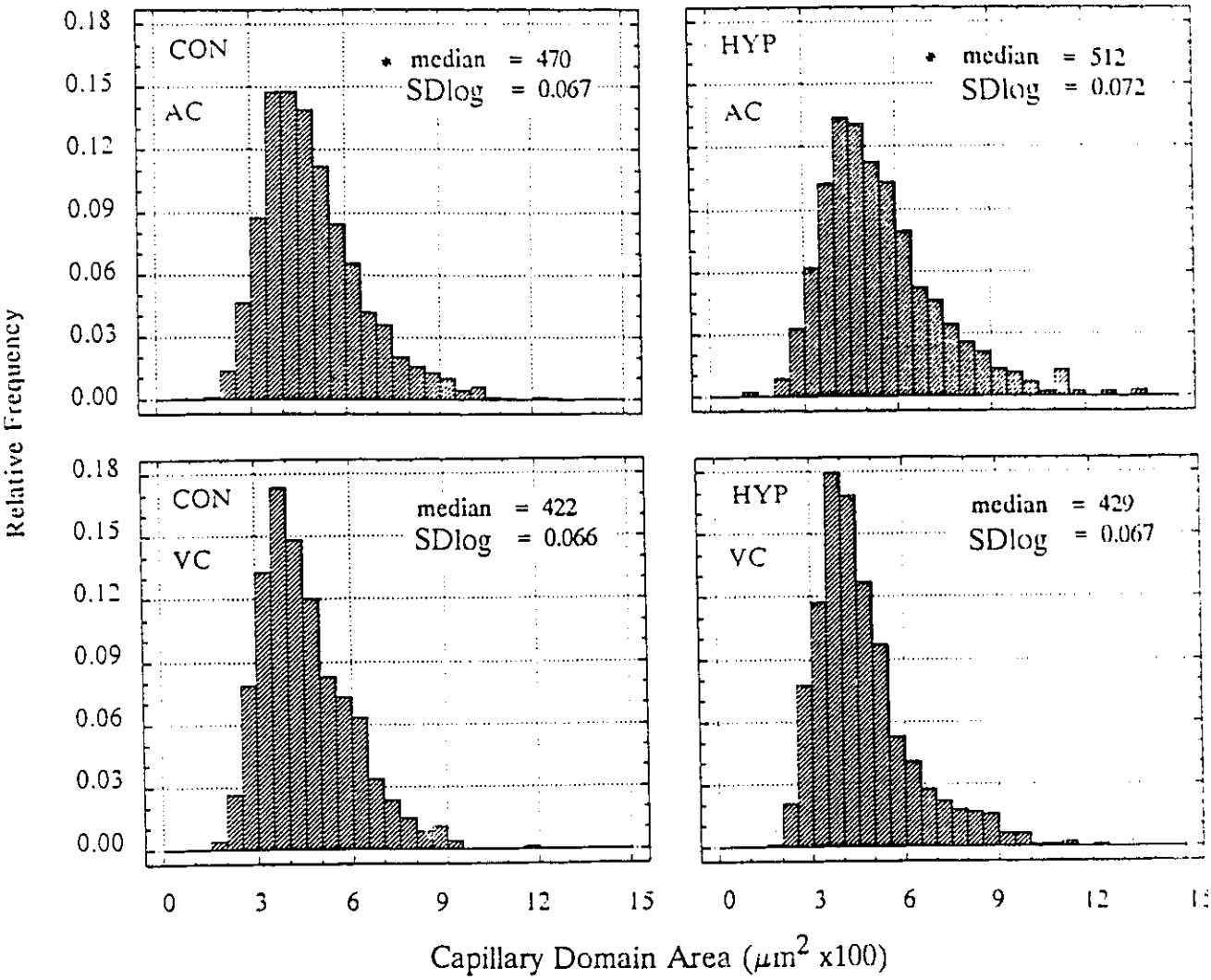

FIG. 3.1 Frequency histograms of arteriolar (AC) and venular (VC) capillary domain areas for control (CON) and hypertrophic (HYP) myocardium. The median values are given as follows: CON-AC = 470 μm; CON-VC = 422 μm; HYP-AC = 512 μm; HYP-VC = 429 μm.

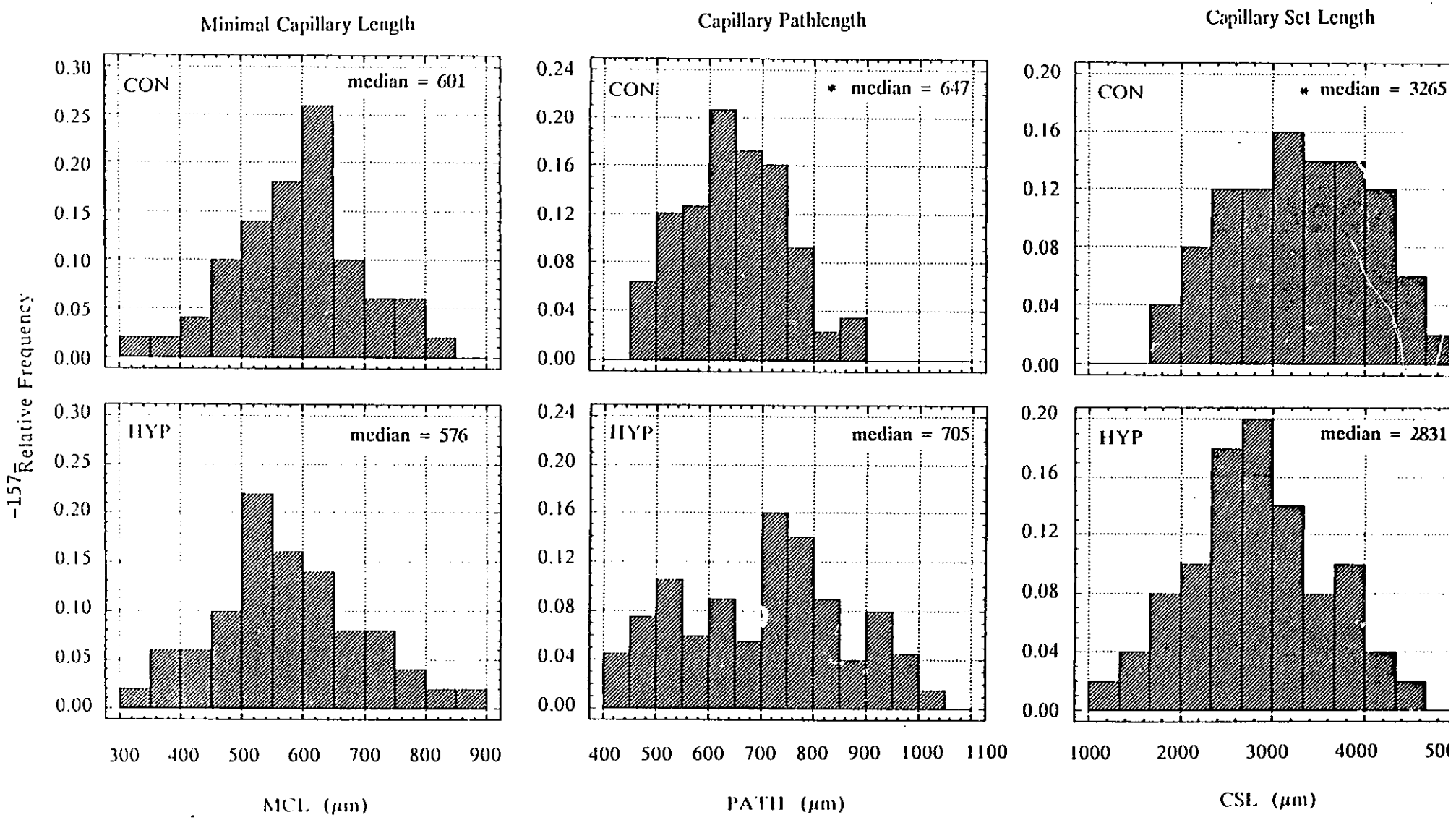

FIG. 3.2 Frequency histograms of minimal capillary length (MCL, left); average capillary pathlength (PATH, middle); and capillary set length (CSL, right) for control (CON, upper) and hypertrophic (HYP, lower) myocardium.

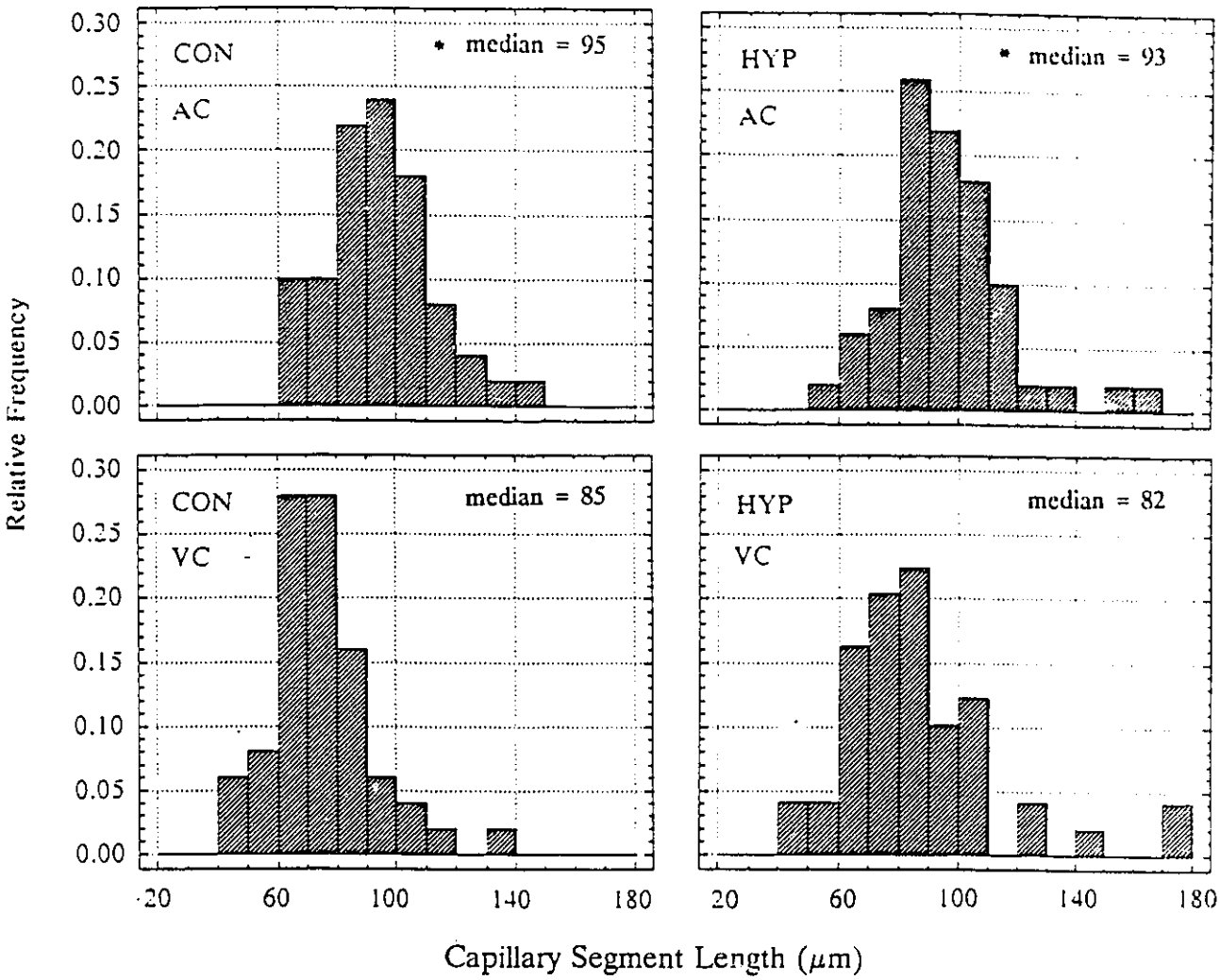

FIG. 3.3 Frequency histograms of arteriolar (AC) and venular (VC) capillary segment lengths for control (CON) and hypertrophic (HYP) myocardium.

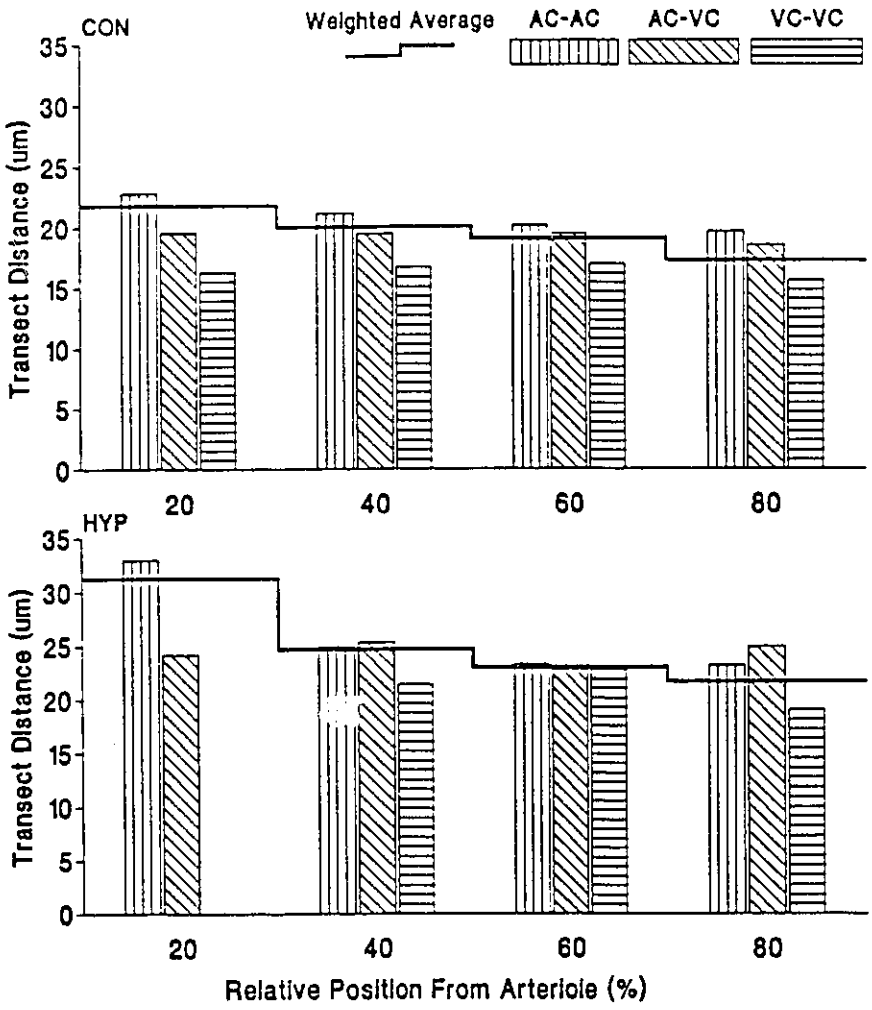

FIG. 3.4 Intercapillary distances measured along a transect line at 20% intervals along the arteriole to venule pathlength for control (upper panel) and hypertrophied (lower panel) hearts.

PLATE 6 Two-dimensional reconstruction of a capillary set, illustrating transect lines (in white), drawn at right angles to a line joining the arteriole and venule, at 20% increments.

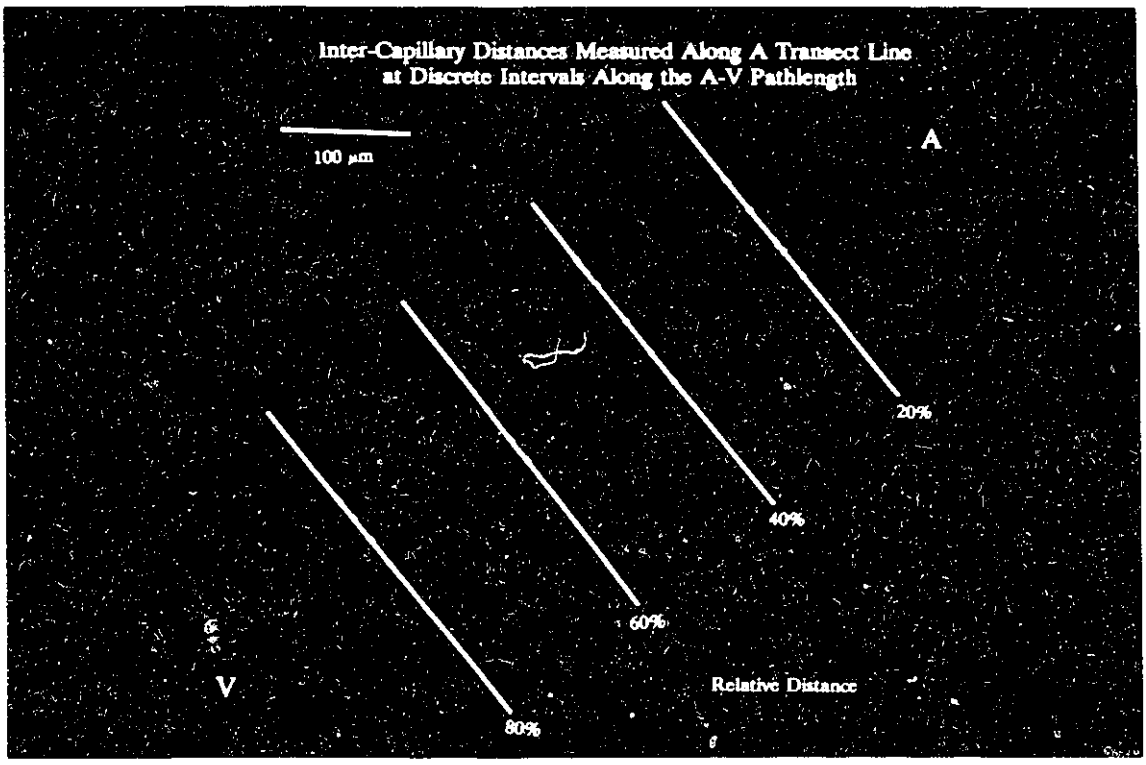

CHAPTER 4: GEOMETRY OF CAPILLARY NETWORKS IN VOLUME OVERLOADED RAT HEART

INTRODUCTION

In Chapter 3, we identified several important changes in capillary geometry following chronic pressure overload due to aortic constriction in neonatal rats. Systematic differences were demonstrated in morphometric parameters from arteriolar to venular capillary regions in both controls and pressure overloaded hearts. In pressure overload, capillary supply was diminished in arteriolar capillary regions while in venular regions it remained unchanged. This distinctive geometry in pressure overloaded hearts served to preserve normal geometric conditions for the diffusion of oxygen towards venular capillary regions where PO_2 values are lower.

These data prompted us to consider what changes occur in capillary geometry following volume overload, where myocyte dimensions and their pattern of organization in the ventricular wall are different from pressure overload. We were interested whether these differences in the tissue remodelling between pressure and volume overload comprised the structural basis for a different pattern of adaptation at the level of the coronary microcirculation.

Pressure and volume overload both lead to increases in myocyte volume. However, the pattern of myocyte remodelling may be different in these two forms of hypertrophy. In pressure overload, it has been shown that myocytes primarily

display increases in cross sectional area (Campbell et al. 1989), whereas in volume overload the increase in cell volume is due primarily to increases in cell length (Gerdes et al. 1988).

Previous studies of capillary geometry following volume overload have generally relied upon estimates of capillary density. This measurement, however, only serves as an overall index of capillary supply, without an assessment of the heterogeneity of capillary spacing. Furthermore, morphometric data are not yet available regarding arterio-venous capillary path lengths, which are necessary for the modelling of oxygen supply to the myocardium. The histochemical methods used in this study, which served to distinguish arteriolar and venular capillary regions, allowed us to directly measure these parameters in normal and volume overloaded rat myocardium.

METHODS

Sixteen male Sprague-Dawley rats were used in this study (body mass = 212 ± 4 g; mean ± SEM). Rats were randomly divided into two groups: volume overload hypertrophy (VOL; n=8) and sham-operated control (CON; n=8). Volume overload was produced by the experimental introduction of an aorto-caval fistula. Animals were anaesthetized with pentobarbital sodium (4 mg/100g ip). Following a mid-line incision, the abdominal contents were reflected to one side to allow identification of the abdominal aorta (between the origin of the left renal artery and aortic bifurcation) and inferior vena cava. Following isolation,

these juxtaposed vessels were clamped off using a rubber covered curved hemostatic forceps. In the wall of both the aorta and vena cava, an elliptical incision (approx 2 mm in length) was made using sharply curved spring scissors. The vessels were then anastomosed side to side, using 7-0 black braided silk with a tapered TE 10 needle. After suturing, the clamp was slowly released and patency of the fistula was visually confirmed. In sham operated controls, the vessels were isolated and clamped off, but the incision was not made.

At 21-23 days post-surgery, following anaesthesia, hearts were quickly excised, weighed, dissected and frozen in liquid nitrogen. Two tissue blocks per heart, one parallel (for cross sections) and one perpendicular (for longitudinal sections) to the principle axis (base-apex) of the heart were prepared for (16 μm) cryostat sectioning. The differential staining protocol was the same as in the previous Chapter, and is detailed in Appendix 1. All morphometric data were prepared and analyzed in the same manner as described in Chapter 3.

Cross Sections

See the corresponding section in Chapter 3 for explanation of morphometric methods used from tissue cross sections.

Longitudinal Sections

A total of 40 capillary sets (4-6 per heart) were delineated for each group. See the corresponding section in Chapter 3 for explanation of morphometric methods used from tissue longitudinal sections.

Statistical Analyses

All results are presented as mean ± SE. As these morphometric data are generally not compatible with the normal distribution, median values as required for non-parametric statistics are reported in the figure legends. See the corresponding section in Chapter 3 for explanation of the statistical methods used in this Chapter.

RESULTS

The introduction of an aorto-caval fistula produced a chronic volume overload, resulting in substantial increases in cardiac mass. Left ventricular mass increased by 70% compared with controls. Left ventricular mass to body mass ratio demonstrated an increase of 85% (Table 4.1). The mortality rate in this study was approximately 55%. In the majority of failures, the animals died within the first 24 hours following surgery. Of the surviving animals, approximately 15% did not develop hypertrophy presumably due to closure of the fistula.

Cross-Sections

Mean values for arteriolar (AC) and venular (VC) capillary domain areas are listed in Table 4.2. In control hearts, AC domain area was significantly larger than VC domain area ($P<0.01$). In volume overloaded hearts, AC domain area was also larger than the VC domain area ($P<0.01$) with only VC domain areas significantly ($P<0.01$) reduced from control values. The frequency histograms of capillary domain areas in Figure 4.1 demonstrate a left shift in VC areas for both the CON and VOL groups. The dispersion of domain areas was also lower in VC regions as illustrated by the interquartile range (IQR): CON-AC = 205 μm; CON-VC = 189 μm; VOL-AC = 174 μm; VOL-VC = 131 μm. The heterogeneity of capillary spacing (SDlog) was significantly lower in volume overloaded hearts as compared to controls ($P<0.01$).

Longitudinal Sections

Mean values of data from longitudinal sections are given in Table 4.3. In control hearts, capillary set length was 3371 $\pm$ 100 μm. Minimal capillary length was 581 $\pm$ 20 μm. The mean capillary path length was approximately one fifth of the capillary set length (656 $\pm$ 9) which would be consistent with about five capillary paths traversing the interval from arteriole to venule. The length of AC segments was significantly longer than VC segments ($P<0.01$). Although few in number, average mixed capillary segment length was more than twice as long as the AC or VC segment length. The lengths of these long transitional segments

may be partly explained by the fact that longer segments have a greater probability of capturing the color transition from blue to red along the capillary path.

In volume overloaded hearts, capillary set length (CSL; Fig. 4.2, right) was significantly longer ($P<0.01$) than in controls. This would indicate an overall increase in capillary material from a given arteriole to venule. Minimal capillary length (MCL; Fig. 4.2, left) also showed a significant increase from control values ($P<0.01$) showing that arteriole to venule distance was increased. Mean capillary path length (PATH; Fig. 4.2, middle) was also significantly longer than control values ($P<0.01$) the degree of increase being similar to the increase in minimal capillary length. In volume overloaded hearts, MCL, PATH and CSL all displayed increases ranging from 17-24% over control values. These data would indicate that in volume overloaded hearts there was a longitudinal expansion of the capillary set. This expansion was entirely uniform, as indicated by the increases in the number of capillary segments in volume overload. The relative proportions of arteriolar, venular and mixed segments in the set were similar to control values.

In control hearts AC segment length was longer than VC segment length (AC = 93±2 μm; VC = 74±1 μm). In volume overloaded hearts a similar pattern existed with only AC segment length displaying an increase ($P<0.01$) from control values (AC = 108±3 μm; VC = 71±2 μm). The frequency histograms of capillary segment length (Fig. 4.3) demonstrated marked differences between control and

volume overloaded hearts. The range and shape of the distribution of segment lengths was much wider in the VOL group. This may be expressed quantitatively by the interquartile range: CON-AC=22 μm; CON-VC=18 μm; VOL-AC=66 μm; VOL-VC=46 μm.

The intercapillary distance (ICD) measurements at 20% intervals along the capillary path length (Fig.4.4), indicate a stepwise decrease in ICD from arteriole to venule in both groups. The decrease in ICD was not only as a function of distance from the terminal arteriole, but even along a given transect line there was a trend for shorter ICD's for VC-VC neighboring capillaries as compared to AC-AC or AC-VC neighbors. In controls the stepwise decrease in ICD was similar at each 20% interval along the capillary path length. Intercapillary distances ranged from 23 $\pm$ 2 μm (at 20% of capillary path length; AC-AC) to 16 $\pm$ 1 μm (at 80% of capillary path length; VC-VC). In volume overload, intercapillary distances displayed a greater range of values than controls, but weighted averages tended to be smaller. The decrease in ICD was greatest from the 40% to the 60% transect line. Values ranged from 25 $\pm$ 4 μm (at 20% of capillary path length; AC-AC) to 12 $\pm$ 1 μm (at 80% of capillary path length; VC-VC) (Table 4.4).

DISCUSSION

Cardiac hypertrophy is generally considered to be a compensatory adjustment when the heart is exposed to an increased pressure or volume overload. There is typically a period of compensated hypertrophy, but this may eventually give way to decompensation and congestive heart failure (Meerson, 1969). The prominent gross morphological features of the hypertrophied myocardium are thickening of the ventricular wall and/or dilatation of the ventricular cavity. Under conditions of pressure overload, such as in aortic stenosis or systemic hypertension, the concentric form of hypertrophy develops which gives rise to increases in ventricular wall thickness. However, in conditions of volume overloading such as in aortic regurgitation or arterio-venous shunting, eccentric hypertrophy develops which is characterized by ventricular dilatation with variable changes in relative wall thickness (Linzbach, 1960; Grossman et al. 1975).

The nature of the stress which elicits the hypertrophic response of the myocardium plays an important role in determining the functional and morphological characteristics of cardiomegaly. Increases in cardiac mass are associated with myocyte hypertrophy rather than hyperplasia after the neonatal period (Rakusan and Poupa, 1966). Notwithstanding this, changes in the gross morphology and tissue geometry of the myocardium are distinct in different types of hypertrophy, even when increases in cardiac mass are similar.

In pressure overload hypertrophy, the ventricle must pump against a greater afterload, which causes an increase in wall stress. As a consequence, hypertrophy

is induced and the compensatory phase returns stress per unit of muscle towards normal levels. There is an increase in wall thickness (Linzbach, 1960) due to increases in myocyte diameter since myofibrils are laid down in parallel (Anversa et al. 1986c). We have shown that the ensuing changes in capillary geometry following aortic constriction in neonatal rats (Chapt. 3) give rise to decreases in capillary density that are specific to arteriolar capillary regions. Capillary length parameters from arteriole to venule were similar to control values as the pattern of myocyte growth was in cross sectional area rather than length. In essence, this pattern of hypertrophy demonstrates increases in myocyte diameter, which would push capillaries further apart, reducing the capillary density. This pattern of hypertrophy is far more pronounced on the arteriolar side of the capillary net. On the venular side of the capillary net, where PO_2 values are lower, capillary morphometric parameters remained similar to control values.

In the present study, volume overload cardiac hypertrophy was induced in male rats by the introduction of an aorto-caval fistula. In this case, there is an increase in cardiac output against a reduced peripheral resistance. The induced cardiac hypertrophy in volume overload is accompanied by ventricular dilatation. This dilatation results from sarcomerogenesis developing in series during the hypertrophic process, which cause an increase in myocyte length (Gerdes et al. 1988) and perhaps slippage between adjacent myofibrils and fibers (Anversa et al. 1986c). In compensated volume overload, the ventricular dilatation and hypertrophy allows maintenance of cardiac function per unit of myocardium

resulting in an increased stroke volume (Flaim et al. 1979) to compensate for the flow fraction diverted through the fistula.

It should be noted that some previous studies have shown a concomitant growth in myocyte cross sectional area and length following volume overload (Linzbach, 1960; Hatt et al. 1980), while other studies have indicated preferential increases in cell length (Thomas et al. 1984; Gerdes et al. 1988). In the present study myocyte dimensions were not measured, however the changes in capillary geometry were likely in concordance with increases in cell length with or without increases in cross sectional area. Another possibility, although not analyzed to the best of our knowledge, is that myocyte diameter may be systematically larger on the arteriolar side of the capillary net. Clearly these changes would depend upon the region of the heart, the time course, and severity of the imposed stress.

The increase in left ventricular mass (70%), which was similar to that observed by others (Dart and Holloszy, 1969; Hatt et al. 1980; Olivetti et al. 1989a) was sufficient to allow for tissue remodelling to occur in the compensated stage of hypertrophy. Previous studies have shown that volume overloading gives rise to decreases in capillary density in the left ventricular subendocardium of the dog (Thomas et al. 1984), and the rat (Rakusan et al. 1980) with no differences in capillary density in the midmyocardium or subepicardium of the dog (Thomas et al. 1984; Legault et al. 1990), midmyocardium of the rat (Rakusan et al. 1980) or entire ventricular wall of the rat (Olivetti et al. 1989a). In agreement with

other studies, we have found no significant differences in capillary density in the midmyocardium of normal and volume overloaded rat hearts.

To the best of our knowledge this is the first study to consider differences in capillary geometry from arteriolar to venular capillary regions in the volume overloaded heart. Our domain method indicated that the tissue area supplied by a single capillary (which is inversely proportional to capillary density) decreased in volume overloaded hearts in only venular capillary regions. This would indicate increased venular capillary branching and/or tortuosity directed at reducing diffusion distances for oxygen. Within both CON and VOL groups, venular capillary domain area was smaller than arteriolar capillary domain area, indicating that any capillary proliferation was likely greater towards the venular end of the capillary net where PO_2 values are generally considered to be lower. A decrease in capillary domain areas, resulting in shorter diffusion distances would lead to improved geometrical conditions for diffusion. The heterogeneity of capillary spacing (SDlog) which is another important determinant of local oxygen supply indicated that capillary spacing was more uniform in volume overloaded hearts. In previous studies of cardiac hypertrophy where the heterogeneity of capillary spacing has been measured, SDlog values have either remained the same or increased (e.g. Rakusan, 1987; Legault et al. 1990). This is the first study where the heterogeneity of capillary spacing has decreased following an experimental intervention. This advantageous adaptation in volume overloaded hearts could be induced by increased capillary branching in regions where capillary spacing is

irregular. This may be viewed as a gap filling measure that would ensure homogeneous capillary spacing to optimize conditions for oxygen supply.

Overall capillary length parameters increased in volume overloaded hearts. This uniform increase would be consistent with the concept of series replication of sarcomeres (Grossman et al. 1975) producing myocyte growth preferentially in length rather than cross sectional area. It is of interest that in a recent paper by Olivetti and coworkers, an increase in the total length of capillaries has been found in the cardiac ventricles of anemic rats. The increase in aggregate length of capillaries in volume overload hypertrophy was more or less comparable to the overall increase in cardiac mass (Olivetti et al. 1989a). These authors raised a question whether the increase in the total capillary length is due to the formation of new capillaries or due to an increase in the length of existing vessels. They also commented about a lack of data concerning the length of capillary units under normal and pathological conditions. Our data indicate that an increase in total capillary length in volume overload hypertrophy may be partly or entirely explained by increases in the length of individual capillaries.

At some critical capillary segment length, additional capillary branching could be induced. This would explain the very long (before new branching) and very short (after new branching) capillary segment lengths demonstrated in volume overloaded hearts (Fig. 3). The relative increases in MCL, PATH and CSL were similar in volume overloaded hearts. The only parameters that did not increase in volume overloaded hearts were the transitional (MIX) and venular (VC)

capillary segment lengths. The maintenance of MIX and VC segment lengths in the face of increases in overall capillary length would imply a greater capillary branching phenomenon in venular capillary regions. Further, there may be some critical segment length operating beyond which proliferation of new branches is induced.

Perhaps the most integral morphometric parameter would be the intercapillary distance measurements at 20% intervals along the capillary path length from arteriole to venule. These data are independent of the staining response of individual capillaries and provide a clear assessment of capillary spacing at relative positions along the capillary path. These measurements indicate stepwise decreases in intercapillary distance from arteriole to venule. In volume overloaded hearts, the smaller intercapillary distances, especially towards venules would reduce diffusion distances for oxygen.

These changes in the geometry of capillaries in the volume overloaded heart would provide the basis for altered capillary flow pattern. The increased minimal and mean capillary lengths may increase red blood cell transit time, allowing for greater red blood cell desaturation towards the venular end of the capillary path. The lower PO_2 values in capillaries towards venules may then play an important role in stimulating capillary branching phenomenon which in turn decreases diffusion distances for oxygen in this region. The point where increases in capillary length and branching parameters may become decompensated is when O_2

extraction cannot be further increased. This would likely occur towards venular capillary regions in the case of very long capillary path lengths.

In this study we have shown that subsequent to the introduction of an aorto-caval fistula, there is considerable expansion of the coronary microvasculature directed at maintaining adequate oxygen supply during the compensated phase of cardiac hypertrophy. The pattern of myocyte remodelling may serve as the structural basis for the specific pattern of capillary adaptation.

TABLE 4.1 Body Mass & Left Ventricular Mass Data for Control and Volume Overloaded Rat Myocardium

	CON (n=8)	**VOL (n=8)**
Initial BM (g)	210 ± 5	214 ± 4
Final BM (g)	342 ± 8	329 ± 7
LVM (mg)	715 ± 14	1212 ± 60 *
LVM/FBM Ratio	2.1 ± 0.1	3.7 ± 0.2*

Note. All values are mean ± SEM; BM = body mass; LVM = left ventricular mass; LVM includes septum.

* Significantly different from CON at $P<0.01$; Student's t test.

TABLE 4.2 Capillary Domain Areas and Heterogeneity Index for Control and Volume Overloaded Rat Myocardium

	CON	VOL
Arteriolar Domain (μm^2)	505 ± 5 #	480 ± 6 #
Heterogeneity index SDlog	0.069 ± 0.02	0.061 ± 0.02*
Venular Domain (μm^2)	452 ± 5	395 ± 5 *
Heterogeneity index SDlog	0.067 ± 0.01	0.059 ± 0.02*
Capillary Density (#/mm^2)	2215 ± 105	2422 ± 180

* Significantly different from CON at $P<0.01$; Mann-Whitney Test.

Significantly different from venular domain area at $P<0.01$; Mann-Whitney Test.

TABLE 4.3 Capillary Length Data for Control and Volume Overloaded Rat Myocardium

	CON	VOL
Minimal Capillary Length (μm)	581 ± 20[a]	723 ± 18[a]
Capillary Set Length (μm)	3371 ±100[b]	3949 ± 104[b]
Capillary Pathlength (μm)	656 ± 9[c]	807 ± 9[c]
Number of Segments per Path	7 ± 1	9 ± 1
Arteriolar Segment Length (μm)	93 ± 0.3[df]	108 ± 3.3[ef]
Venular Segment Length (μm)	74 ± 0.2[d]	71 ± 2.4[e]
Mixed Segment Length (μm)	220 ± 12.3[dg]	149 ± 5.8[eg]
Arteriolar Segment Number	18 ± 1[hj]	21 ± 2[ij]
Venular Segment Number	10 ± 1[hk]	15 ± 1[ik]
Mixed Segment Number	3 ± 1[h]	4 ± 1[i]

Variables denoted by the same letter are significant from one another at $P<0.01$.

[abcfgjk] Mann-Whitney Test.

[dehi] Kruskal-Wallis ANOVA.

TABLE 4.4 Transect Distances (μm) measured at Discrete Intervals Along the Capillary Path for Control and Volume Overloaded Rat Myocardium.

	CON				VOL			
	AC-AC	**AC-VC**	**VC-VC**	**X_a**	**AC-AC**	**AC-VC**	**VC-VC**	**X_a**
20%	23 ± 1	20 ± 1	17 ± 2	22 ± 2	25 ± 7	24 ± 2	22 ± 3	24 ± 4
40%	22 ± 1	20 ± 1	17 ± 1	21 ± 1	27 ± 1	22 ± 2	19 ± 4	23 ± 1
60%	20 ± 1	19 ± 1	16 ± 1	19 ± 1	20 ± 2	21 ± 2	13 ± 1	16 ± 1*
80%	20 ± 1	19 ± 1	16 ± 1	17 ± 1*	19 ± 5	17 ± 4	12 ± 1	13 ± 2*
X_b	22 ± 1	19 ± 1	16 ± 1#		24 ± 2	20 ± 1#	14 ± 1#	

AC = arteriolar capillary; VC = venular capillary; X_a = weighted mean by transect line; X_b = weighted mean by histochemical type;

* Significantly different from X_a value at 20% interval;

Significantly different from X_b value for AC-AC.

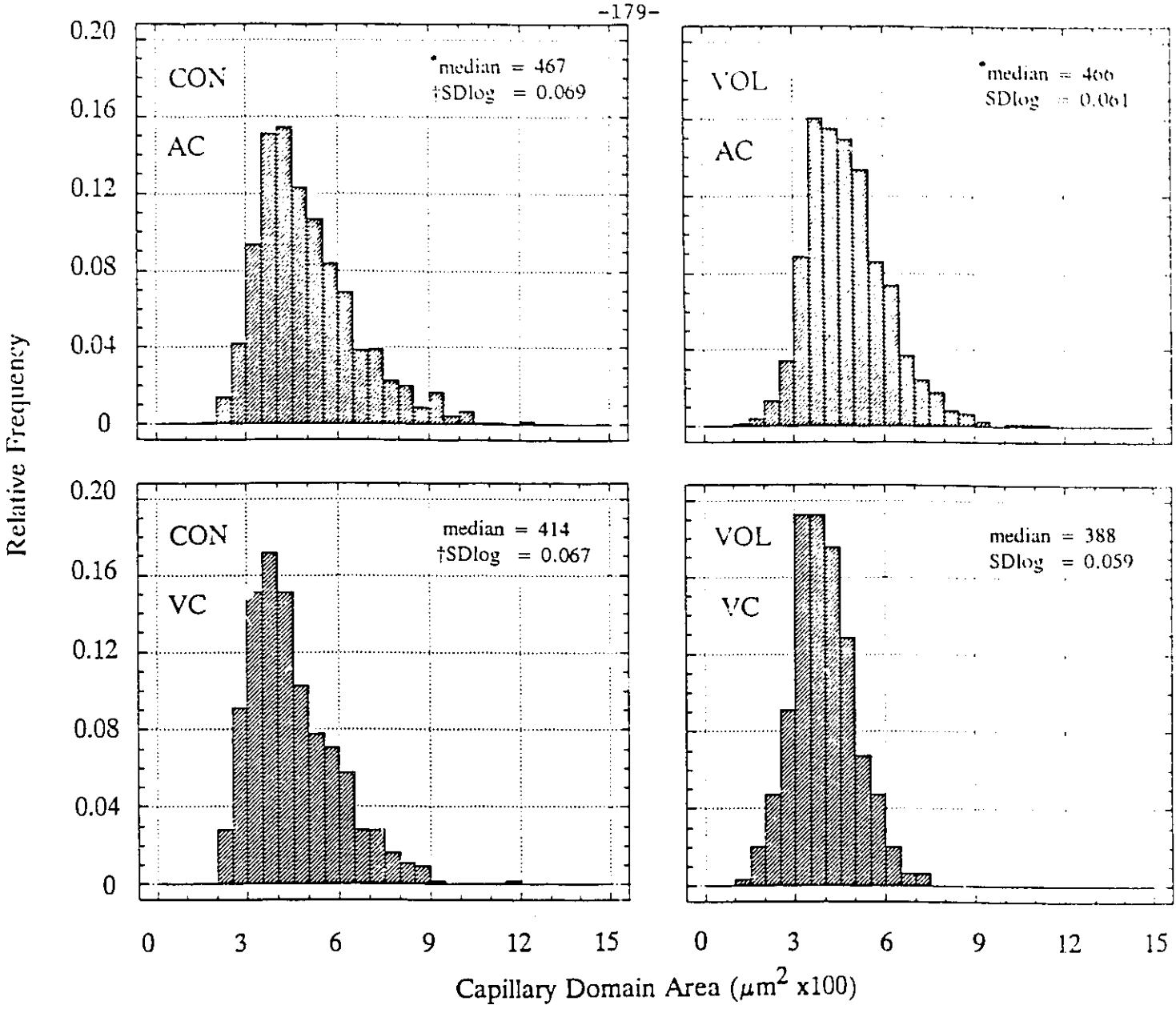

FIG. 4.1 Frequency histograms of arteriolar (AC) and venular (VC) capillary domain areas for control (CON) and volume overloaded (VOL) myocardium.

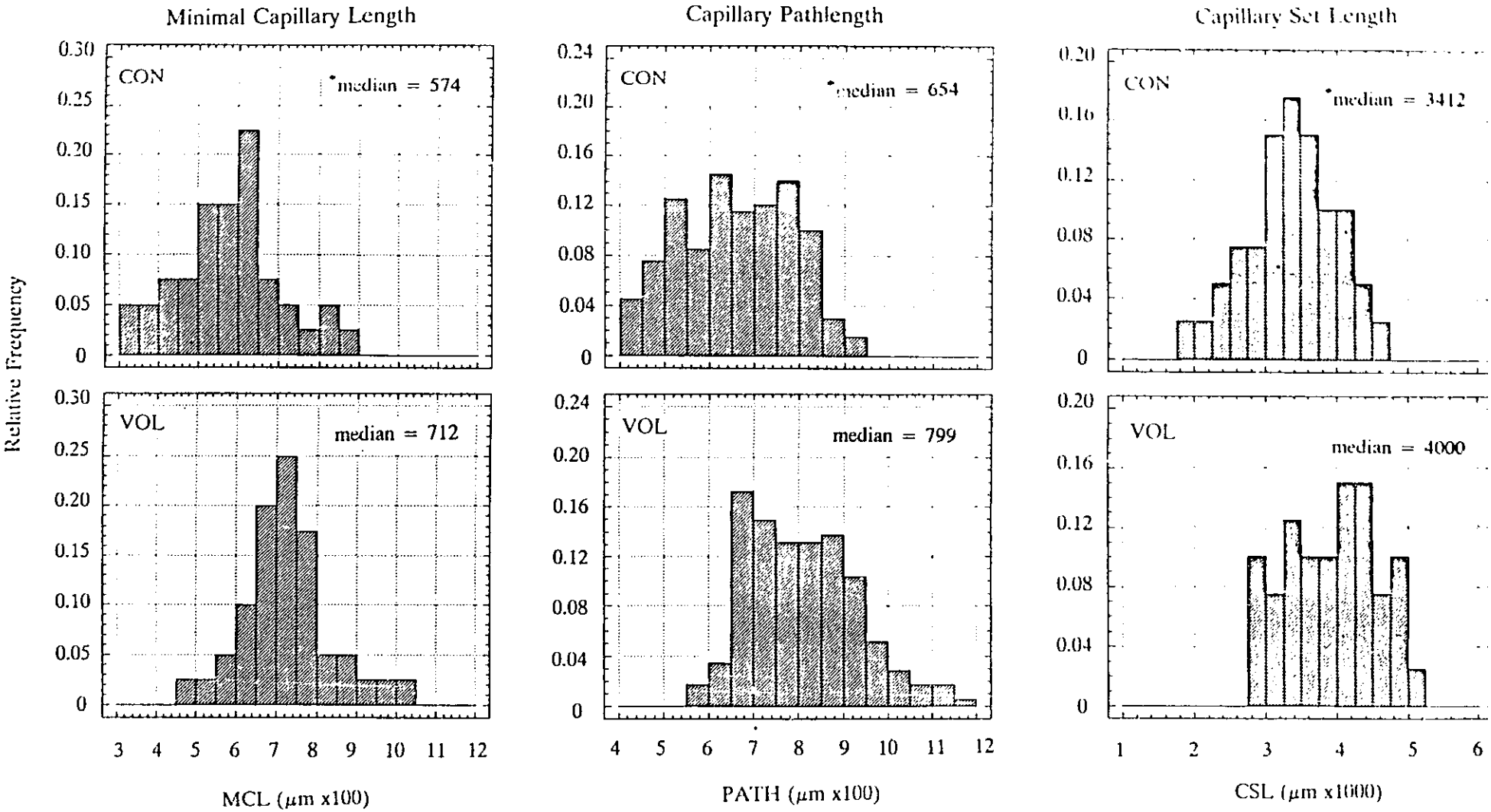

FIG. 4.2 Frequency histograms of minimal capillary length (MCL, left); average capillary path length (PATH, middle); and capillary set length (CSL, right) for control (CON, top) and volume overloaded (VOL, bottom) myocardium.

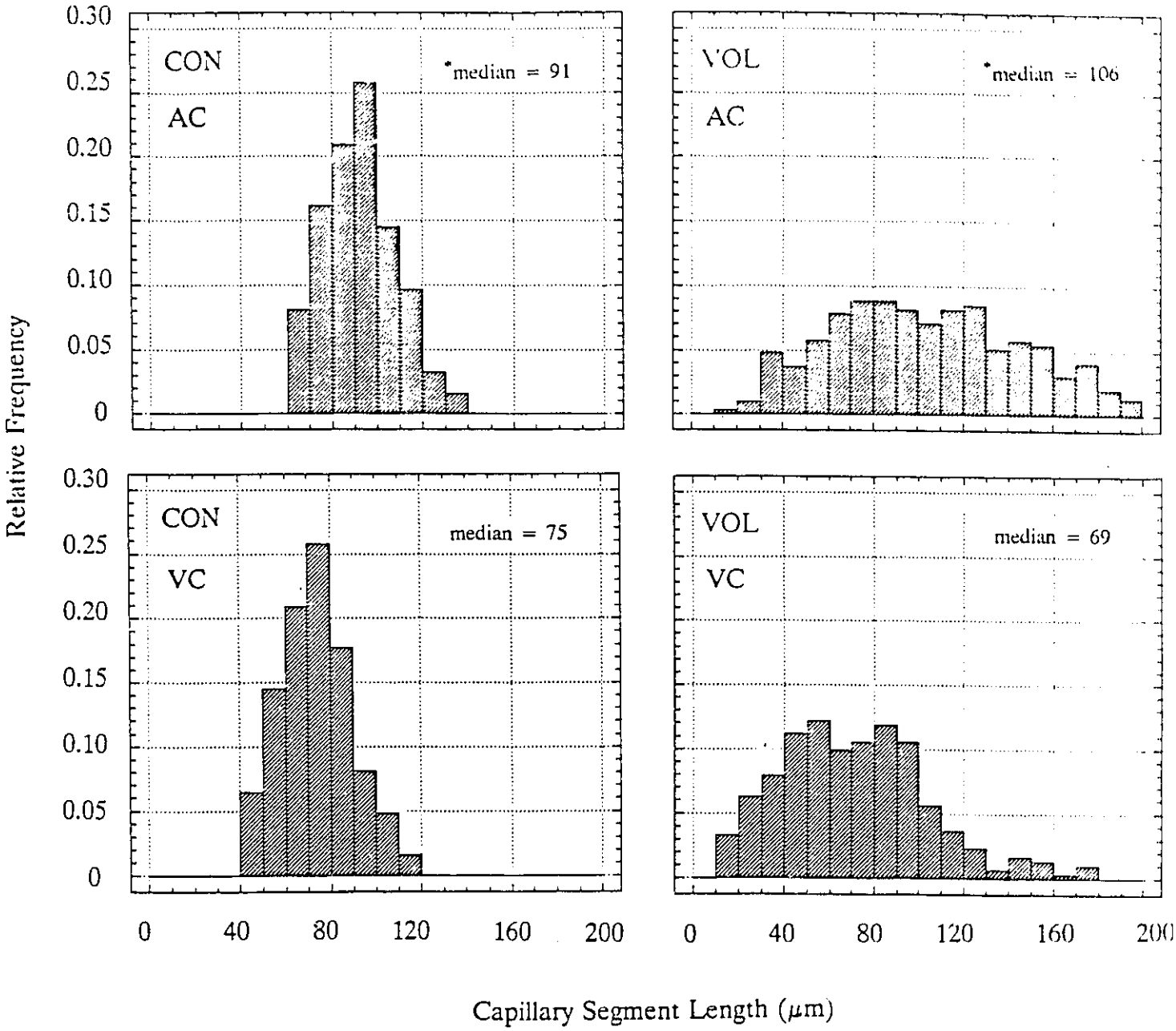

FIG. 4.3 Frequency histograms of arteriolar (AC) and venular (VC) capillary segment lengths for control (CON) and volume overloaded (VOL) myocardium.

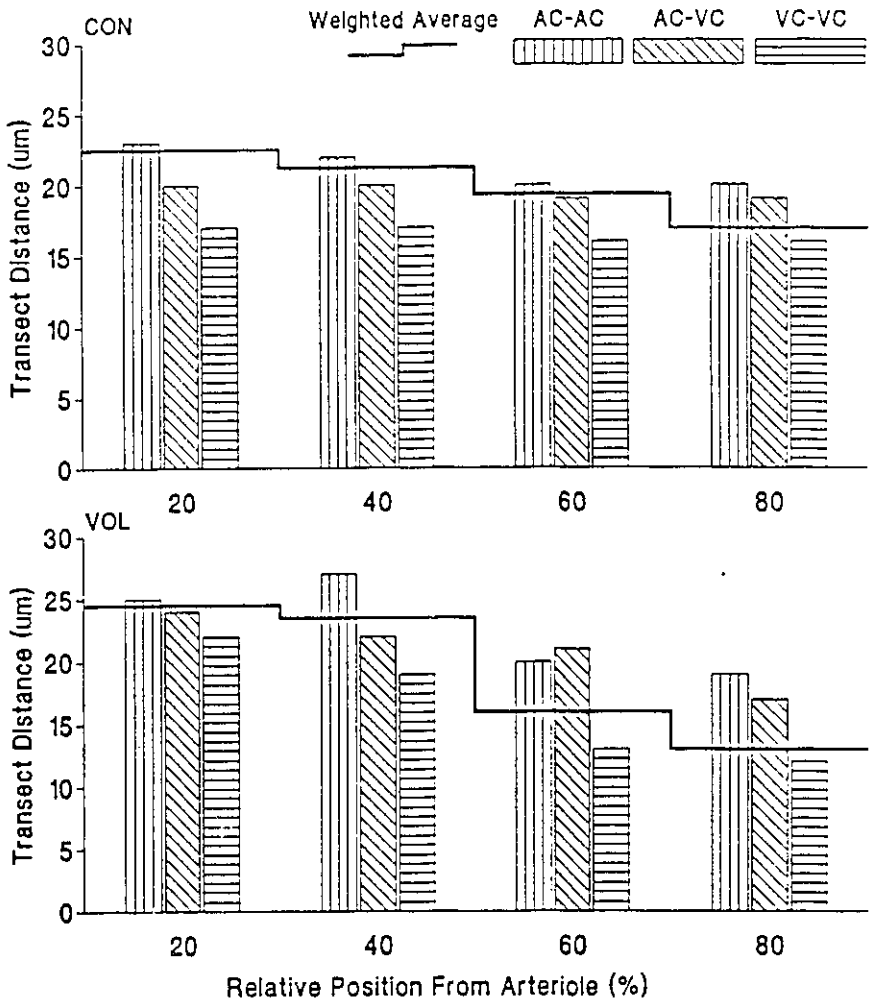

FIG. 4.4 Intercapillary distances measured along a transect line at 20% intervals along the arteriole to venule pathlength for control (top) and volume overloaded (bottom) rat myocardium.

CHAPTER 5: OVERALL SUMMATION AND CONCLUSIONS

The data presented in this dissertation has served to address several important questions related to oxygen supply in the heart muscle. These questions are listed as follows:

1. Is capillary geometry affected by myocardial fiber shortening? i.e. is there an increase in capillary tortuosity at reduced sarcomere length?
2. Are there systematic differences in capillary geometry from arteriolar to venular capillary regions?
3. What is the pattern of capillaries at different stages of postnatal growth of the heart? During postnatal growth, is the expansion of the capillary network commensurate to overall increases in myocyte size?
4. Is experimentally induced pressure overload cardiac hypertrophy simply a well compensated form of accelerated normal growth? What changes occur in capillary geometry following chronic pressure overloading in neonatal rat?
5. Is experimentally induced volume overload cardiac hypertrophy simply a well compensated form of accelerated normal growth? What changes occur in capillary geometry following chronic volume overloading? Are there differences in these two models of cardiac hypertrophy at the level of the microcirculation?

6. What are the implications of these morphometric adaptations to models of oxygen supply of the myocardium? Do differences at the level of capillary geometry influence calculations of tissue PO_2 profiles?

The advent of the differential staining technique provided a novel and yet very practical approach to the study of capillary geometry in the heart muscle. This technique allowed for the unambiguous identification of capillary pathways from terminal arteriole to collecting venule from both transverse and longitudinal sections. The pilot studies (as described in the Introduction) served as a basis for the application of this technique to the analysis of capillary geometry under various conditions. From transverse sections, we first described the nonrandom distribution of capillaries as a function of their arteriolar and venular ends. The concept of staggering of arteriolar inputs has been qualitatively described in the literature (Brown, 1965; Fabel, 1968; Ludwig, 1971; Rakusan, 1971b). However, this was the first attempt to systematically characterize this phenomenon based upon the registration of arteriolar and venular capillary regions. This proposed schema, of a transverse arteriole running at an oblique angle to the fiber axis and furnishing capillaries at different levels in the heart muscle suggests a higher pattern organization than previously considered.

In addition, our pilot studies illustrated that the domain method was superior to the triangulation method for the quantitative description of capillary supply from transverse sections. Differences in these two methods became appreciable

when capillaries were reduced to a bivariate (two subtypes, AC and VC) point configuration over a diverse range of capillary grouping patterns. The domain method was shown to be more sensitive to the local capillary environment, thus providing more meaningful data regarding capillary supply geometry.

These pilot studies served to establish the differential staining technique, as well as to validate morphometric methods previously used for the (univariate) analysis of capillaries from transverse sections. To reiterate, the domain method was the method of choice, and was therefore used in all subsequent studies. It should be stressed that from longitudinal sections, there were previously very few, if any, established methodologies available for the quantitative description of coronary capillary geometry. We therefore defined and measured parameters that we felt would be most important for the characterisation of the capillary bed in meaningful terms. Some parameters (e.g. capillary pathlength, and capillary segment length) have been previously used in studies of skeletal muscle. The other parameters, including respective terminology, were introduced in the dissertation.

From the studies of capillary geometry at discrete phases of the cardiac cycle (Chapter 1), it may be generally concluded that fiber shortening gives rise to a an overall reduction in sarcomere length, up to and beyond those values predicted from measurements of ejection fraction and end systolic volume in humans. It would be of interest to consider the ultrastructure of these fibers following calcium (or barium) induced systole, to consider the extent of fiber disruption or

other non-physiological changes associated with contracture rather than physiological systole. In contrast to skeletal muscle, capillary tortuosity does not significantly increase over the range of sarcomere lengths observed in these studies. The development of capillary tortuosity may be dampened by the presence of capillary-to-myocyte collagenous struts (Borg and Caulfield, 1980; Caulfield and Borg, 1979; Borg and Caulfield, 1981) or alternatively by the high degree of capillary branching found in cardiac as compared to most skeletal muscles.

In the special case of arterio-venous tortuosity in the midmyocardium, the increase in the tortuosity index in systole suggests that the difference may be due to a shift in the orientation of contiguous capillary segments rather than increases in intra-segment tortuosity. Perhaps the high intramuscular pressures generated in systole, and the presence of collagenous strut preclude a substantial increase in capillary segment tortuosity. Alternatively, at capillary branch points, the angle from parent to daughter branches become less acute, resulting in an "observed" increase in capillary path tortuosity, which may be better described as a reduction in anisotropy. It is not known whether there is a structural basis for an adjustment in capillary branching angles due to fiber shortening.

It should further be noted that measurements of arterio-venous tortuosity index were only applied to the midmyocardium. It is not known whether a similar pattern along individual capillary pathlength may occur in the subepi and subendocardium. We are not aware of any studies that have systematically looked

at transmural differences in capillary pathlength. As a first step in addressing this question, Ludwig (1971) suggested that arterio-venous distances where longer in the subepi and subendocardial layers as compared to the intramural layers of the rabbit heart.

The findings in Chapter 1, regarding changes in capillary geometry due to fiber shortening were based on young adult rats (approx. 2 months of age). We chose this age since most data in the literature are based upon a similar group. Nonetheless, it is possible that these data may not be representative in animals at different stages of postnatal growth. To consider this possibility further, in Chapter 2, we have considered capillary geometry in the rat myocardium from the time of weaning (21 days) to adulthood (240 days).

This study focused on the post-weaning period of cardiac development, where increases in cardiac mass are due to myocyte hypertrophy (Rakusan et al. 1965). We observed systematic differences in capillary geometry from arteriolar to venular capillary regions. These differences were already present at 21 days of age, and persisted throughout the age range of the study. Unfortunately, we were not able to study animals before 21 days of age as the histochemical methods yielded incomplete and therefore unreliable results at these earlier stages of development. It appears that the enzyme profiles were not fully laid down in the capillary endothelium prior to 21 days of age.

The principle finding in this study was that in all age groups venular capillary domain areas were significantly smaller than arteriolar domain areas ($P<0.01$).

This indicates that venular capillaries are situated closer together, which may be explained in one of two ways. Firstly, myocyte cross sectional areas may be systematically smaller towards venular capillary regions, i.e. along the capillary length, myocyte diameter would taper. This would imply that the several myocytes in series that traverse the capillary path, do not form an elongated cylinder, but are rather shaped in the form of a truncated cone, resulting in smaller capillary domain areas towards venular capillary regions. We are not aware of any studies that have considered the prospect that myocytes may have smaller cross-sectional areas towards venular capillary regions. The other possibility, and the one that we regard as more plausible, is that there was an increased capillary proliferation towards venular capillary regions. This increased proliferation would be manifest by an increase in capillary branching and/or tortuosity, which would result in smaller venular capillary domain areas. This reduction in domain area would provide advantageous conditions for the diffusion of oxygen in capillary regions with generally lower PO_2.

Another important determinant of oxygen supply, the heterogeneity of capillary spacing (SDlog), was also determined at four stages of postnatal growth. SDlog values remained the same on the venular side of the capillary net with increasing age. In contrast, SDlog was significantly increased in arteriolar capillary regions with increasing age. These data from transverse sections suggest that with normal postnatal growth, capillarization is well preserved towards venular capillary regions, with a progressive impairment in capillarization in

arteriolar capillary regions. The overall reduction in capillary supply parameters suggest that with growth, capillary proliferation does not match myocyte hypertrophy. Similar results were obtained from longitudinal capillary sections. In summary, the (longitudinal and lateral) expansion of the capillary set with normal growth was not accompanied by a commensurate increase in the aggregate capillary length. Rather, capillaries were spread less densely with normal growth, resulting in an impairment in the geometric conditions for oxygen supply.

In light of these data regarding capillary geometry during normal growth, we were interested in whether experimentally induced pathological growth represented an extension, albeit accelerated, of normal cardiac growth. Under conditions of pathological growth, it has been proposed that the type of overload influences the resulting adaptation at the level of the microcirculation. To this end, we introduced two forms of pathological cardiac growth in the rat myocardium. These models served to address the following question: how does pathological growth under conditions of chronic pressure or volume overload compare with normal cardiac growth?

Our method of chronic pressure overloading was innovative in that the overload state was introduced in neonatal rats (5 postnatal days of age). This approach resulted in a slow-onset pressure overload, with significant increases in cardiac mass, due to myocyte hypertrophy and hyperplasia. It has previously been shown that when pressure overloading is induced in younger animals, greater compensatory capillary proliferation occurs as compared to pressure overloading

in adult animals (for a review see Rakusan, 1987). Our data suggested that the decreases in capillary supply following six weeks of pressure overloading were specific to arteriolar capillary regions. As myocytes increased in cross-sectional area, capillaries were pushed further apart, resulting in an increase in arteriolar capillary domain areas. On the venular side of the capillary net, capillary supply was similar to sham-operated controls. This preservation of venular capillary domain areas, once again, may have been due to a relatively smaller increase in myocyte cross-sectional area in regions adjacent to venular capillaries; or due to an increased venular capillary proliferation.

Capillary length parameters, as determined from longitudinal sections, were essentially the same as in controls as the pattern of myocyte growth was likely due to increases in cross sectional area rather than length. Our method of volume overloading was based upon the introduction of an aortocaval fistula. Despite similar increases in cardiac mass to our model of pressure overload, we noticed profound differences in adaptation at the level of the coronary microvasculature. In volume overloaded hearts, there was surprisingly a reduction in overall capillary domain areas, resulting in shorter diffusion distances for oxygen. In addition, the heterogeneity of capillary spacing (SDlog) was significantly reduced in volume overloaded hearts. These advantageous adaptations in the volume overloaded heart may have resulted from the induction of capillary proliferation in regions where capillary spacing was nonuniform, i.e. some gap filling adaptation directed

at ensuring a homogeneous capillary distribution in the tissue. Capillary length parameters were significantly increased in volume overloaded hearts.

In these studies of chronic pressure and volume overloading, we have documented considerable adaptations in the coronary microvasculature in the face of substantial increases in cardiac mass. It is clear that both of these forms of hypertrophy lead to increases in myocyte volume, however the pattern of myocyte-capillary remodeling appears to be quite distinct. The changes in capillary geometry may be secondary to specific changes in the arrangement and dimensions of myocytes in the ventricular wall following chronic pressure or volume overload. Although both models of hypertrophy appear to be well compensated, the model of volume overloading appears to result in additional capillary proliferation directed at preserving geometrical conditions for the diffusion of oxygen.

The concept of differences in capillary network geometry in normal versus pathological cardiac growth was already introduced in Chapter 2, in several Figures (2.5, 2.7-2.10) that contained data from normal as well as pressure and volume overloaded rat myocardium. To recapitulate, capillary set geometry changed with increases in left ventricular mass during normal growth. Our results from volume overloaded hearts generally followed the extrapolated regression lines of normal growth better than the data from pressure overloaded hearts. It should be noted that in both models of pathological growth, capillary proliferation was significantly greater than would be predicted from the regression lines derived

from normal growth. The index of capillary supply from longitudinal sections, the capillary set length/area, illustrates that the geometric conditions for oxygen supply deteriorate with normal growth. With both models of hypertrophy, there is a greater level of capillary adaptation than would be predicted from the linear regression line, indicating additional capillary growth, which was however, not commensurate to the increase in cardiac mass. Volume overload appears to improve these geometric conditions for oxygen supply more than the model of pressure overload.

It is of interest to note that Rossi and Carillo (1991), have recently evaluated different structural and functional characteristics of the pressure and volume overloaded myocardium. In their review, they suggest that the cardiac hypertrophy induced by pressure and volume overloading, are clearly distinct biological phenomena, mediated through different mechanisms.

The data presented in this dissertation have served to rigorously document capillary geometry from transverse and longitudinal sections in the rat myocardium under several different conditions. A natural extension of this study would be to consider what functional implication these structural changes may have. Specifically, would alterations at the level of the coronary microvasculature influence myocardial PO_2? To address this question, we have considered a multicylindrical model of oxygen transport, that represents myocardial tissue as a set of overlapping Kroghian tissue cylinders (Turek et al. 1991).

This model allows for the calculation of PO_2 histograms as a function of various input conditions including cylinder radius, heterogeneity of capillary spacing (SDlog), and myoglobin facilitated oxygen diffusion (calculations done by Dr. Z. Turek, University of Nijmegen, The Netherlands). In the basic model, tissue cylinders are divided longitudinally into different slabs. For each slab, PO_2 profiles are calculated from the edge of the capillary to the periphery of the tissue cylinder using an iterative procedure. We assumed that each slab was composed of concentric rings, and oxygen gradients were accordingly calculated across each concentric layer by the Fick equation. The oxygen flux out of each layer was given by the flux into the layer minus the oxygen consumed, and assumed to follow zero-order kinetics. The flux value at the capillary was adjusted until the flux at the periphery of the tissue cylinder was equal to zero (zero-flux boundary conditions).

A value for additional resistance to diffusion, the capillary barrier had an Ohmic character. In other words, the PO_2 gradients due to this barrier depend on the oxygen flux which is equivalent to the oxygen consumption in the slab. Therefore, for a given rate of oxygen consumption, PO_2 gradients in thicker cylinders would be greater than in thinner cylinders. This barrier resistance was expressed quantitatively as a pressure drop for the mean cylinder radius and mean oxygen consumption. This pressure drop (10 mmHg) is based upon recent experimental and theoretical findings that suggest that PO_2 values are low and uniform in the muscle cells, i.e. a barrier to diffusion exists between red cell

hemoglobin and the surrounding tissue, resulting in steep perivascular, and low uniform intracellular PO_2 gradients (e.g. Gayeski and Honig, 1986; Groebe, 1990). Specific reference data used in our calculations are given in Table 5.1.

Of particular interest to the results obtained in this dissertation was the difference in capillary geometry from arteriolar to venular capillary regions. To illustrate the effect of changes in capillary geometry on myocardial oxygenation, we have chosen as an illustration, the results obtained from pressure overloaded hearts (Chapt. 2). The 2 layer arrangement incorporated data from measurements of AC and VC domain area. The 4 layer arrangement incorporated data from transect measurements at 20% intervals along the capillary set. The salient variables and input data are listed in Table 5.2.

2 Layer. The cylinder is divided longitudinally into 2 layers representing arteriolar and venular capillary regions. These layers comprised 70% and 30%, respectively of the cylinder length. Computed PO_2 profiles are based upon the truncated cone model (data from this dissertaion, Table 3.2), as well as the traditional Krogh cylinder model (no differences from arteriolar to venular capillary regions).

4 Layer. The cylinder is divided longitudinally into 4 equal layers. PO_2 profiles are similarly based upon the truncated cone model (data from this dissertation, Table 3.4) and Krogh cylinder model.

For both arrangements, the illustrations presented here have been derived from conditions of myoglobin facilitation, zero-order kinetics, and the inclusion of capillary barrier. The radial PO_2 profiles from all slabs of the entire distribution of tissue cylinders were used for the calculation of PO_2 histograms. The histograms are expressed as the percentage of the total tissue volume having a PO_2 value between the identified limits. In the following examples, class intervals of 10 mmHg were used. PO_2 values of less than 0.005 mmHg were defined as anoxic, and values greater than 0.005 mmHg but less than 10 mmHg were defined as hypoxic. Figures 5.1 - 5.5 illustrate the effect of different capillary geometries (domain area and heterogeneity of capillary spacing) on computed myocardial PO_2.

In Figure 5.1, histograms are shown for the 2 layer arrangement, using the Krogh cylinder model. Input morphometric data for arteriolar capillary (AC) and venular capillary (VC) regions are the same (see Table 5.2). The distribution of PO_2 values is notably wide, especially for AC regions. Note the low PO_2 values observed in venular capillary regions, corresponding to the notion of lethal corners. The percent anoxic tissue was increased almost 5-fold from AC to VC regions (AC = .36%; VC = 1.75%).

Figure 5.2 illustrates a similar situation to Figure 5.1, except with the truncated cone rather than the Krogh cylinder model. This more realistic geometry, with smaller VC domains and reduced VC heterogeneity of capillary spacing, results in improved myocardial oxygenation. It is evident that, for VC

regions, the histogram is markedly right-shifted, towards higher PO_2 values. The percent anoxic tissue increases from AC to VC regions is increased much less than in the Krogh cylinder model, by approximately 1.6-fold (AC = .54%; VC = .86%). This improved oxygenation would serve to attenuate the occurrences of these lethal corners.

Figure 5.3 demonstrates the computed PO_2 histograms for the 4 layer arrangement using the Krogh cylinder model. It is evident that from the first layer (0-25) to the fourth layer (75-100) the shapes of the respective histograms become progressively narrower, and tend towards lower PO_2 values. Accordingly, the percent anoxic tissue is progressively increased from the first to the fourth layer of the tissue cylinder (1st = .04%; 2nd = .25%; 3rd = .70%; 4th = 1.51%) resulting in an overall increase in percent anoxic tissue of 38-fold. It is interesting to note that the percent anoxic tissue was lower in the 4th layer, as compared to the VC layer of the Krogh cylinder model (1.51% and 1.75%, respectively). This surprising finding serves to illustrate the important effect of cylinder radius on calculations of PO_2 profiles. An increase in cylinder radius, as described for the 2 layer model, serves to increase the percent anoxic tissue within the cylinder.

When a similar computation is made using the truncated cone rather than the Krogh cylinder model, the previously observed reduction in PO_2 from the first to forth cylinder layer is dramatically averted. These histograms in Figure 5.4 clearly suggest that the truncated cone model tends to normalize PO_2 values within the tissue cylinder, resulting in a more homogeneous tissue oxygenation. The percent

anoxic tissue from the first to the fourth layer of the tissue cylinder, in fact, **decreases** (1st = .71%; 2nd = .28%; 3rd = .19%; 4th = .32%).

Figure 5.5 serves to integrate the results of Figs. 5.3 and 5.4, by combining the individual data from each of the four layers. It is again clear from this Figure that when more realistic capillary geometry is used in the modelling of oxygen supply, computed histograms suggest that myocardial oxygenation is improved and more uniform throughout the tissue cylinder. It is also notable that the percent anoxic tissue is appreciably reduced in the truncated cone model (cylinder = .63%; cone = .37%). Figure 5.6 serves to summarize percent anoxic tissue as determined for both models and arrangements.

When realistic morphometric data are used as input parameters in the computations of myocardial PO_2, computed histograms are significantly altered. The effect of realistic morphometric data, as those collected in this dissertation (truncated cone model), show that myocardial oxygenation is markedly increased and more uniform than calculations based upon the traditional Krogh cylinder model.

TABLE 5.1 Input and Reference Data used for the Calculation of Myocardial PO_2 Histograms.

VARIABLE	VALUE
Capillary radius (μm)	2.4
PaO_2 (mmHg)	100
$PaCO_2$ (mmHg)	40
pH_a	7.4
Blood O_2 capacity (ml/100ml)	20
P_{50} of hemoglobin (mmHg)	37
Blood flow ($ml \cdot min^{-1} \cdot g^{-1}$)	4.0
Arterial hematocrit	45
Tissue O_2 permeability ($ml \cdot s^{-1} \cdot cm^{-1} \cdot mmHg^{-1}$)	2.1×10^{-8}
Facilitation pressure (P_F, mmHg)	14
Myoglobin P_{50} (mmHg)	5.3
Tissue O_2 consumption ($ml \cdot min^{-1} \cdot g^{-1}$)	0.4
Tissue temperature (°C)	37
Respiratory Quotient	0.8
Oxygen pressure = ½ VO_{2max} (q_{50}, mmHg)	3

See Turek et al. (1991) for original citations for these data.

TABLE 5.2 Input Morphometric Data from Pressure Overloaded Myocardium used for the Calculation of Myocardial PO_2 Histograms.

2 Layer	**Cylinder**	**Cone**
AC Cylinder Radius (μm)	12.9	13.2
AC SDlog	0.070	0.072
VC Cylinder Radius (μm)	12.9	12.2
VC SDlog	0.070	0.067

4 Layer	**Cylinder**	**Cone**
1st Quarter Cylinder Radius (μm)	12.6	15.5
1st Quarter SDlog	0.070	0.072
2nd Quarter Cylinder Radius (μm)	12.6	12.5
2nd Quarter SDlog	0.070	0.072
3rd Quarter Cylinder Radius (μm)	12.6	11.5
3rd Quarter SDlog	0.070	0.067
4th Quarter Cylinder Radius (μm)	12.6	11.0
4th Quarter SDlog	0.070	0.067

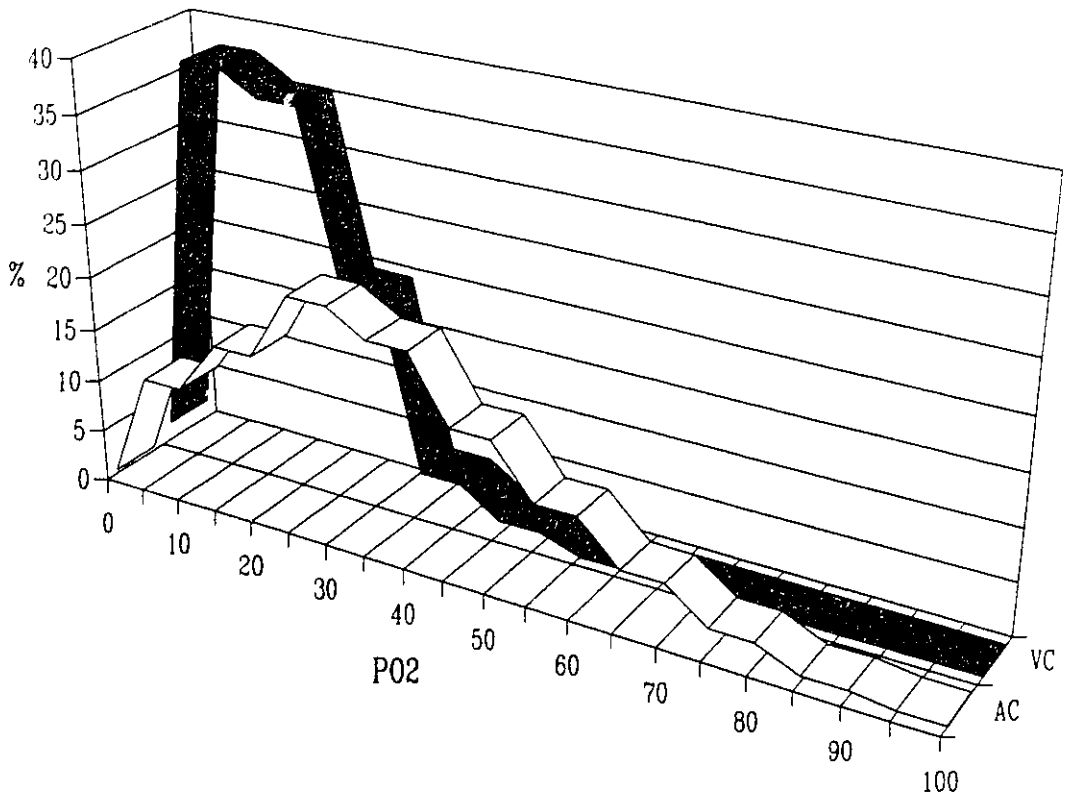

Fig. 5.1 Computed myocardial PO_2 histograms from morphometric data of pressure overloaded rat myocardium. Two layer case (AC, arteriolar capillary; VC, venular capillary), employing the **Krogh cylinder model** with the inclusion of capillary barrier.

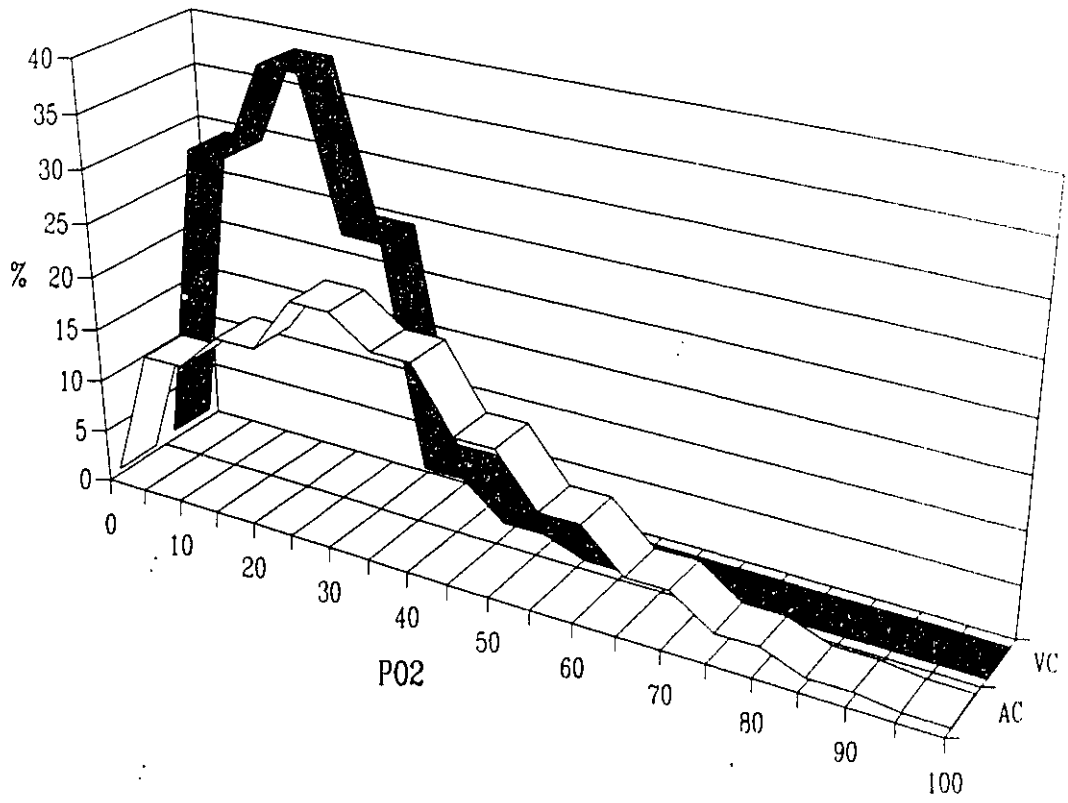

Fig. 5.2 Computed myocardial PO_2 histograms from morphometric data of pressure overloaded rat myocardium. Two layer case (AC, arteriolar capillary; VC, venular capillary), employing the **truncated cone model** with the inclusion of capillary barrier.

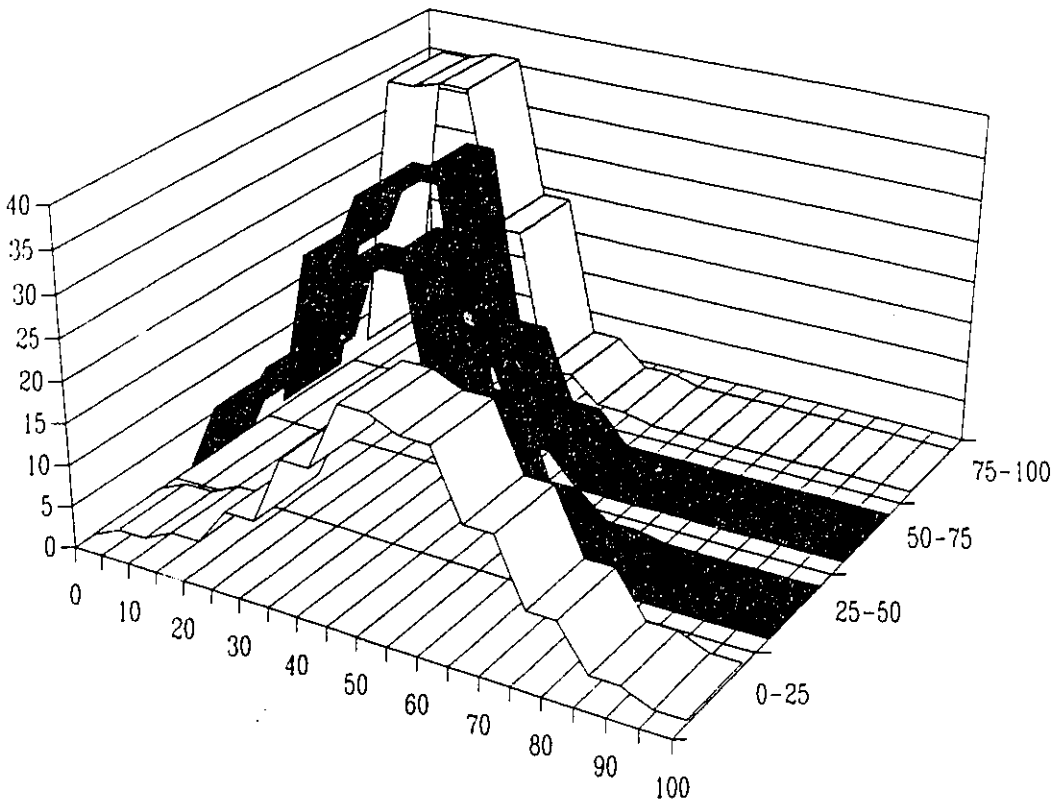

Fig. 5.3 Computed myocardial PO_2 histograms from morphometric data of pressure overloaded rat myocardium. Four layer case, employing the **Krogh cylinder model**, with the inclusion of capillary barrier.

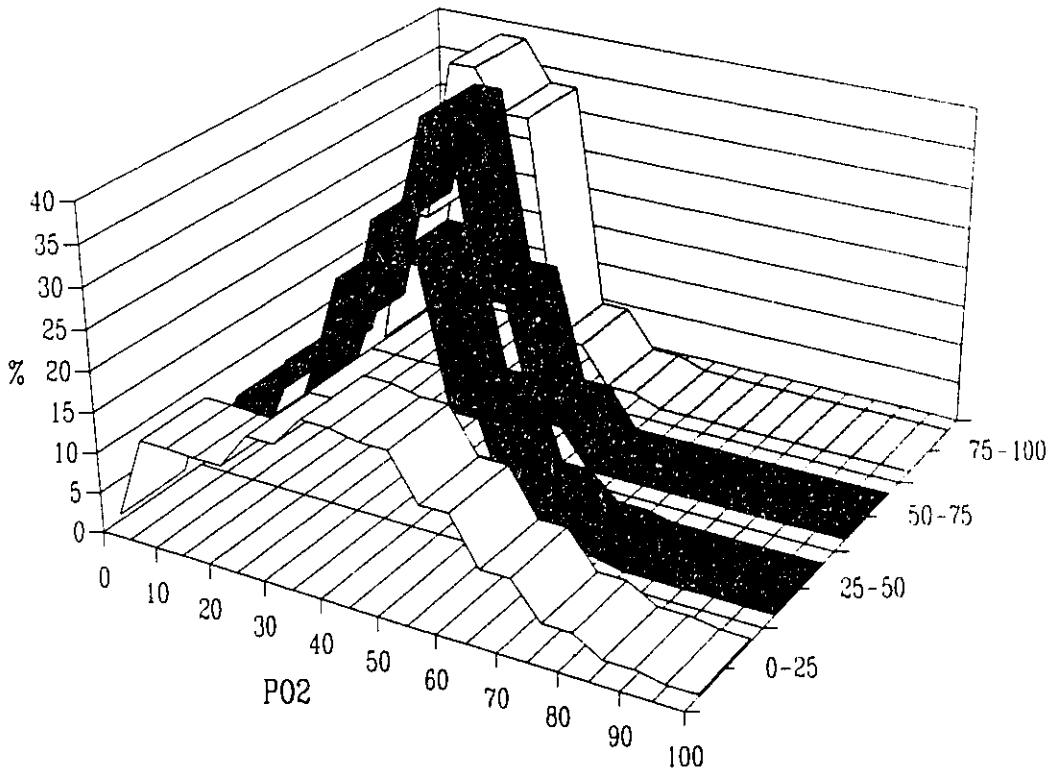

Fig. 5.4 Computed myocardial PO_2 histograms from morphometric data of pressure overloaded rat myocardium. Four layer case, employing the **truncated cone model**, with the inclusion of capillary barrier.

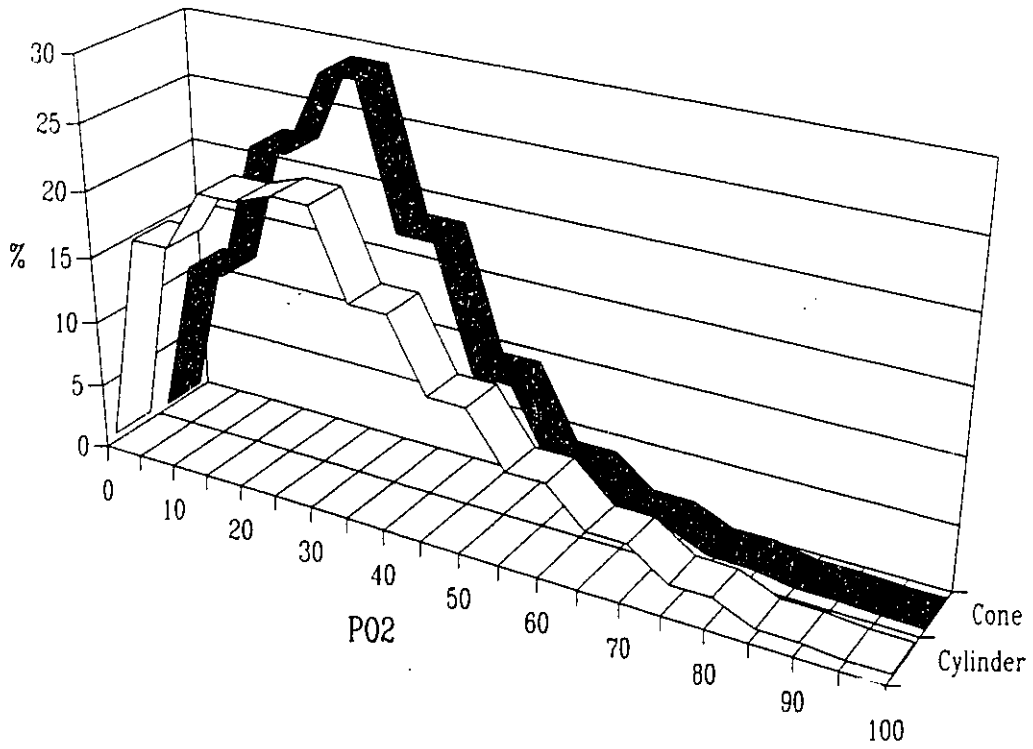

Fig. 5.5 Computed myocardial PO_2 histograms from morphometric data of pressure overloaded rat myocardium. The four layers of Figs. 5.3 and 5.4, respectively, have been combined, resulting in integrated PO_2 histograms based upon both **Krogh cylinder** and **truncated cone models.**

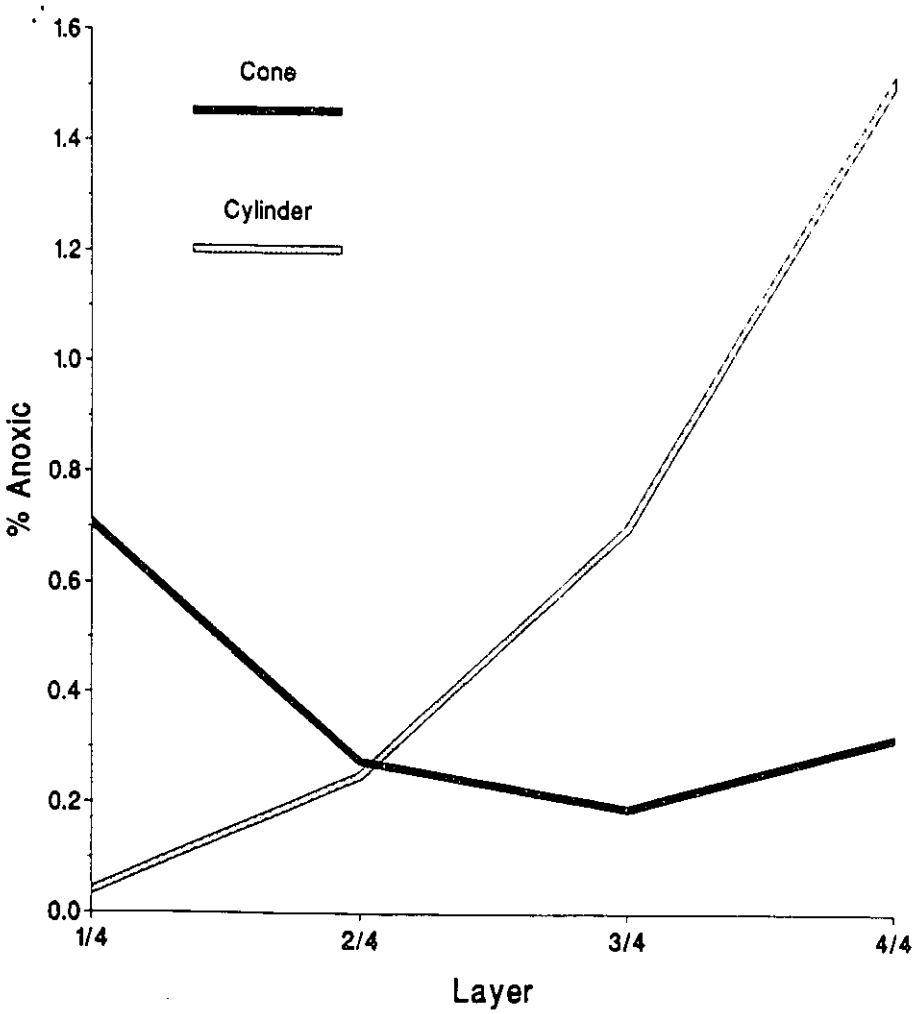

Fig. 5.6 Summary of the computed percent anoxic tissue (PO_2 < 0.005 mmHg) for 4 layer arrangement of the Krogh cylinder and truncated cone models.

The data presented in this dissertation have served to address several important questions related to oxygen supply in the heart muscle under normal and pathological conditions. It is becoming increasingly evident that the structure-function relationship at the level of the coronary microvascular bed is very dynamic. Indeed, coronary capillaries demonstrate marked plasticity in the face of physiological and pathological challenge.

Inevitably, the results of this dissertation will raise more questions than have been answered. There is still a lot of work to be done!

REFERENCES

Anversa, P., Loud, A.V., Giacomelli, F. and Wiener, J. (1978). Absolute morphometric study of myocardial hypetrophy in experimental hypertension. Lab. Invest. **38**, 597-609.

Anversa, P., Olivetti, G. and Loud, A.V. (1980). Morphometric study of early postnatal development in the left and right ventricular myocardium of the rat. I. Hypertrophy, hyperplasia and binucleation of myocytes. Circ. Res. **48**, 495-502.

Anversa, P., Beghi, C., Levicky, V., McDonald, S.L. and Kikkawa, Y. (1982). Morphometry of right ventricular hypertrophy induced by strenous exercise in the rat. Am. J. Physiol. **243**, H856-H861.

Anversa, P., Levicky, V., Beghi, C., McDonald, S.L. and Kikkawa, Y. (1983). Morphometry of exercise-induced right ventricular hypertrophy in the rat. Circ. Res. **52**, 57-64.

Anversa, P., Melissari, M., Beghi, C. and Olivetti, G. (1984). Structural compensatory mechanisms in rat heart in early spontaneous hypertension. Am. J. Physiol. **246**, H739-H746.

Anversa, P., Ricci, R. and Olivetti, G. (1986a). Coronary capillaries during normal and pathological growth. Can. J. Cardiol. **2**, 104-113.

Anversa, P., Beghi, C., Kikkawa, Y. and Olivetti, G. (1986b). Myocardial infarction in rats. Infarct size, myocyte hypertrophy, and capillary growth. Circ. Res. **58**, 26-37.

Anversa, P., Ricci, R. and Olivetti, G. (1986c). Quantitative structural analysis of the myocardium during physiologic growth induced cardiac hypertrophy: A review. J. Am. Coll. Cardiol. **7**, 1140-1149.

Anversa, P. and Capasso, J.M. (1991). Loss of intermediate-sized coronary arteries and capillary proliferation after left ventricular failure in rats. Am. J. Physiol. **260**, H1552-H1660.

Artigue, R.S. and [illegible]nan, W.A. (1976). The effect of myoglobin on the oxygen concentration in skeletal muscle subjected to ischemia. Ann. Biomed. Eng. **4**, 128-136.

Auerbach, L. (1865). Ueber den Bau der Lymph- und Blut-Capillaren. Zbl. med. Wiss. **3**, 177-192.

Azizkhan, R.G., Azizkhan, J.C., Zetter, B.R. and Folkman, J. (1980). Mast cell heparin stimulates migration of capillary endothelial cells in vitro. J. Exp. Med. **152**, 931-944.

Banchero, N. (1987). Capillarity and distribution of capillaries and mitochondria in cardiac growth. In: The stressed heart, edited by Legato, M.J. Boston: Martinus Nijhoff, p. 67-86.

Bassingthwaighte, J.B., Yipintsoi, T. and Harvey, R.B. (1974). Microvasculature of the dog left ventricular myocardium. Microvasc. Res. **7**, 229-249.

Bassingthwaighte, J.B., King, R.B. and Roger, S.A. (1989). Fractal nature of regional myocardial blood flow heterogeneity. Circ. Res. **65**, 578-590.

Bennett, R.A., Pittman, R.N. and Sullivan, S.M. (1991). Capillary spatial pattern and muscle fiber geometry in three hamster striated muscles. Am. J. Physiol. **260**, H579-H585.

Blum, J. (1960). Concentration profiles in and around capillaries. Am. J. Physiol. **198**, 991-998.

Borg, T.K. and Caulfield, J.B. (1980). Morphology of connective tissue in skeletal muscle. Tiss. Cell **12**, 197-207.

Borg, T.K. and Caulfield, J.B. (1981). The collagen matrix of the heart. Federation Proc. **40**, 2037-2041.

Borsi, L., Carnemolla, B., Castellani, P., Rosellini, C., Vecchio, D., Allemanni, G., Chang, S.E., Taulor-Papadimitrion, J., Pande, E. and Zardi, Z. (1987). Monoclonal antibodies in the analysis of fibronectin isoforms generated by alternative splicing on mRNA precursors in normal and transformed human cells. J. Cell Biol. **104**, 595-600.

Brown, R.E. (1965). The pattern of the microcirculatory bed in the ventricular myocardium of domestic mammals. Am. J. Anat. **116**, 355-374.

Campbell, S.E., Rakusan, K. and Gerdes, A.M. (1989). Change in cardiac myocyte distribution in aortic-constricted neonatal rats. Basic Res. Cardiol. **84**, 247-258.

Casscells, W., Speir, E., Sasse, J., Klagsbrun, M., Allen, P., Lee, M., Calvo, B., Chiba, M., Haggroth, L., Folkman, J. and Epstein, S.E. (1990). Isolation, characterization and localization of heparin-binding growth factors in the heart. J. Clin. Invest. **85**, 433-441.

Caulfield, J.B. and Borg, T.K. (1979). The collagen network of the heart. Lab. Invest. **40**, 364-372.

Chambers, R. and Zweifach, B.W. (1944). Topography and function of the mesenteric capillary circulation. Am. J. Anat. **75**, 173-205.

Clark, P.J. and Evans, F.C. (1954). Distance to nearest neighbor as a measure of spatial relationships in populations. Ecology **35**, 445-453.

Claycomb, W.C. (1976). Biochemical aspects of cardiac muscle differentiation. J. Biol. Chem. **251**, 6082-6089.

Cliff, A.D. and Ord, J.K. (1973). Spatial autocorrelation, London:Pion.

Cousineau, D., Rose, C.P., Lamoureux, D. and Goresky, C.A. (1983). Changes in cardiac transcapillary exchange with metabolic coronary vasodilation in the intact dog. Circ. Res. **53**, 719-730.

Covell, D.G. and Jacquez, J.A. (1987). Does myoglobin contribute significantly to diffusion of oxygen in red skeletal muscle?. Am. J. Physiol. **252**, R341-R347.

Crisman, R.P., Rittman, B. and Tomanek, R.J. (1985). Exercise-induced myocardial capillary growth in the spontaneously hypertensive rat. Microvasc. Res. **30**, 185-194.

Cutts, A. (1986). Sarcomere length changes in the wing muscles during the wing beat cycle of two bird species. J. Zool. (Lond.) **209**, 183-185.

Cutts, A. (1989). Sarcomere length changes in muscles of human thigh during walking. J. Anat. **166**, 77-84.

Dart, C.H. and Holloszy, J.O. (1969). Hypertrophied non-failing rat heart. Circ. Res. **25**, 245-253.

Dawson, J.M., Tyler, K.R. and Hudlicka, O. (1987). A comparison of the microcirculation in rat fast glycolytic and slow oxidative muscles at rest and during contractions. Microvasc. Res. **33**, 167.

Dowell, R.T. and McManus, R.E. (1978). Pressure induced cardiac enlargement in neonatal and adult rats. Circ. Res. **42**, 303-310.

Ellis, C.G., Safranyos, R.G.A. and Groom, A.C. (1983). Television-computer method for in vivo measurement of capillary diameter, based on the passage of red cells. Microvasc. Res. **26**, 139-150.

Ellis, C.G., Fraser, S., Hamilton, G. and Groom, A.C. (1984). Measurement of the lineal density of red blood cells in capillaries in vivo, using a computerized frame-by-frame analysis of video images. Microvasc. Res. **27**, 1-13.

Ellis, C.G., Mathieu-Costello, O., Potter, R.F., MacDonald, I.C. and Groom, A.C. (1990). The effect of sarcomere length on total capillary length in skeletal muscle: in vivo evidence for longitudinal stretching of capillaries. Microvasc. Res. **40**, 63-72.

Ellsworth, M.L., Popel, A.S. and Pittman, R.N. (1988). Assessment and impact of heterogeneities of convective oxygen transport parameters in capillaries of striated muscle: experimental and theoretical. Microvasc. Res. **35**, 341-362.

Eriksson, E. and Myrhage, R. (1972). Microvascular dimensions and blood flow in skeletal muscle. Acta. Physiol. Scand. **86**, 211-222.

Fabel, H. (1968). Normale und kritische Sauerstoffversorgung des Herzens. In: Oxygen transport in blood and tissue, Stuttgart: Thieme, p. 159-225.

Federspiel, W.J. (1986). A model study of intracellular oxygen gradients in a myoglobin-containing skeletal muscle fiber. Biophys. J. **49**, 857-868.

Flaim, S.F., Minteer, W.J., Clark, D.P. and Zelis, R. (1979). Cardiovascular response to acute aquatic and treadmill exercise in the untrained rat. J. Appl. Physiol. **46**, 302-308.

Flanagan, M.F., Fujii, A.M., Colan, S.D., Flanagan, R.G. and Lock, J.E. (1991). Myocardial angiogenesis and coronary perfusion in left ventricular pressure-overload hypertrophy in the young lamb. Circ. Res. **68**, 1458-1470.

Fletcher, J.E. (1980). On facilitated oxygen diffusion in muscle tissues. Biophys J. **29**, 437-445.

Frasher, W.G. and Wayland, H. (1972). The repeating modular organization of the microcirculation of cat mesentery. Microvasc. Res. **4**, 62-76.

Frolkis, V.V. and Bogatskaya, L.N. (1968). The energy metabolism of myocardium and its regulation in animals of various age. Exp. Gerontol. **3**, 199-210.

Gay, W.A. and Johnson, E.A. (1967). The anatomical evaluation of the myocardial length-tension diagram. Circ. Res. **21**, 33-43.

Gayeski, T.E.J. and Honig, C.R. (1986). O2 gradients from sarcolemma to cell interior in a red muscle at maximal VO2. Am. J. Physiol. **251**, 789-799.

Gayeski, T.E.J. and Honig, C.R. (1988). Intracellular PO2 in long axis of individual fibers in working dog gracilis muscle. Am. J. Physiol. **254**, H1179-H1186.

Gerdes, A.M., Campbell, S.E. and Hilbelink, D.R. (1988). Structural remodelling of cardiac myocytes in rats with arteriovenous fistulas. Lab. Invest. **59**, 857-861.

Gibbons, J.D. (1985). Nonparametric statistical inference, New York:Dekker.

Gobel, U., Theilen, H. and Kuschinsky, W. (1990). Congruence of total and perfused capillary network in rat brains. Circ. Res. **66**, 271-281.

Gordon, A.M., Huxley, A.F. and Julian, F.J. (1966). The variation in isometric tension with sarcomere length in vertebrate muscle fibers. J. Physiol. (Lond.) **184**, 170-192.

Gore, R.W. and Bohlen, H.G. (1977). Microvascular pressures in rat intestinal muscle and mucosal villi. Am. J. Physiol. **233**, H685-H693.

Grayson, J., Davidson, J.W., Fitzgerald-Fitz, A. and Scott, C. (1974). The functional morphology of the coronary microcirculation in the dog. Microvasc. Res. **8**, 20-43.

Groebe, K. (1990). A versatile model of steady state O2 supply to tissue. Application to skeletal muscle. Biophys. J. **57**, 485-498.

Groom, A.C., Ellis, C.G. and Potter, R.F. (1984a). Microvascular architecture and red cell perfusion in skeletal muscle. Changes during shortening and possible improvement in oxygen transport to tissue. In: Prog. appl. Microcirc, edited by Hammersen, F. and Messmer, K. Basel: Karger, p. 64-83.

Groom, A.C., Ellis, C.G. and Potter, R.F. (1984b). Microvascular geometry in relation to modeling of oxygen transport in contracted skeletal muscle. Amer. Rev. Resp. Dis. **129**, Suppl. S6-S9.

Groom, A.C., Ellis, C.G., Wrigley, S. and Potter, R.F. (1986). Architecture and flow patterns in capillary networks of skeletal muscle of frog and rat. In: Microvascular networks: experimental and theoretical studies, edited by Popel, A.S. and Johnson, P.C. Basel: Karger, p. 6[illegible].

Grossman, W., Jones, D. and McLaurin, L.P. (1975). Wall stress patterns of hypertrophy in the human left ventricle. J. Clin. Invest. **56**, 56-64.

Grote, J. and Thews, G. (1962). Die bedingungen fur die Sauerstoffversorgung des Herzmuskelgewebes. Pflugers Arch. **276**, 142.

Grunewald, W.A. and Sowa, W. (1977). Capillary structures and O_2 supply to tissue. An analysis with a digital diffusion model as applied to the skeletal muscle. Rev. Physiol. Biochem. Pharmacol. **77**, 149-209.

Hall, M. (1831). A critical and experimental essay on the circulation of the blood; expecially as observed in the minute and capillary vessels of the batrachia and of fishes, London:Seely and Burnside.

Hammersen, F. (1968). The pattern of the terminal vascular bed and the ultrastructure of capillaries in skeletal muscle. In: Oxygen transport in blood and tissue, edited by Lubbers, D.W., Luft, U.C., Thews, G. and Witzleb, E. Stuttgart: Georg Thieme Verlag, p. 184-197.

Harris, T.E. (1989). The theory of branching processes, New York:Dover.

Hatt, P.Y., Rakusan, K., Gastineau, P. and Laplace, M. (1980). Morphometry and ultrastructure of the heart hypertrophy induced by chronic volume overload (aorto-caval fistula in the rat). J. Mol. Cell. Cardiol. **11**, 989-998.

Henquell, L. and Honig, C.R. (1976). Intercapillary distances and capillary reserve in right and left ventricles: significance for control of tissue PO2. Microvasc. Res. **12**, 35-41.

Henquell, L., Odoroff, C.L. and Honig, C.R. (1977). Intercapillary distance and capillary reserve in hypertrophied rat hearts beating in situ. Circ. Res. **41**, 400-408.

Hill, A.V. (1928). The diffusion of oxygen and lactic acid through tissues. Proc. Roy. Soc. Ser. B. **104**, 39-96.

Honig, C.R., Feldstein, L. and Frierson, J.L. (1977). Capillary lengths, anastomoses, and estimated capillary transit times in skeletal muscle. Am. J. Physiol. **233**, H122-H129.

Honig, C.R., Gayeski, T.E.J., Federspiel, W., Clark, A.Jr. and Clark, P. (1984). Muscle O_2 gradients from hemoglobin to cytochrome: new concepts, new complexities. Adv. Exp. Med. Biol. **169**, 23-37.

Honig, C.R., Gayeski, T.E.J. and Groebe, K. (1991). Myoglobin and oxygen gradients. In: The Lung, edited by Crystal, R.G. and West, J.B. New York: Raven, p. 1489-1496.

Hoofd, L., Turek, Z., Kubat, K., Ringnalda, B.E.M. and Kazda, S. (1985). Variability of intercapillary distance estimated on histological sections of rat heart. Adv. Exp. Med. Biol. **227**, 239-247.

Hort, W. and Hort, A. (1958). Beitrage zur Histochemie der Blutgfassendothelien und der Kapillargrundhautchen. Virchows arch. A **331**, 591-598.

Hudlicka, O., West, D., Kumar, S., El Khelly, F. and Wright, A.J.A. (1989). Can growth of capillaries in the heart and skeletal muscle be explained by the presence of an angiogenic factor? Br. J. Exp. Pathol. **70**, 237-246.

Hudson, J.A. and Cater, D.B. (1965). An analysis of factors affecting tissue oxygen tension. Proc. Roy. Soc. London. B. **161**, 247-256.

Jacobs, T.B., Bell, R.D. and McClements, J.D. (1984). Exercise, age and the development of the myocardial vasculature. Growth **48**, 148-157.

Kardami, E. and Fandrich, R.R. (1989). Basic fibroblast growth factor in atria and ventricles of the vertebrate heart. J. Cell Biol. **109**, 1865-1875.

Kayar, S.R., Archer, P.G., Lechner, A.J. and Banchero, N. (1982a). The closest-individual method in the analysis of the distribution of capillaries. Microvasc. Res. **24**, 326-341.

Kayar, S.R., Archer, P.G., Lechner, A.J. and Banchero, N. (1982b). Evaluation of the concentric-circles method for estimating capillary-tissue diffusion distances. Microvasc. Res. **24**, 342-353.

Kety, S. (1970). Determinant of tissue oxygen tension. Fed. Proc. **16**, 666-670.

King, R.B., Weissman, L.J. and Bassingthwaighte, J.B. (1990). Fractal descriptions for spatial statistics. Ann. Biomed. Eng. **18**, 111-121.

Korecky, B. and Rakusan, K. (1978). Normal and hypertrophic growth of the rat heart: changes in cell dimensions and number. Am. J. Physiol. **234**, 123-128.

Korecky, B., Hai, C.M. and Rakusan, K. (1982). Functional capillary density in normal and transplanted rat hearts. Can. J. Physiol. Pharmacol. **60**, 23-32.

Kreuzer, F. (1982). Oxygen supply to tissues: the Krogh model and its assumptions. Experientia Basel **38**, 1415-1426.

Kreuzer, F., Turek, Z. and Hoofd, L. (1991). Oxygen transfer from blood to mitochondria. In: The lung:Scientific Foundations, edited by Crystal, R.G. and West, J.B. New york: Raven Press, p. 1479-1488.

Krogh, A. (1919). The number and distribution of capillaries in muscles with calculations of the oxygen pressure head necessary for supplying the tissue. J. Physiol. **52**, 409-415.

Krogh, A. (1922). The Anatomy and Physiology of Capillaries, New Haven:Yale U.P.,

Laks, M.M., Nisenson, M.J. and Swan, H.J.C. (1967). Myocardial cell and sarcomere lengths in the normal dog heart. Circ. Res. **21**, 671-678.

Legault, F., Rouleau, J.L., Juneau, C., Rose, C. and Rakusan, K. (1990). Functional and morphological characteristics of compensated and decompensated cardiac hypertrophy in dogs with chronic infrarenal aorto-caval fistulas. Circ. Res. **66**, 846-859.

Linzbach, A.J. (1947). Mikrometrische und histologische Analyse hypertrophischer menschlicher Herzen. Virchows arch. A **314**, 534-543.

Linzbach, A.J. (1960). Heart failure from the point of view of quantitative anatomy. Am. J. Cardiol. **5**, 370-382.

Ljungqvist, A., Tornling, G., Unge, G., Jurdahl, E.B. and Larrson, B. (1984). Capillary growth in the heart and skeletal muscle during dipyridamole treatment and exercise. Prog. Appl. Microcirc. **4**, 9-15.

Loats, J.T., Sillau, A.H. and Banchero, N. (1978). How to quantify skeletal muscle capillarity. Adv. Exp. Med. Biol. **94**, 41-48.

Lojda, Z. (1979). Studies on dipeptidyl(amino) peptidase IV (Glycyl-proline naphthlyamidase). Histochem. **59**, 153-166.

Ludwig, G. (1971). Capillary pattern of the myocardium. In: Methods of achievement in experimental pathology, edited by Bajusz, E. and Jasmin, G. Basel: Karger, p. 238-271.

Lund, N., Damon, D.H., Damon, D.N. and Duling, B.R. (1987). Capillary grouping in hamster tibialis anterior muscles: flow patterns, and physiological significance. Int. J. Microcirc.: Clin. Exp. **5**, 359-372.

Mall, G., Mattfeldt, T. and Volk, B. (1980). Ultrastructural morphometric study on the rat heart after chronic ethanol feeding. Virchows arch. A **389**, 59-77.

Mall, G., Mattfeldt, T., Hasslacher, C. and Mann, J. (1986). Morphological reaction patterns in experimental cardiac hypertrophy - a quantitative stereological study. Basic Res. Cardiol. **81(Suppl. 1)**, 193-203.

Mall, G., Klingel, K., Hasslacher, C.H., Mann, J., Mattfeldt, T., Baust, H. and Waldherr, R. (1987). Synergistic effects of diabetes mellitus and renovascular hypertension on the rat heart-stereological investigations on papillary muscles. Virchows arch. A **411**, 531-542.

Mall, G. and Mattfeldt, T. (1990). Capillary growth patterns in cardiac hypertrophy and normal growth-a stereological study on papillary muscles. In: Cardiac dilatation, edited by Jacob, Seipel and Zucker Stuttgart: Gustav Fischer Verlag, p. 51-67.

Mall, G., Zimmer, G., Baden, S. and Mattfeldt, T. (1990). Capillary neoformation in the rat heart-stereological studies on papillary muscles in hypertrophy and physiologic growth. Basic Res. Cardiol. **85**, 531-540.

Martini, J. and Honig, C.R. (1969). Direct measurement of intercapillary distance in beating rat heart in situ under various conditions of O2 supply. Microvasc. Res. **1**, 244-256.

Mathieu, O., Cruz-Orive, L.M., Hoppeler, H. and Weibel, E.R. (1983). Estimating length density and quantifying anisotropy in skeletal muscle capillaries. J. Microsc. **131**, 131-146.

Mathieu-Costello, O. (1987). Capillary tortuosity and degree of contraction or extension of skeletal muscles. Microvasc. Res. **33**, 98-117.

Mathieu-Costello, O., Potter, R.F., Ellis, C.G. and Groom, A.C. (1988). Capillary configuration and fiber shortening in muscles of the rat hindlimb: correlation between corrosion casts and stereological measurements. Microvasc. Res. **36**, 40-55.

Mathieu-Costello, O., Poole, D.C. and Logemann, R.B. (1989a). Muscle fiber size and chronic exposure to hypoxia. Adv. Exp. Med. Biol. **248**, 305-311.

Mathieu-Costello, O., Hoppeler, H. and Weibel, E.R. (1989b). Capillary tortuosity in skeletal muscles of mammals depends on muscle contraction. J. Appl. Physiol. **66**, 1436-1442.

Mathieu-Costello, O. (1991). Morphometric analysis of capillary geometry in pigeon pectoralis muscle. Am. J. Anat. **191**, 74-84.

Mattfeldt, T., Kramer, K.L., Zeitz, R. and Mall, G. (1985). Stereology of myocardial hypertrophy induced by physical exercise. Virchows arch. A **409**, 473-485.

Mattfeldt, T. and Mall, G. (1984). Estimation of length and surface of anisotropic capillaries. J. Microsc. **135**, 181-190.

Mattfeldt, T. and Mall, G. (1987). Growth of capillaries and myocardial cells in the normal rat heart. J. Mol. Cell. Cardiol. **19**, 1237-1246.

Mattfeldt, T., Drautz, M. and Mall, G. (1989). Experimentelle Herzhypertrophie durch Thyroxingabe. Pathologe **10**, 206-211.

Meerson, F.Z. (1969). The myocardium in hyperfunction, hypertrophy and heart failure. Circ. Res. **25(no. 1 suppl. 11)**, 1-163.

Myers, W.W. and Honig, C.R. (1964). Number and distribution of capillaries as determinants of myocardial oxygen tension. Am. J. Physiol. **207**, 653.

Myrhage, R. and Hudlicka, O. (1976). The microvascular bed and capillary surface area in rat extensor hallucis proprius muscle (EHP). Microvasc. Res. **11**, 315-323.

Olivetti, G., Anversa, P. and Loud, A.V. (1980). Morphometric study of early postnatal development in the left and right ventricular myocardium of the rat. II. Tissue composition, capillary growth, and sarcoplasmic alterations. Circ. Res. **46**, 503-512.

Olivetti, G., Lagrasta, C., Quaini, F., Ricci, R., Moccia, G., Capasso, J.M. and Anversa, P. (1989a). Capillary growth in anemia-induced ventricular wall remodeling in the rat heart. Circ. Res. **65**, 1182-1192.

Olivetti, G., Lagrasta, C., Ricci, R., Sonnenblick, E.H., Capasso, J.M. and Anversa, P. (1989b). Long-term pressure-induced cardiac hypertrophy: capillary and mast cell proliferation. Am. J. Physiol. **257**, H1766-H1772.

Olivetti, G., Capasso, J.M., Sonnenblick, E.H. and Anversa, P. (1990). Side-to-side slippage of myocytes participates in ventricular wall remodeling acutely after myocardial infarction in rats. Circ. Res. **67**, 23-34.

Olivetti, G., Capasso, J.M., Meggs, L.G., Sonnenblick, E.H. and Anversa, P. (1991). Cellular basis of chronic ventricular remodeling after myocardial infarction in rats. Circ. Res. **68**, 856-869.

Opitz, E. and Schneider, M. (1950). The oxygen supply of the brain and the mechanism of deficiency effects. Ergeb. Physiol. **46**, 126-260.

Phillips, S.J., Rosenberg, A., Meir-Levi, D. and Pappas, E. (1979). Visualization of the coronary microvascular bed by light and scanning electron microscopy and x-ray in the mammalian heart. Scanning Electron Microsc. **3**, 735-742.

Poole, D.C., Batra, S., Mathieu-Costello, O. and Rakusan, K. (1990). Effect of fiber shortening on capillary geometry in rat myocardium. Physiologist **33**, A99.

Popel, A.S. (1980a). Oxygen diffusion from capillary layers with concurrent flow. Math. Biosci. **50**, 171.

Popel, A.S. (1980b). Mathematical modeling of convective and diffusive transport in the microcirculation. In: Mathematics of microcirculation phenomena, edited by Gross, J.G and Popel, A.S. New York: Raven Press, p. 63-88.

Popel, A.S. (1982). Oxygen diffusive shunts under conditions of heterogeneous oxygen delivery. J. Theor. Biol. **96**, 533.

Potter, R.F. and Groom, A.C. (1983). Capillary diameter and geometry in cardiac and skeletal muscle studied by means of corrosion casts. Microvasc. Res. **25**, 68-84.

Potter, R.F., Houghton, S. and Groom, A.C. (1989). Capillary lengths and anastomoses in rat hindlimb muscles, studied by aquablack perfusion during rest versus exercise. Adv. Exp. Med. Biol. **248**, 313-322.

Poupa, O., Rakusan, K. and Ostadal, B. (1970). The effect of physical activity upon the heart of vertebrates. Medicine sport **4**, 202-235.

Rakusan, K. (1971a). Quantitative morphology of capillaries of the heart. In: Meth. achievm. exp. path, edited by Bajusz, E. and Jasmin, G. Basel: Karger, p. 272-286.

Rakusan, K. (1971b). Oxygen in the heart muscle, Springfield :Charles C Thomas,

Rakusan, K. (1984). Cardiac growth, maturation, and aging. In: Growth of the heart in health and disease, edited by Zak, R. New York: Raven Press, p. 131-164.

Rakusan, K. (1984). Assessment of cardiac growth. In: Growth of the heart in health and disease, edited by Zak, R. New York: Raven Press, p. 25-40.

Rakusan, K. (1987). Microcirculation in the stressed heart. In: The stressed heart, edited by Legato, M.J. Boston: Martinus Nijhoff, p. 107-124.

Rakusan, K. and Poupa, O. (1963). Changes in the diffusion distance in the rat heart muscle during development. Physiol. Bohemoslov. **12**, 220-227.

Rakusan, K., Jelinek, J., Soukupova, B., Korecky, B. and Poupa, O. (1965). Postnatal development of muscle fibers and capillaries in the rat heart. Physiol. Bohemoslov. **14**, 32-37.

Rakusan, K. and Poupa, O. (1966). Differences in capillary supply of hypertrophic and hyperplastic hearts. Cardiologia **49**, 293-298.

Rakusan, K., du Mesnil de Rochemont, W., Braasch, W., Tschopp, H. and Bing, R.J. (1967). Capacity of the terminal vascular bed during normal growth, in cardiomegaly, and in cardiac atrophy. Circ. Res. **21**, 209-215.

Rakusan, K., Moravec, J. and Hatt, P-Y. (1980). Regional capillary supply in the normal and hypertrophied rat heart. Microvasc. Res. **20**, 319-326.

Rakusan, K. and Korecky, B. (1982). The effect of growth and aging on functional capillary supply of the rat heart. Growth **46**, 275-281.

Rakusan, K., Hoofd, L. and Turek, Z. (1985). The effect of cell size and capillary spacing on myocardial oxygen supply. Adv. Exp. Med. Biol. **180**, 463-475.

Rakusan, K. and Turek, Z. (1985). Protamine inhibits capillary formation in growing rat hearts. Circ. Res. **57**, 393-398.

Rakusan, K., Korecky, B., Sarkar, K. and Turek, Z. (1986). Merits and pitfalls in morphological assessment of cardiac growth. Fed. Proc. **45**, 2580-2584.

Rakusan, K., Wicker, P., Abdul-Samad, M., Healy, B. and Turek, Z. (1987). Failure of swimming exercise to improve capillarization in cardiac hypertophy of renal hypertensive rats. Circ. Res. **61**, 641-647.

Rakusan, K., Sarkar, K., Turek, Z. and Wicker, P. (1990). Mast cells in the rat heart during normal development and in cardiac hypertrophy. Circ. Res. **66**, 511-516.

Reid, M.B., Gonvea, W.J. and Johnson, R.L.Jr. (1982). Capillary density in the canine diaphragm: comparison of alkaline ATPase stain with vasodilated, in situ fixation. Fed. Proc. **41**, 1272. (Abstract)

Renkin, R.E., Gray, S.D., Dodd, L.R. and Lia, B.D. (1981). Heterogeneity of capillary distribution and capillary circulation in mammalian skeletal muscles. In: Underwater physiology, edited by Bacharach, A.V. and Matzemm, M.M. Bethesda: Undersea medical society, p. 464-474.

Ripley, B.D. (1981). Spatial statistics, Ney York:Wiley, pp. 33-41.

Roberts, J.T. and Wearn, J.T. (1941). Quantitative changes in the capillary-muscle relationship in human hearts during normal growth and hypertrophy. Amer. Heart J. **21**, 617-633.

Rome, L.C., Funke, R.P., Alexander, R.M., Lutz, G., ALdridge, H., Scott, F. and Freadmans, M. (1988). Why animals have different muscle fiber types. Nature **335**, 824-827.

Roos, K.P. (1987). Sarcomere length uniformity determined from three-dimensional reconstructions of resting isolated heart cell striation patterns. Biophys. J. **52**, 317-327.

Rossi, M.A. and Carillo, S.V. (1991). Cardiac hypertrophy due to pressure and volume overload: distinctly different biological phenomena? Int. J. Cardiol. **31**, 133-142.

Roughton, F. (1952). Diffusion and chemical reaction velocity in cylindrical and spherical systems of physiological interest. Proc. Roy. Soc. Ser. B. **140**, 203-229.

Safranyos, R.G.A., Ellis, C.G., Tyml, K. and Groom, A.C. (1983). Heterogeneity of capillary diameters in the skeletal muscle of the frog. Microvasc. Res. **26**, 151-156.

Sarelius, I.H. (1990). An analysis of microcirculatory flow heterogeneity using measurements of transit time. Microvasc. Res. **40**, 88-98.

Sasaki, H., Hoshi, H., Hong, Y.-M., Suzuki, T., Kato, T., Saito, M., Youki, H., Karube, K., Konno, S., Onodera, M., Saito, T. and Aoyagi, S. (1989). Purification of acidic fibroblast growth factor from bovine heart and its localization to the cardiac myocytes. J. Biol. Chem. **264**, 17606-17612.

Schmid-Schonbein, G.W., Skalak, R., Usami, S. and Chien, S. (1980). Cell distribution in capillary networks. Microvasc. Res. **19**, 18-44.

Schuchhardt, S. (1985). Myocardial oxygen pressure: mirror of oxygen supply. Adv. Exp. Med. Biol. **180**, 21-35.

Shipley, R.A., Shipley, J. and Wearn, J.T. (1937). The capillary supply in normal and hypertophied hearts of rabbits. J. Exp. Med. **65**, 29-44.

Skalak, T.C. and Schmid-Schonbein, G.W. (1986). The microvasculature of skeletal muscle. IV. A model of the capillary network. Microvasc. Res. **32**, 333-347.

Smaje, L., Zweifach, B.W. and Intaglietta, M. (1970). Micro-pressures and capillary filtration coefficients in single vessels of the cremaster muscle of the rat. Microvasc. Res. **2**, 96-110.

Sonnenblick, E.H., Spiro, D. and Cottrell, T.S. (1963). Fine structural changes in heart muscle in relation to the length-tension curve. Proc. Nat. Acad. Sci. **49**, 193-200.

Sonnenblick, E.H., Spiro, D. and Spotnitz, H.M. (1964). The ultrastructural basis of Staring's law of the heart. The role of the sarcomere in determining ventricular size and stroke volume. Am. Heart J. **68**, 336-346.

Sonnenblick, E.H., Ross, J., Covell, J.W., Spotnitz, H.M. and Spiro, D. (1967). The ultrastructure of the heart in systole and diastole. Circ. Res. **21**, 423-431.

Spiro, D. and Sonnenblick, E.H. (1964). Comparison of the ultrastructural basis of the contractile process in heart and skeletal muscle. Circ. Res. (Suppl. II) **14 and 15**, II-14-II-37.

Spotnitz, H.M., Sonnenblick, E.H. and Spiro, D. (1966). Relation of ultrastructure to function in the intact heart: sarcomere structure relative to pressure volume curves of intact left ventricles of dog and cat. Circ. Res. **28**, 49-66.

Steinhausen, M., Tillmans, H. and Thederan, H. (1978). Microcirculation of the epimyocardial layer of the heart. Pflugers Arch. **378**, 9-14.

Taylor, S. and Folkman, J. (1982). Protamine is an inhibitor of angiogenesis. Nature **297**, 307-311.

ter Keurs, H.E.D.J., Bucx, J.J.J., de Tombe, P.P., Backx, P. and Iwazumi, T. (1988). The effects of sarcomere length and Ca++ on force and velocity of shortening in cardiac muscle. Adv. Exp. Med. Biol. **226**, 581-593.

Thews, G. (1960). Oxygen diffusion in the brain, a contribution to the question of the oxygen supply of the organs. Pflugers Archiv. **271**, 197-226.

Thomas, D.P., Phillips, S.J. and Bove, A.A. (1984). Myocardial morphology and blood flow distribution in chronic volume-overload hypertrophy in dogs. Basic Res. Cardiol. **79**, 379-388.

Thomas, D.P., McCormick, K.M., Gosselin, L.E., Julin, D.M., Raab, D.M. and Wanta, D. (1990). Age-training interactions on cell size and vascularity in the rat heart. In: Sports, Medicine and Health, edited by Hermans, G.P.H. : Elsevier, p. 943-948.

Tillich, G., Mendoza, L., Wayland, H. and Bing, R.J. (1971). Studies of the coronary microcirculation of the cat. Am. J. Cardiol. **27**, 93-98.

Tillmans, H., Ikeda, S., Hansen, H., Sarma, J.S.M., Fauvel, J.M. and Bing, R.J. (1974). Microcirculation in the ventricle of the dog and turtle. Circ. Res. **34**, 561-569.

Toborg, M. (1972). The microcirculatory bed in the myocardium of the rat and the cat. Z. Zellforsch. **123**, 369-394.

Tomanek, R.J. (1970). Effects of age and exercise on the extent of the myocardial capillary bed. Anat. Rec. **167**, 55-62.

Tomanek, R.J., Searls, J.C. and Lachenbruch, P.A. (1982). Quantitative changes in the capillary bed during developing, peak, and stabilized cardiac hypertrophy in the spontaneously hypertensive rat. Circ. Res. **51**, 295-304.

Tomanek, R.J., Aydelotte, M.R. and Butters, C.A. (1990). Late-onset renal hypertension in old rats alters myocardial microvessels. Am. J. Physiol. **259**, H1681-H1687.

Turek, Z. and Rakusan, K. (1981). Lognormal distribution of intercapillary distance in normal and hypertrophic rat heart as estimated by the method of concentric circles: its effect on tissue oxygenation. Pflugers Arch. **391**, 17-21.

Turek, Z., Kubat, K., Kazda, S., Hoofd, L. and Rakusan, K. (1987). Improved myocardial capillarisation in spontaneously hypertensive rats treated with nifedipine. Cardiovasc. Res. **21**, 725-729.

Turek, Z., Rakusan, K., Olders, J., Hoofd, L. and Kreuzer, F. (1991). Computed myocardial PO2 histograms: effects of various geometrical and functional conditions. J. Appl. Physiol. **70(4)**, 1845-1853.

Tyml, K. (1986). Capillary recruitment and heterogeneity of miscrovascular flow in skeletal muscle before and after contraction. Microvasc. Res. **32**, 84-98.

Tyml, K. and Mikulash, K. (1988). Evidence for increased perfusion heterogeneity in skeletal muscle during reduced flow. Microvasc. Res. **35**, 316-324.

Venema, H.W. (1988). Spatial distribution of fiber types in skeletal muscle: test for a random distribution. Muscle & nerve **2**, 301-311.

Wearn, J.T. (1928). The extent of the capillary bed of the heart. J. Exp. Med. **47**, 273-292.

Weibel, E.R. (1984). The pathway for oxygen, Cambridge:Harvard university press, pp. 180.

Wiedeman, M. (1984). Architecture. In: Handbook of Physiology, Section 2, Microcirculation, edited by Renkin, E.M. and Michel, C.C. Bethesda: Am. Physiol. Soc., p. 11.

Wieringa, P.A., Spaan, J.A.E., Stassen, H.G. and Laird, J.D. (1982). Heterogeneous flow distribution in a three dimensional network simulation of the myocardial microcirculation. Microcirculation **2**, 195-216.

Wolff, J.R., Goerz, C., Bar, T. and Guldner, F.H. (1975). Common morphogenetic aspects of various organotypic microvascular patterns. Microvasc. Res. **10**, 373-395.

Wright, A.J.A. and Hudlicka, O. (1981). Capillary growth and changes in heart performance induced by chronic bradycardial pacing in the rabbit. Circ. Res. **49**, 469-478.

Wright, A.J.A., Hudlicka, O. and Brown, M.D. (1989). Beneficial effect of chronic bradycardial pacing on capillary growth and heart performance in volume overload heart hypertrophy. Circ. Res. **64**, 1205-1212.

Yoran, C., Covell, J.W. and Ross, J. (1973). Structural basis for the ascending limb of left ventricular function. Circ. Res. **32**, 297-303.

Ziada, A.M.A.R., Hudlicka, O., Tyler, K.R. and Wright, A.J.A. (1984). The effect of long-term vasodilatation on capillary growth and performance in rabbit heart and skeletal muscle. Cardiovasc. Res. **18**, 724-732.

APPENDIX

Incubating media for the demonstration of enzyme activities in the endothelium of arteriolar and venular capillary regions (Lojda, 1979; Batra et al., 1989).

Alkaline Phosphatase (AP)	**Dipeptidyl Peptidase IV (DPP IV)**
40 mg Naphthol AS-MX Phosphate	16 mg Glycy-L-proline-4-methoxy
2 ml N,N-dimethylformamide	B-naphthylamide
80 mg Variance Blue Salt Rt	2 ml N,N-dimethylformamide
40 ml 0.1M tris-HCl buffer pH 9.2	40 mg Fast Blue B salt
	40 ml 0.1M acetate buffer pH 5.4

Staining Method

1. Prepare frozen sections (16 μm thick)
2. Fix in chloroform-acetone (1:1): 5 min.
3. Wash in distilled water: 3 changes
4. Incubation for DPP reaction in room temperature: 90 min.
5. Wash in distilled water: 3 changes
6. Incubation for AP reaction: 25 min. (room temperature)
7. Wash in distilled water
8. Postfix in 4% formalin: 2 hrs.
9. Wash in running water: 2 min.
10. Wash in distilled water
11. Mount with APATHY'S MOUNTING MEDIA or GLYCEROL-GELATIN

APATHY'S MOUNTING MEDIA

Acacia (gum arabic)	50 gm
Cane sugar (sucrose)	50 gm
Distilled water	150.0 ml
Sodium chloride	10.0 gm
Thymol	0.1 gm

Mix the acacia, cane sugar, and distilled water in a flask. Place the flask in a pan of boiling water until ingredients are dissolved. Dissolve the sodium chloride and thymol in this solution. Filter with a Seitz filter while the solution is still warm, or use coarse filter paper and place in 60C oven, changing filter paper frequently. Refrigerate to remove air bubbles. Sodium chloride is added to prevent bleeding and thymol is added as a preservative.

Incubation Solution

A. DPP (filter)

1. Glycy-L-proline-4-methoxy-β-Naphthylamide-8 mg
   dissolved in
2. N, N-dimethylformamide - 1 ml
   mix with
3. Fast blue B salt - 20 mg
4. 0.1M Acetate Buffer - 20 ml, pH - 5.4-5.6

B. AP (filter)

1. Naphthol AS-MX phosphate - 20 mg
   dissolve in — Mix
2. N, N-dimethylformamide - 1 ml
   add to — Mix well
3. Variamine Blue Salt RT - 40 mg
4. 0.1 M Tri-HCl buffer - 20 ml, pH 9.2 — Mix

*All the chemicals are from SIGMA

Acetate Buffer

Stock Solutions

A: 0.2M solution of acetic acid (11.55 ml. in 1000 ml.).

B: 0.2M solution of sodium acetate (16.4 g. of $C_2H_3O_2Na$ or 27.2 g. of $C_2H_3O_2Na.3H_2O$ in 1000 ml.).

x ml. of A + y ml. of B, diluted to a total of 100 ml.

x	y	pH
46.3	3.7	3.6
44.0	6.0	3.8
41.0	9.0	4.0
36.8	13.2	4.2
30.5	19.5	4.4
25.5	24.5	4.6
20.0	30.0	4.8
14.8	35.2	5.0
10.5	39.5	5.2
8.8	41.2	5.4
4.8	45.2	5.6

Tris (hydroxymethyl)aminomethane (Tris) Buffer

Stock Solutions

A:0.2M solution of tris(hydroxymethyl)aminomethane (24.2 g. in 1000 ml.).

B:0.2M HCl.

50 ml. of A + x ml. of B, diluted to a total of 200 ml.

x	pH
5.0	9.0
8.1	8.8
12.2	8.6
16.5	8.4
21.9	8.2
26.8	8.0
32.5	7.8
38.4	7.6
41.4	7.4
44.2	7.2

VITA

NAME:	Sanjay Batra.
DATE OF BIRTH:	July 12, 1963.
CITIZENSHIP:	Canadian.
PRESENT ADDRESS:	21 Wellfleet Crescent Nepean, Ontario, Canada. K2J 2Y3
	(613) 825-2518

EDUCATION

1987-1991 Ph.D. Physiology, University of Ottawa
Thesis Advisor - Dr. Karel Rakusan

1982-1986 B.Sc. Kinanthropology, University of Ottawa

SCHOLARSHIPS AND AWARDS

1991 Japan Society for the Promotion of Science Postdoctoral Fellowship [pending]
1991 Heart and Stroke Foundation of Canada Research Fellowship [declined]
1991 International Society of Heart Research Travel Award
1991 Department of Physiology Student Seminar Award
1991 The Jerry Taichman Award for Best Research Achievement by a Graduate Student in the Department of Physiology

1989 Melvin H. Knisely Young Investigator Award. Presented at the XI Meeting of the International Society on Oxygen Transport To Tissue, GÖttingen, F.R.G., 21-24 July 1989.

1988-1991 Ontario Graduate Student Scholarship
1988-1991 University of Ottawa Merit Scholarship
1989 University of Ottawa Travel Award
1988-1989 University of Ottawa Rector's Scholarship
1988-1989 Department of Physiology Student Seminar Award
1987-1988 University of Ottawa Entrance Scholarship

PUBLICATIONS

Batra, S., Kuo, C., and Rakusan, K. (1989). Spatial Distribution of Coronary Capillaries: A-V Segment Staggering. *Adv. Exp. Med. Biol.* **248:** 241-247.

Batra, S., and Rakusan, K. (1990). Morphometric Analysis of Capillary Nets in Rat Myocardium. *Adv. Exp. Med. Biol.* **227:** 377-385.

Rakusan, K., Batra, S., Turek, Z., and Wicker, P. (1990). Geometry of Coronary Capillary Net and it's Effect on Myocardial Oxygenation. *Microcirc. Ann.* 1-4.

Batra, S., Rakusan, K. and Campbell, S. (1991). Geometry of Capillary Networks in Hypertrophied Rat Heart. *Microvasc. Res.* **41,** 29-40.

Batra, S., and Rakusan, K. (1991). Capillarization of the Hypertrophic Heart: Discrepancy of the Results Obtained by the Triangulation and Domain Methods. *J. Cardiovasc. Pharmacol.* **17 (Suppl. 2),** S151-S153.

Batra, S., and Rakusan, K. (1991). Geometry of capillary networks in volume overloaded rat heart. *Microvasc. Res. 42, 39-50.*

Batra, S. and Rakusan, K. (under revision). Capillary network geometry during postnatal growth in the rat heart. *Am. J. Physiol.*

Poole, D.C., Batra, S., Mathieu-Costello, O., and Rakusan, K. (under revision). Capillary geometrical changes with fiber shortening in rat myocardium: implications for oxygen delivery. *Circ. Res.*

Batra, S., Veprek, P., and Rakusan, K. (in press). Gradients of capillarization in the subendocardium of the rat heart septum. *Adv. Exp. Med. Biol.*

Batra, S., and Rakusan, K. (in press). Morphometric methods for the evaulation of capillary grouping patterns in hypertrophied rat heart. *Adv. Exp. Med. Biol.*

Turek, Z., Hoofd, L., Batra, S., and Rakusan, K. (in press). The effect of realistic geometry of capillary networks on tissue PO_2 in hypertrophied rat heart. *Adv. Exp. Med. Biol.*

Veprek, P., Batra, S., and Rakusan, K. (in press). Isoproteronol induced necrosis in relationship to local capillary geometry. *Bas. Res. Cardiol.*

Batra, S., Poole, D.C., and Rakusan, K. (in preparation). Capillary segment branching and orientation at discrete phases of the cardiac cycle in the rat heart. *Cardiovasc. Res.*

POSTER PRESENTATIONS/ABSTRACTS

Spatial distribution of coronary capillaries: A-V segment staggering. Presented at the X Meeting of the International Society on Oxygen Transport To Tissue, Ottawa, Canada, 7-11 August 1988.

Capillary network architecture: minimal capillary lengths and branching patterns in rat myocardium. Presented at the XIII Congress of the International Society for Heart Research, Ann Arbor, U.S.A., 14-18 May 1989. **Abstract:** Journal of Molecular and Cellular Cardiology. **21**:Supplement II, April 1989.

The effect of cardiac hypertrophy on capillary network architecture. Presented at Microvascular Networks: Fractal Structure, Hemodynamic Properties and Physiological Functions [A satellite Symposium of the XXXI International Congress of Physiological Sciences], West Berlin, F.R.G., 16-19 July 1989. **Abstract:** International Journal of Microcirculation Clinical and Experimental. **8**:Supplement 1, May 1989.

Morphometric analysis of capillary nets in rat myocardium. Presented at the XI Meeting of the International Society on Oxygen Transport To Tissue, GÖttingen, F.R.G., 21-24 July 1989.

Capillarization of the hypertrophic heart: discrepency of the results obtained by the triangulation and domain methods. Presented at Cardiovascular Hypertrophy: It's Implication for Pathophysiology, Outcome and Management of Hypertension [A satellite Symposium of the XIII Scientific Meeting of the International Society of Hypertension], Ottawa, Canada, 29-30 June 1990.

Morphometric methods for the evaluation of capillary grouping patterns in rat heart. Presented at the XII Meeting of the International Society on Oxygen Transport To Tissue, Townsville, Australia, 18-22 July 1990.

Effect of fiber shortening on capillary geometry in rat myocardium. Presented at the Fall meeting of the American Physiological Society, Tampa, U.S.A., 6-10 October 1990. **Abstract:** The Physiologist. Vol. **33, No. 4**, August 1990.

Differences in capillary-tissue geometry from arteriole to venule in rat heart. Presented at the Winter meeting of the Canadian Physiological Society, St. Adele, Canada., 16-20 January 1991. **Abstract:** Can. J. Physiol. Pharmacol.

Geometry of capillary nets during postnatal growth in rat myocardium. Presented at the XV Congress of the International Society for Heart Research, Cinncinati, U.S.A., 29 May - 2 June, 1991. **Abstract:** Journal of Molecular and Cellular Cardiology. **23:**Supplement III, April 1991.

Coronary capillary nets in pressure and volume overloaded rat heart. Presented at the XV Congress of the International Society for Heart Research, Cinncinati, U.S.A., 29 May - 2 June, 1991. **Abstract:** Journal of Molecular and Cellular Cardiology. **23:**Supplement III, April 1991.

Gradients of capillarization in the subendocardium of the rat heart septum. Presented at the XIII Meeting of the International Society on Oxygen Transport To Tissue, Curacao, Netherlands Antilles, 23-30 August 1991 (**ORAL**).

The effect of realistic geometry of capillary networks on tissue PO_2 in hypertrophied rat heart. Presented at the XIII Meeting of the International Society on Oxygen Transport To Tissue, Curacao, Netherlands Antilles, 23-30 August 1991.

3D Domain